# **Extracellular Vesicles as Intercellular Messengers in Aortic Valve Stenosis**

Dissertation

zur

Erlangung des Doktorgrades (Dr. rer. nat.)

der

Mathematisch-Naturwissenschaftlichen Fakultät

der

Rheinischen Friedrich-Wilhelms-Universität Bonn

vorgelegt von

### **Neda Mohammadi**

aus

Ghazvin, Iran

Bonn, 2025

## Angefertigt mit Genehmigung der Mathematisch-Naturwissenschaftlichen Fakultät der Rheinischen Friedrich-Wilhelms-Universität Bonn

Gutachter/Betreuer: Prof. Dr. Alexander Pfeifer

**Gutachter: Prof. Dr. Alf Lamprecht** 

Tag der Promotion: 05.11.2025

Erscheinungsjahr: 2025

#### **Acknowledgements**

Coming to Germany to pursue my PhD opened up a new chapter in both my personal life and scientific career. I am immensely grateful to everyone who facilitated and supported me on this journey, especially those who actively contributed to my scientific development and growth: Prof. Alexander Pfeifer, Prof. Felix Jansen, Prof. Alf Lamprecht, Dr Elisabeth Mies-Klomfass, and Dr. Staffan Hildebrand. I would also like to express my sincere appreciation to my friends and colleagues at the Institute of Pharmacology and Toxicology and the Department of Internal Medicine II at the University Hospital Bonn.

Furthermore, I would like to thank TRR259 and Bigs Drugs for providing outstanding opportunities for PhD students. I would like to thank the Microscopy Core Facility of the Medical Faculty at the University of Bonn for providing support and instrumentation funded by the Deutsche Forschungsgemeinschaft (DFG, German Research Foundation) project number 388171357.

I feel incredibly fortunate to have had the opportunity to conduct some parts of my research at Harvard Medical School. I am particularly grateful to Prof. Elena Aikawa, Dr. Mandy Turner (her postdoctoral fellow), and their group at the Center for Interdisciplinary Cardiovascular Sciences (CICS) for providing such a valuable experience.

Finally, my deepest and most heartfelt thanks go to my family. Their unwavering love, encouragement, and consistent support have been the greatest source of motivation throughout my life.

### **Table of contents**

Acknowledgements	I
Table of contents	II
Abbreviations	VI
1. Introduction	1
1.1. Structure and Function of Aortic Valve	1
1.1.1. Anatomy of aortic root	1
1.1.2. Aortic valve leaflet structure	1
1.1.2.1. Aortic valve cell types: VECs and VICs	2
1.2. Aortic Valve Stenosis (AVS)	3
1.2.1. Prevalence and history	3
1.2.2. Symptoms	4
1.2.3. Diagnosis	5
1.2.4. Treatment	6
1.2.5. Pathophysiological mechanisms of AVS	6
1.2.5.1. Endothelial to mesenchymal transition (EndMT)	8
1.2.5.2. Calcification in AVS	10
1.3. Extracellular Vesicles (EVs) as Regulators of Cardiovascular Disease	11
1.3.1. Biogenesis of EVs	11
1.3.2. Role of EVs in AVS and other cardiovascular diseases	12
1.4. MicroRNAs and Post-transcriptional Regulation in AVS	13
1.4.1. miRNA biogenesis and molecular mechanism	13
1.4.2. Role of miRNAs in AVS and other cardiovascular disease	16
1.5. Aim of PhD Thesis	17
2. Material and Methods	18
2.1. Obtaining Human Aortic Valve Tissue	18
2.2. Cell Culture Methods	18
2.2.1. Materials in cell culture	18
2.2.2. Equipment in cell culture	19
2.2.3. VIC isolation from human aortic valve	20
2.2.4. Cell culture of commercial VICs and VECs	21
2.2.5. VEC culture under the laminar flow	21
2.2.6. Trypsinization and cryo-preservation of VECs and VICs	22
2.2.7. Lentiviral transduction for immortalization and overexpression of miRNA	23

	2.2.8. EndMT induction	23
	2.2.9. Scratch assay to assess VEC migration	23
	2.2.10. Tube formation assay	24
	2.2.11. Cell proliferation	24
	2.2.12. Cellular uptake of IEVs	25
	2.2.13. Co-incubation of IEV with VECs and EndMT assay	25
	2.2.14. Osteogenic differentiation of VICs (calcification assay)	25
	2.2.15. Alizarin red staining	25
	2.2.16. Tissue non-specific alkaline phosphatase (TNAP) activity	26
2	.3. Extracellular Vesicle Methods	26
	2.3.1. Materials	26
	2.3.2. Equipment	26
	2.3.3. IEVs and sEV isolation from aortic valve tissue and cell culture medium	27
	2.3.4. Nano particle tracking analysis (NTA)	27
	2.3.5. Scanning electron microscopy (SEM)	27
2	.4. Immunological Methods	27
	2.4.1. Materials	27
	2.4.2. Equipment	28
	2.4.3. Immunofluorescence (IF) staining	28
2	.5. Cloning and Lentiviral Vector Generation	29
	2.5.1. Materials	29
	2.5.2. Equipment	30
	2.5.3. Preparation of insert DNA	30
	2.5.4. Digest insert DNA and vector	32
	2.5.5. Ligation of insert DNA into the vector	33
	2.5.6. Bacteria transformation	33
	2.5.7. Miniprep	34
	2.5.8. Verification of plasmid integrity via restriction digestion and sequencing	35
	2.5.9. Maxiprep	36
	2.5.10 Lentivirus production	36
2	.6. Protein Methods	37
	2.6.1. Materials	37
	2.6.2. Equipment	37
	2.6.3. Protein isolation and quantification	37
2	7 RNA Methods	38

	2.7.1. Materials	38
	2.7.2. Equipment	38
	2.7.3. Isolation of RNA	39
	2.7.4. RNA isolation from aortic and ventricular sides of aortic valve	39
	2.7.5. qPCR (SYBR green)	40
	2.7.5.1. cDNA synthesis	40
	2.7.5.2. Quantitative real-time polymerase chain reaction (qRT-PCR)	40
	2.7.6. TaqMan qPCR	41
	2.7.6.1. cDNA synthesis	41
	2.7.6.2. TaqMan PCR	43
	2.7.7. miRNA array	43
	2.8. Next Generation Sequencing (NGS)	44
	2.8.1. Library preparation and miRNA deep sequencing	44
	2.8.2. Library preparation and mRNA sequencing (transcriptomics)	44
	2.9. Bioinformatic Analysis	45
	2.9.1. miRNA and mRNA differential expression analysis (DEA)	45
	2.9.2. Prediction of miRNA target genes	46
	2.9.3. Gene ontology (GO) and pathway enrichment analysis	46
	2.9.4. Protein protein interaction (PPI) and gene regulatory network (GRN)	46
	2.9.5. miRNA-mRNA Prediction	46
	2.9.6. Statistical analysis	46
	2.9.7. Image modification	46
3.	Results	47
	3.1. Next Generation Sequencing of EV-miRNAs in AVS	47
	3.1.1. High throughput miRNA sequencing identified dysregulated miRNAs in tissue-de	
	3.1.2. GO Analysis of differentially expressed EV-miRNAs	50
	3.1.3. Validation of dysregulated EV-miRNAs in AVS	53
	3.2. Effects of Candidate miRNAs in VECs	54
	3.2.1. Characterization of VECs and their assessments for VIC contamination	54
	3.2.2. TNFα is the potent inducer of EndMT in VECs	56
	3.2.3. hsa-miRNA-150-5p reduces EndMT in VECs treated with TNFα	58
	3.2.4. hsa-miRNA-150 increases tube formation in VECs	62
	3.2.5. hsa-miRNA-150-5p inhibits cell migration in VECs	63

3.2.8.1. Immortalization of VECs	3.2.7. hsa-miRNA-150-5p expression is increased under laminar shear stress	
3.2.8.3. IEV-miRNA-150-5p is taken up and reduces EndMT in recipient VECs	· ·	
3.2.9. Next generation sequencing of hsa-miRNA-150-5p target genes in VECs	3.2.8.2. IEV characterization	69
3.2.9.1. mRNA sequencing identified dysregulated genes in VECs overexpressing miRNA-150-5p	3.2.8.3. IEV-miRNA-150-5p is taken up and reduces EndMT in recipient VECs	70
150-5p	3.2.9. Next generation sequencing of hsa-miRNA-150-5p target genes in VECs	72
3.2.9.3. Protein-protein interaction (PPI) analysis and gene regulatory network (GRN) analysis	, , , , , , , , , , , , , , , , , , , ,	
analysis	3.2.9.2. GO analysis of differentially expressed miRNA-150-5p target genes	74
150-5p in VECs		•
3.3.1. Primary VIC isolation from calcific aortic valve	·	
3.3.2. miRNA-150-5p reduces calcification in VICs	3.3. Effects of Candidate miRNAs in VICs	81
3.3.3. miRNA-150-5p and Let-7c-5p reduces calcific markers in calcified VICs	3.3.1. Primary VIC isolation from calcific aortic valve	81
3.3.4. miRNA-150-5p and Let-7c-5p reduces TNAP activity in VICs cultured in OM	3.3.2. miRNA-150-5p reduces calcification in VICs	82
4.1. Identification of Dysregulated Tissue-derived EV-miRNAs in AVS	3.3.3. miRNA-150-5p and Let-7c-5p reduces calcific markers in calcified VICs	85
4.1. Identification of Dysregulated Tissue-derived EV-miRNAs in AVS	3.3.4. miRNA-150-5p and Let-7c-5p reduces TNAP activity in VICs cultured in OM	87
4.2. Effects of Candidate miRNAs in VECs	l. Discussion	88
4.3. hsa-miRNA-150-5p in VECs Cultured under the Laminar Flow	4.1. Identification of Dysregulated Tissue-derived EV-miRNAs in AVS	88
4.4. Role of IEV-Mediated Transfer of miRNA-150-5p in Intracellular Communication in VECs 92 4.5. Identification of miRNA-150-5p Target Genes in VECs	4.2. Effects of Candidate miRNAs in VECs	90
4.5. Identification of miRNA-150-5p Target Genes in VECs	4.3. hsa-miRNA-150-5p in VECs Cultured under the Laminar Flow	91
4.6. Effects of Candidate miRNAs in VICs	·	
5. Summary97	4.5. Identification of miRNA-150-5p Target Genes in VECs	92
•	4.6. Effects of Candidate miRNAs in VICs	95
Publication bibliography99	5. Summary	97
	Publication bibliography	99

#### **Abbreviations**

**ACS**-Acute coronary syndrome

**ACE**-Angiotensin converting enzyme

ACTA2-Alpha smooth muscle actin

**ADIPOR**-Adiponectin receptor

Al-Aortic insufficiency

**ALP**-Alkaline phosphatase

AT2-Angiotensin II type 2 receptors

**ATX**-Autotoxin

**AVA-**Aortic valve area

**AVS**-Aortic valve stenosis

**AV-**Aortic valve

**BMP**-Bone morphogenetic protein

**BSA**-Bovine serum albumin

**CAD**-Coronary artery disease

CASP3-Caspase-3

**CCG**-Cologne center for genomics

**CCNA**-Cyclin A

**CDH**-Cadherin

**CHF**-Chronic heart failure

**CM-**Cardiomyocyte

**CO**-Cardiac output

COL1A1-Collagen Type I Alpha 1 Chain

**CPC**-Cetylpyridinium chloride

**CPM**-Counts per million

DAPI-4',6-diamidino-2-phenylindole

**DEA**-Differential expression analysis

**DMEM**-Dulbecco's modified eagle medium

**DMSO**-Dimethyl sulfoxide

**DNA**-Deoxyribonucleic acid

EC-Endothelial cells

**ECM**-Extracellular matrix

EDTA-Ethylenediaminetetraacetic acid

**EFNA1**-Ephrin A1 and

**EtOH**-Ethanol

EndMT-Endothelial to mesenchymal transition

**EMT**-Epithelial to mesenchymal transition

**ERK-**Extracellular-regulated kinases

**ESCRT**-Endosomal sorting complex required for transport

**eNOS**-Endothelial nitric oxide synthase 3

**EV**-Extracellular vesicle

FBS-Fetal bovine serum

**FDR**-False discovery rate

FGF-Fibroblast growth factor

**FP**-Forward primer

FSA-Fibroblast surface antigen

FSP-1-Fibroblast-specific protein-1

**GAPDH**-Glycerol aldehyde-3-phosphate dehydrogenase

gDNA-Genomic DNA

**GFP**-Green fluorescent protein

**GO**-Gene ontology

**GRN-**Gene regulatory network

**HBSS**-Hank's balanced salt solution

**HCAEC**-Human coronary artery endothelial cell

HMEC-1-Human microvascular endothelial cell

**HMMR**-Hyaluronan mediated motility receptor

HIF-2-Hypoxia-inducible factor-2

hnRNPU-Heterogeneous nuclear ribonucleoprotein U

HPASMC-Human pulmonary artery smooth muscle cell

ICAM1-Intercellular adhesion molecule 1

IF-Immunofluorescence

IgG-Immunoglobulin G

IGF-1-Insulin-like growth factor 1

**IL**-Interleukin

**INSR-Insulin receptor** 

ITGA-Integrin subunit alpha

I-VECs-Immortalized VECs

**KLF**-Kruppel-like factor

IEV-Large extracellular vesicle

IncRNA-long-non doing RNAs

Lp-PLA2-Lipoprotein-associated phospholipase A2

LRP5-LDL receptor-related protein 5

**LVC-**Lentivirus control

**LVOT**-Left ventricular outflow tract

MAPK-Mitogen-activated protein kinase

MCP-1-Monocyte chemoattractant protein-1

**MFE**-Minimum free energy

**MI**-Myocardial Infarction

**MPs**-Metalloproteinases

**MMP**-Matrix metalloproteinase

mRNA-Messenger ribonucleic acid

**MVBs**-Multivesicular bodies

NaCI-Sodium chloride

Na2HPO4-Disodium hydrogen phosphate

NaN3-Sodium azide

**NaF**-Natriummonovanadat

ncRNAs-Non-coding RNAs

**NF**-Nuclear factor

**NGS**-Next generation sequencing

Nm-Nanometer

**NM**-Nanomolar

**NO-**Nitric oxide

NP-40-Nonidet® P 40 Substitute

**NTA**-Nano particle tracking analysis

**OM**-Osteogenic medium

oxLDL-Oxidized LDL

oxPLs-Oxidized phospholipids

**OD**-Optical density

P/S-Penicillin/ streptomycin

**PABP-**Poly(A)-binding protein

**PAH-**Pulmonary arterial hypertension

**PBS**-Phosphate buffered saline

**PCR**-Polymerase chain reaction

PDLIM1-Protein PDZ and LIM domain

PECAM/CD31-Platelet and endothelial cell adhesion molecule 1

**PFA-**Paraformaldehyde

**PGK**-Phosphoglycerate-kinase

PM-Pro-calcifying medium

Pmean-Mean pressure gradient

pNP-p-Nitrophenol

pNPP-p-Nitrophenyl phosphate

**PPi**-Pyrophosphate

pre-miRNA-Precursor-miRNA

pri-miRNA-Primary-miRNA

**PPI-**Protein protein interaction

PPi-Pyrophosphate

**PS**-Phosphatidylserine

qRT-PCR-Quantitative real-time polymerase chain reaction

RAPGEF2-Rap quanine nucleotide exchange factor 2

**RBP**-RNA binding protein

**RISC-RNA-induced silencing complex** 

**RT**-Room temperature

**RT**-Reverse transcription

Runx2-Runt-related transcription factor 2

**SAG-**Smoothened agonist

**SAVR**-Surgical aortic valve replacement

SCD-Stearoyl-CoA desaturase-1

**SDS**-Sequence detection system

SDS-PAGE Sodium dodecyl-sulphate polyacrylamide gel electrophoresis

**SEM**-Standard error of the mean

**SEM**-Scan electron microscopy

**sEV**-Small extracellular vesicle

SHC2-SHC adaptor protein 2

**SMC**-Smooth muscle cell

**α-SMA**-Alpha smooth muscle actin

**SMAD-**Small mothers against decapentaplegic

NaH2PO4-Sodium dihydrogen phosphate

**SV40**-Simian virus 40

TAg SV40-Tumor antigen SV40

**TAVR**-Transcatheter aortic valve replacement

TBS-T-Tris buffered saline -Tween 20

**TC**-Telocytes

TCA-Tricarboxylic acid cycle

**TAVR**-Transcatheter aortic valve replacement

**TG**-Triglyceride

**TGF-**β-Transforming growth factor-β

**TGFBR2**-TGF-β receptor 2

**TNAP**-Tissue non-specific alkaline phosphatase

**TNF**α-Tumor necrosis factor alpha

**UNG**- Uracyl N-glycosylase

**URP**-Universal reverse primer

VCAM-1-Vascular cell adhesion molecule-1

**VEGFR**-Vascular endothelial growth factor receptor

**VEC**-Valvular endothelial cell

VWF-Von Willebrand factor

**VIC**-Valvular interstitial cell

**VIM**-Vimentin

**WB**-Western blot

**ZEB**-Zinc finger e-box binding homeobox

#### 1. Introduction

#### 1.1. Structure and Function of Aortic Valve

#### 1.1.1. Anatomy of aortic root

The term "aortic root" encompasses the segment of the aortic valve (AV) extending from the left ventricular outflow tract (LVOT) which is joined to the ascending aorta, and is interposed between the mitral valve orifice and the muscular ventricular septum (Ho 2019). The aortic root forms a bulge outward and creates three sinuses including the right and left coronary sinuses and non-coronary aortic sinus (Figure 1A and B) (Ho 2019). When the aortic valve is closed, triangular junctions can be observed between adjacent leaflets, extending towards the peripheral commissures and surrounded by the aortic wall (Ho 2019). The proper function of the aortic root is of utmost importance for maintaining optimal coronary flow, left ventricular performance, and the preservation of a healthy myocardium (Piazza et al. 2008).

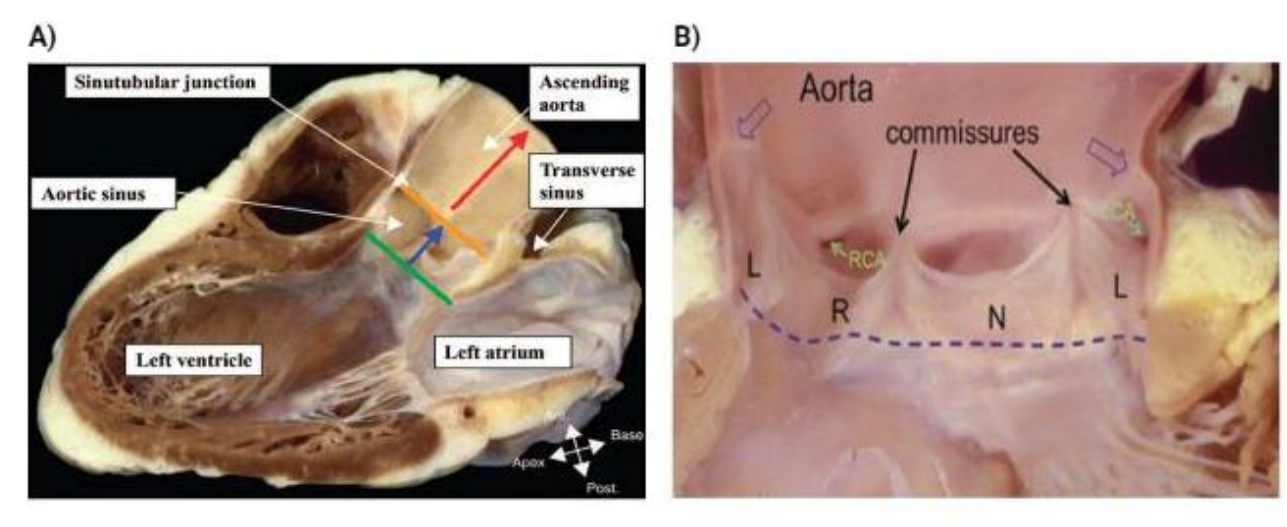


Figure 1. Schematic figure of the aortic root.

**A)** The aortic root is the continuation of the left ventricular outflow tract (LVOT). The key parts of aortic root are indicated with different colors including the basal attachment of aortic valve (AV) leaflets (green line), the aortic root itself (blue arrow), the sinutubular junction (orange line), and the ascending aorta (red arrow) (picture adapted from Rozeik et al.) (Rozeik et al. 2014) **B)** The LVOT is shown incised longitudinally and displayed flat. The three aortic sinuses (R, N, L), RCA and LCA are visible after leaflet removal. R: Right coronary aortic sinus, L: Left coronary aortic sinus, N: non-coronary aortic sinus, RCA: Right Coronary Artery, and LCA: Left Coronary Artery (picture adapted from Ho et al.) (Ho 2019).

#### 1.1.2. Aortic valve leaflet structure

The aortic valve is located between the left ventricle and the aorta and normally has three cusps or leaflets which are covered by valvular endothelial cells (VEC) on the aortic and ventricular side. Pulsatile blood flow generates hydrodynamic pressure, leading to the

cyclic opening of the AV leaflets, which consist of three distinct connective tissue layers: fibrosa, spongiosa and ventricularis (Figure 2) (Kostyunin et al. 2019). The fibrosa positioned on the aortic side is an extension of the aortic annulus and characterized by an abundance of type I and III collagen fibers that provide mechanical strength to the valve. The spongiosa, located in the central layer, contains proteoglycans and glycosaminoglycans, which facilitate the reorganization of the collagenous and elastic layers during the cardiac cycle. Lastly, the ventricularis is composed of elastic fibers that absorb and distribute the hydrodynamic pressure, contributing to the proper function and elasticity of the valve (Kostyunin et al. 2019). This trilaminar structure plays a crucial role in providing load-bearing capacity and lubrication to the cusps while reducing radial strain when the valve opens (Ho 2019; Vesely 1998; Simionescu et al. 2003). The second cell type in AV is valvular interstitial cells (VICs) which are mainly located within these three layers and under the endothelium and play an important role together with VECs in maintaining valve homeostasis (Charitos and Sievers 2013).

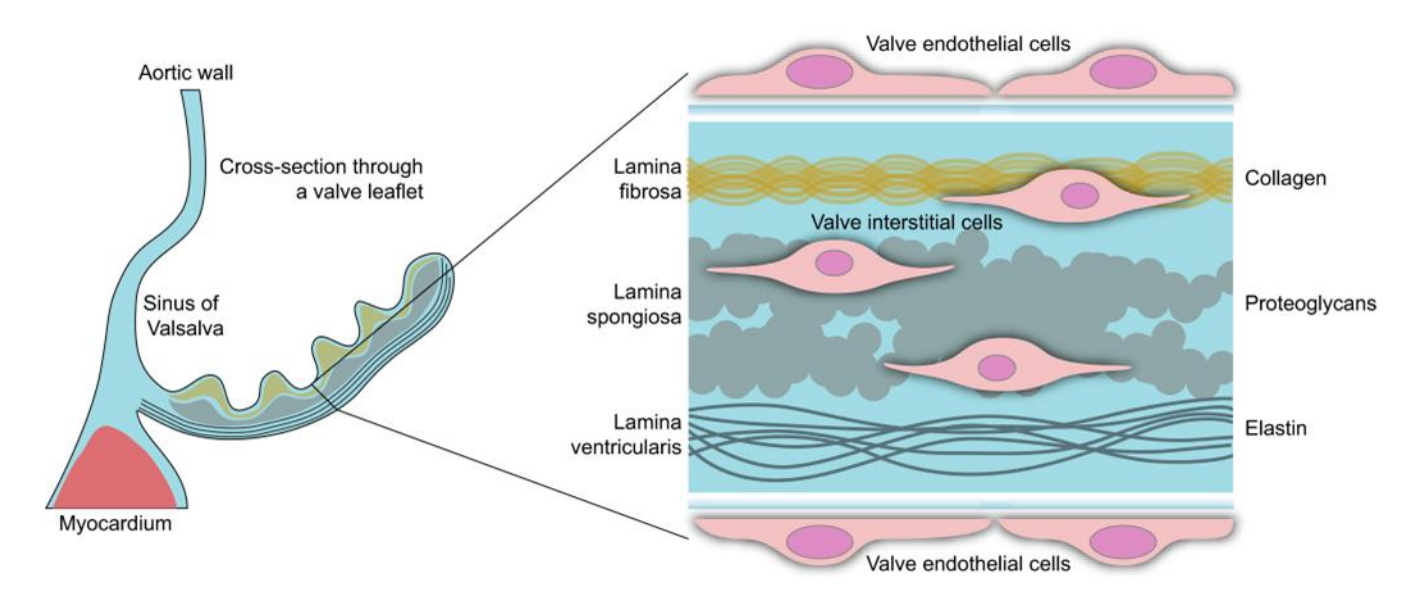


Figure 2. Aortic valve structure.

Aortic valve (AV) consists of three layers: fibrosa, spongiosa and ventricularis from the aortic to the ventricular side. The AV is covered from both aortic and ventricular sides by valve endothelial cells (VECs) and contains valvular interstitial cells (VICs) within the layers (picture adapted from Rutkovskiy et al.) (Rutkovskiy et al. 2017).

#### 1.1.2.1. Aortic valve cell types: VECs and VICs

Both aortic and ventricular sides of VECs play essential protective roles for the underlying tissue. Aortic valve leaflets facilitate the unidirectional blood flow from the left ventricle into the aorta during cardiac cycle. During systole, the aortic valve leaflets open, exposing VECs to high laminar flow on the ventricular side (inflow surface). Conversely, during diastole, the valve leaflets are stretched, and VECs on the aortic side (outflow surface) encounter high turbulent flow due to the reverse blood flow direction. This dynamic

interaction serves to preserve the integrity of the valve leaflets (Rajamannan et al. 2011). Under normal physiological conditions, VECs have a similar morphology to endothelial cells (ECs) that line blood vessels. They display a characteristic flat shape, possess cell junctions, and express specific endothelial markers including platelet and endothelial cell adhesion molecule 1 (PECAM/CD31), von Willebrand factor (vWF), VE-cadherin (CD144), and endothelial nitric oxide synthase 3 (eNOS) (Ma et al. 2020). However, unlike vascular endothelial cells that align with the blood flow, VECs are arranged in a circumferential orientation across the leaflets, perpendicular to the direction of blood flow. During embryogenesis, VECs undergo a process called endothelial to mesenchymal transition (EndMT) via complex signaling cascades and invade into the underlying cardiac jelly to form endocardial cushions, and subsequently heart valve (Ma et al. 2020). Besides their role in preserving aortic valve integrity and embryonic development, VECs also play crucial roles in regulating cell adhesion, permeability and inhibiting VIC differentiation into osteoblast-like cells under pathological conditions (Mongkoldhumrongkul et al. 2016).

VICs are distributed throughout aortic valve leaflets and can be distinguished from VECs by their expression of fibroblast surface antigen (FSA), vimentin (VIM), prolyl-4-hydrolase, CD105, desmin, smooth muscle myosin, and ACTA2, as well as the absence of endothelial markers vWF and CD31 (Rutkovskiy et al. 2017). VICs are responsible for synthesizing the extracellular matrix (ECM), as well as matrix metalloproteinases and their inhibitors, contributing significantly to a rtic valve remodeling (Mongkoldhumrongkul et al. 2016). VICs exhibit a heterogeneous and dynamic cell population based on their response to the mechanical and environmental stimuli. These phenotypes include quiescent, activated, progenitor and osteoblastic cells (Kostyunin et al. 2019). In healthy adult leaflets, VICs primarily exhibit a quiescent fibroblastic phenotype without any synthetic or destructive activities. The activation of VICs mainly occurs during heart growth and the transition from fetus to adult stages. However, in adult life, VICs can be activated in response to mechanical injury and stress. Activated VICs demonstrate the myofibroblast characteristics with enhanced proliferation rates and increased ECM production to repair minor injuries (Mongkoldhumrongkul et al. 2016). Under pathological conditions in AVS, VICs differentiate into the osteoblast-like cells. The exact origin of osteoblastic VICs remains largely unknown. While some studies suggest that they originate from guiescent VICs and mesenchymal stem cells from EndMT, others propose they differentiate from progenitor VICs, and circulating progenitors (Ground et al. 2023).

#### 1.2. Aortic Valve Stenosis (AVS)

#### 1.2.1. Prevalence and history

AVS is now recognized as the third most common heart disease and the most common form of valvular disease in western countries characterized by the narrowing of the aortic valve due to calcification (Freeman and Otto 2005). AVS was first described by a french physician Lazare Rivière in 1663, who reported associated symptoms and anatomical

findings (Leopold 2012). He suggested that the disease might be linked to infective endocarditis. However, Möenkeberg later in 1904 characterized AVS as a passive degenerative process resulting from the deposition of serum calcium on the aortic valve (Leopold 2012). In recent years, AVS is considered as an active disease which is characterized by a long asymptomatic phase followed by a short symptomatic phase (Ross and Braunwald 1968). The disease begins with aortic sclerosis, which involves limited thickening and focal calcification of the valve. At this stage the hemodynamics remain unchanged (Otto et al. 1994). However, over time, increased fibrosis and calcification result in stenotic aortic valve with reduced flexibility and obstruction of the left ventricular outflow. Studies have shown an annual increase of 7mm Hg in transacrtic pressure gradient and a decrease of 0.1cm<sup>2</sup> per year in aortic valve area (AVA) in patients with AVS (Otto et al. 1989). About 1.8-1.9% of sclerotic valves progress to aortic stenosis each year. Although the prevalence of aortic sclerosis and aortic stenosis is low in the general population, it rises significantly after the age of 65 (Coffey et al. 2014). In the US, the prevalence of aortic stenosis was estimated at 0.4% in general population, 1.3% between 65 and 75 years, and 2.8% after 75 years, rising to 48% in those over 85 years old, and males accounting for 80% of the cases (lung and Vahanian 2012)

#### 1.2.2. Symptoms

The initial phase of AVS can last for decades without causing any symptoms. During this phase, the left ventricle adapts to the increasing obstruction of the left ventricular outflow by undergoing hypertrophy and remodeling of the myocardium (Goody et al. 2020). As long as the aortic stenosis remains asymptomatic, intervention is usually not necessary. However, once symptoms develop, the replacement of the aortic valve becomes crucial (Ross and Braunwald 1968). Without valve intervention, the two-year survival rate is only 50%. Moreover, if the patient is over 70 years of age, the survival rates are even worse, with two- and three-year survival rates of 37% and 26%, respectively (Cowell et al. 2004).

Symptoms associated with severe AVS often include dyspnea, angina pectoris, syncope, and congestive heart failure (Cowell et al. 2004; Ljungberg 2018). Angina pectoris is prevalent in 35% of patients with severe AVS. In severe AVS, angina can develop due to reduced left ventricular outflow resulting from increased obstruction in the aortic valve. This obstruction triggers compensatory hypertrophic changes in the left ventricular myocardium, ultimately impairing systolic function. Additionally, the increased left ventricular hypertrophy can elevate myocardial oxygen demands, while simultaneously compressing intramural coronary arteries, leading to restricted blood flow within the coronary arteries. This further leads to the chest pain or angina pectoris (Cowell et al. 2004; Ljungberg 2018). During exercise, peripheral resistance decreases, leading to a decreased cardiac afterload. However, the left ventricle may face challenges in increasing cardiac output due to the high resistance of the aortic valve. This can potentially lead to syncope due to hypotension or reduced coronary blood flow (Da Silva and Brugada 2022). The third symptom of AVS is left ventricular failure. This ventricular failure is likely caused by impaired left ventricular function due to prolonged myocardial hypertrophy and

persistent pressure overload which lead to the destruction of cardiomyocytes (CM) and thereby a left ventricular dysfunction (Cowell et al. 2004; Ljungberg 2018).

#### 1.2.3. Diagnosis

Echocardiography is the standard diagnostic tool for AVS. It is safe, widely available, and cost-effective. It is highly valuable tool for assessing the etiology, level of obstruction, valve calcification, leaflet motion, aortic root anatomy, left ventricular function, wall thickness, and other hemodynamic consequences (Otto 2006). Concurrent valve pathologies like aortic regurgitation, and mitral stenosis and regurgitation should also be evaluated (Stewart et al. 1997). Three parameters are commonly used to classify AVS including peak transvalvular velocity (Vmax), mean pressure gradient (Pmean) and aortic valve area (AVA) (Rana 2022). AVA is a valuable index for the clinical management of AVS and ranged from 3.0 to 4.0cm² in healthy aortic valve. As AVS develops, the AVA decreases and transvalvular pressure gradient increases, leading to the decrease of blood flow from the left ventricle into the aorta. The AVA is measured using Gorlin formula (Rana 2022):

### AVA (cm²) = Cardiac output/ Heart rate × Systolic ejection period × 44.3 × $\sqrt{\Delta P} \ (mmHG)$

AVA= Aortic valve area ΔP = mean gradient

AVA can be calculated using data from cardiac catheterization or Doppler echocardiography. Cardiac catheterization considers actual stroke volume, accounting for flow changes affecting the gradient (Baumgartner 2006). Doppler echocardiography estimates AVA by dividing flow in LVOT by transvalvular velocity. However, inaccuracies may occur due to imprecise measurements of LVOT (Baumgartner 2006). In severe stenosis with normal cardiac output, the mean transvalvular pressure gradient is usually over 40mm Hg. However, in low-flow/low-gradient AVS with left ventricular dysfunction, stress echocardiography using dobutamine can help to assess the severity. Dobutamine stimulates β1-adrenergic receptors in heart, increasing heart rate and contractility. It is used in stress echocardiography to assess cardiac function by mimicking the effects of exercise. An increase in valve area and minimal change in gradient during dobutamine stress suggests moderate stenosis, while a fixed valve area with increased gradient indicates severe AVS, preferable for surgery (Rana 2022).

Despite the pivotal role of echocardiography in the diagnosis of AVS, evidence showed that the hemodynamic change during AVS is relevant to the population body size. Therefore, Indexing AVA by body surface area (BSA) can be the solution to decrease the inconsistency in assessment of AVS severity caused by differences in body size and gain a better predictive accuracy (Jander et al. 2014). Therefore, cut-off for defining the severity is <1 for AVA and <0.6 for AVA index (Table 1). Different hemodynamic

classifications of AVS from mild to severe based on peak velocity, mean gradient, AVA and AVA index are shown in Table 1.

Table 1. Grading of AVS (Rana 2022)

Calcific Aortic Valve Stenosis	Peak velocity (m/s)	Mean gradient (mm Hg)	AVA (cm²)	AVA index (cm²/M²)
Mild	2.6-2.9	< 20	> 1.5	> 0.85
Moderate	3.0-4.0	20-40	1.0-1.5	> 0.6 to 0.85
Severe	≥ 4.0	≥ 40	<1.0	≤ 0.6

#### 1.2.4. Treatment

Surgical aortic valve replacement (SAVR) has been the main treatment for a long time and remains the preferred option for certain patients. It involves replacing the aortic valve with either a mechanical or biological prosthesis (Gleason et al. 2018).

Mechanical valves are recommended for patients under 65 years old without contraindications to anticoagulation. These valves offer excellent durability and a low risk of complications. However, they require lifelong anticoagulation to prevent valve dysfunction and embolisms and face some lifestyle restrictions. Bioprosthetic valves are derived from bovine pericardium, porcine pericardium, and porcine arterial valves and preferred for elderly patients. They do not require anticoagulation but have a limited lifespan, and reoperation is potentially necessary (Gleason et al. 2018).

In recent years, transcatheter aortic valve implantation (TAVI) or replacement (TAVR) has emerged as an alternative treatment for high surgical risk patients, becoming the standard approach for some severe symptomatic AVS cases. TAVI involves implanting an aortic valve prosthesis through less invasive procedures. Large randomized controlled trials have shown that TAVI is as effective as SAVR, leading to its widespread utilization (Gleason et al. 2018). TAVI implantation is performed by inserting a small catheter with a guide wire through various vessels, such as transfemoral arterial, subclavian, transcarotid, transaortic, transaxillary, and transapical, depending on the patient's health and the condition of their blood vessels. The guide wire has a balloon at its tip, which inflates to push the valve leaflets aside upon reaching the aortic valve. Afterwards, catheter is removed and the bioprosthetic aortic valve surrounded by the stent is placed in the aortic valve opening (Ferrari and Segesser 2010).

#### 1.2.5. Pathophysiological mechanisms of AVS

AVS is an age-related valvular degenerative disease characterized by multi-step molecular mechanisms involving endothelial dysfunction/injury, lipid accumulation, sterile inflammation, and excessive production, degradation, and re-deposition of the valve

ECM, ultimately leading to irreversible calcification of aortic valve leaflets (Figure 3) (Kostyunin et al. 2019).

Endothelial integrity is crucial for valve homeostasis, and laminar flow plays crucial role in maintaining endothelial homeostasis by enhancing nitric oxide (NO) signaling and suppressing the expression of adhesion molecules (Mohler 2004). Under pathological conditions, disrupted blood flow and increased turbulent flow on inflow surfaces promote endothelial dysfunction and injury (Atkins and Sucosky 2014). Consequently, VECs lose their protective and regulatory functions, leading to disrupted adhesions, macrophage infiltration, lipid or calcium deposits, and the appearance of fibrotic areas (Mohler 2004). Other risk factors such as dyslipidemia and diabetes mellitus are associated with an increased risk and progression of AVS, likely due to pathological activation of VECs and the increase of proliferation (Kostyunin et al. 2019).

Lipid accumulation plays a significant role in development of AVS (Figure 3). Lipid deposition is facilitated by interactions between positively charged amino acids on lipoproteins and negatively charged glycosaminoglycans within proteoglycans (Osman et al. 2013). Oxidized LDL (oxLDL) and oxidized phospholipids (oxPLs) contribute to inflammation and promote a pro-osteogenic environment. Lipoprotein-associated phospholipase A2 (Lp-PLA2) and autotoxin (ATX) generate bioactive lipids that further enhance inflammation and osteogenic differentiation (Figure 3) (Yeang and Wilkinson 2016). Immune cell infiltration including macrophages, T cells, and mast cells are other inducers of AVS. These immune cells are attracted to VECs through monocyte chemoattractant protein-1 (MCP-1), vascular cell adhesion molecule-1 (VCAM-1) and intercellular adhesion molecule 1 (ICAM1) released upon exposure to oxLDL. Macrophages differentiate from infiltrating monocytes and form foam cells, contributing to inflammation and fibrosis through the release of pro-inflammatory cytokines (Rao et al. 2007). Tumor necrosis factor- $\alpha$  (TNF- $\alpha$ ) is particularly important in AVS and induces a cascade of inflammatory responses, promoting osteogenic differentiation and mineralization. Other cytokines, such as IL (interleukin)-1β, IL-6, IL-18, and IL-32, also play roles in inflammation and matrix remodeling. Transforming growth factor-β (TGF-β) stimulates fibrosis and calcification, while ECM proteins like tenascin C and osteopontin contribute to immune cell migration and ECM remodeling (Figure 3) (Rao et al. 2007). Fibrosis leads to thickening of the leaflets and remodeling of the ECM in the aortic valve, impairing valve mobility (Figure 3). In an aortic valve, collagen fibers are organized and abundant throughout the ECM. However, in AVS collagen accumulation increases significantly, resulting in denser and disorganized fibers (Schoen 2008). Fibrosis and proteolysis are two opposing processes that contribute to ECM remodeling. Fibrosis involves excessive accumulation of disorganized fibrous tissue, while proteolysis which mainly occurs by matrix-degrading enzymes such as matrix metalloproteinase (MMPs) and cathepsins in aortic valve promotes active degradation of the matrix. An imbalance in these processes can contribute to the formation of chaotic fibrotic cores and sporadic cavities (Schoen 2008). MMPs are upregulated in AVS, while tissue inhibitors of MMPs remain unchanged (Kaden et al. 2005). Elastin-degrading cathepsins and their inhibitor

cystatin C are increased in affected valves. However, the increased expression level of cystatin C cannot fully inhibit the elevated cathepsin activity leading to the fragmentation of elastin fibers and increased valve stiffness (Helske et al. 2006). Inflammation induces activation and differentiation of VICs into myofibroblasts, which exhibit characteristics of both fibroblasts and smooth muscle cells (SMCs), and play a pivotal role in ECM remodeling (Kostyunin et al. 2019; Schoen 2008).

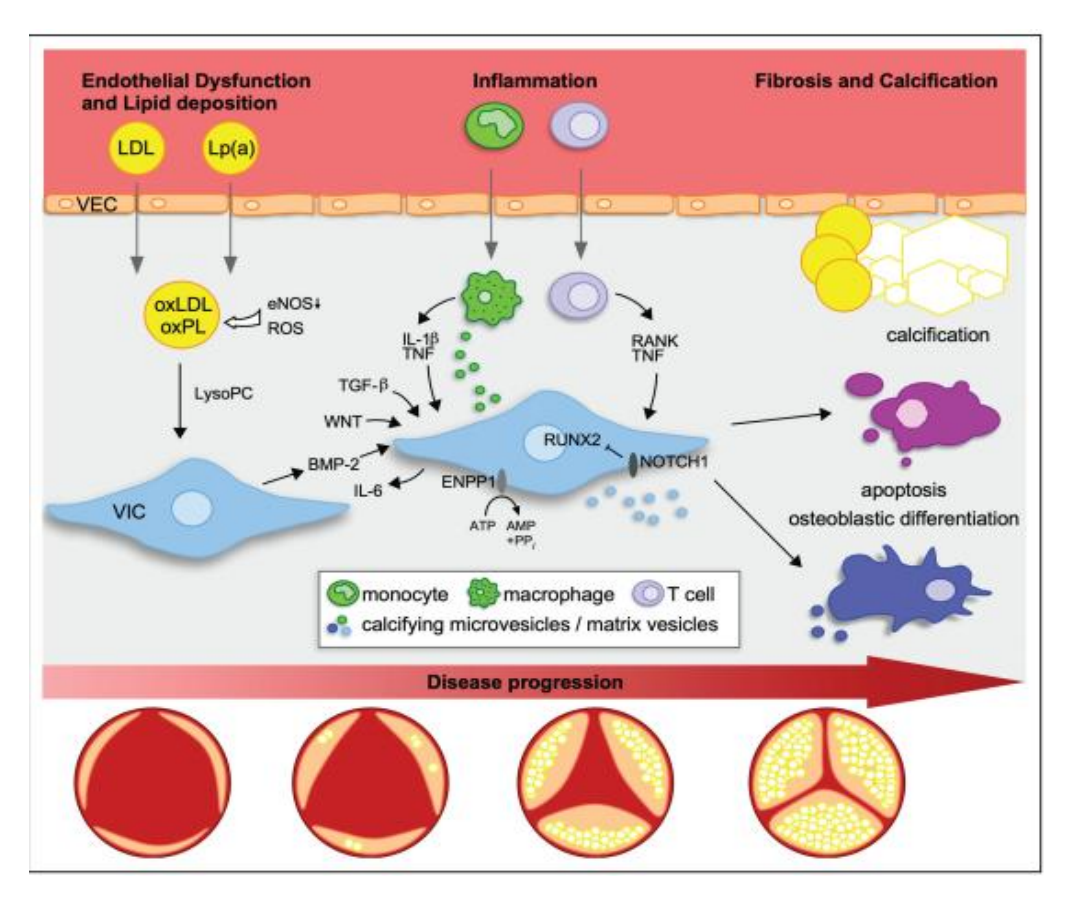


Figure 3. Pathophysiology and progression of aortic valve stenosis (AVS). Calcification is an active process, initiated by endothelial dysfunction/activation followed by accumulation of lipid and/or by inflammation and resulting in mineralization (Picture taken from Goody et al.) (Goody et al. 2020).

#### 1.2.5.1. Endothelial to mesenchymal transition (EndMT)

In AVS, oscillatory flow and inflammatory stimuli can promote EndMT (Figure 4) (Goody et al. 2020). During EndMT, VECs differentiate into the myofibroblast-like VICs and further into the osteoblast-like VICs, promoting fibrosis and calcification, respectively (Goody et al. 2020). In this transition, activated VECs progressively lose cell-cell contact, increase cellular invasion and acquire mesenchymal cell markers such as vimentin, ACTA2, N-cadherin, calponin, fibroblast-specific protein-1 (FSP-1), fibronectin, collagen types I and

III, and MMP-2/9, while also decreasing the expression of endothelial markers such as PECAM/CD31, vWF, VE-cadherin, and eNOS (Ma et al. 2020). Besides, it has been shown that several transcription factors such as SNAI1 and 2 (Snail/Slug), Zinc Finger E-Box Binding Homeobox (ZEB)1, and ZEB2 mediate EndMT in AVS via controlling the expression levels of EndMT markers (Figure 4) (Ma et al. 2020). Proliferative, migratory, secretory, productive ECM synthesis and above all, pro-inflammatory capacities are hallmarks of EndMT (Goody et al. 2020). The co-expression of CD31, ACTA2 and osteocalcin, as a calcific marker, in human AVS explants indicate the potential role for EndMT in calcification (Figure 4) (Hjortnaes et al. 2015). *In vitro* studies revealed that inflammatory cytokines including TNF- $\alpha$ , IL-6 and TGF- $\beta$  contribute to the EndMT process. Specifically, TGF- $\beta$  inhibits the expression of CD31 and decreases the expression of VE-Cadherin which results in the loss of endothelial barrier via Snail/Slug. TNF- $\alpha$  inhibits eNOS and CD31 expression and promotes the expression of ACTA2 (Figure 4) (Goody et al. 2020).

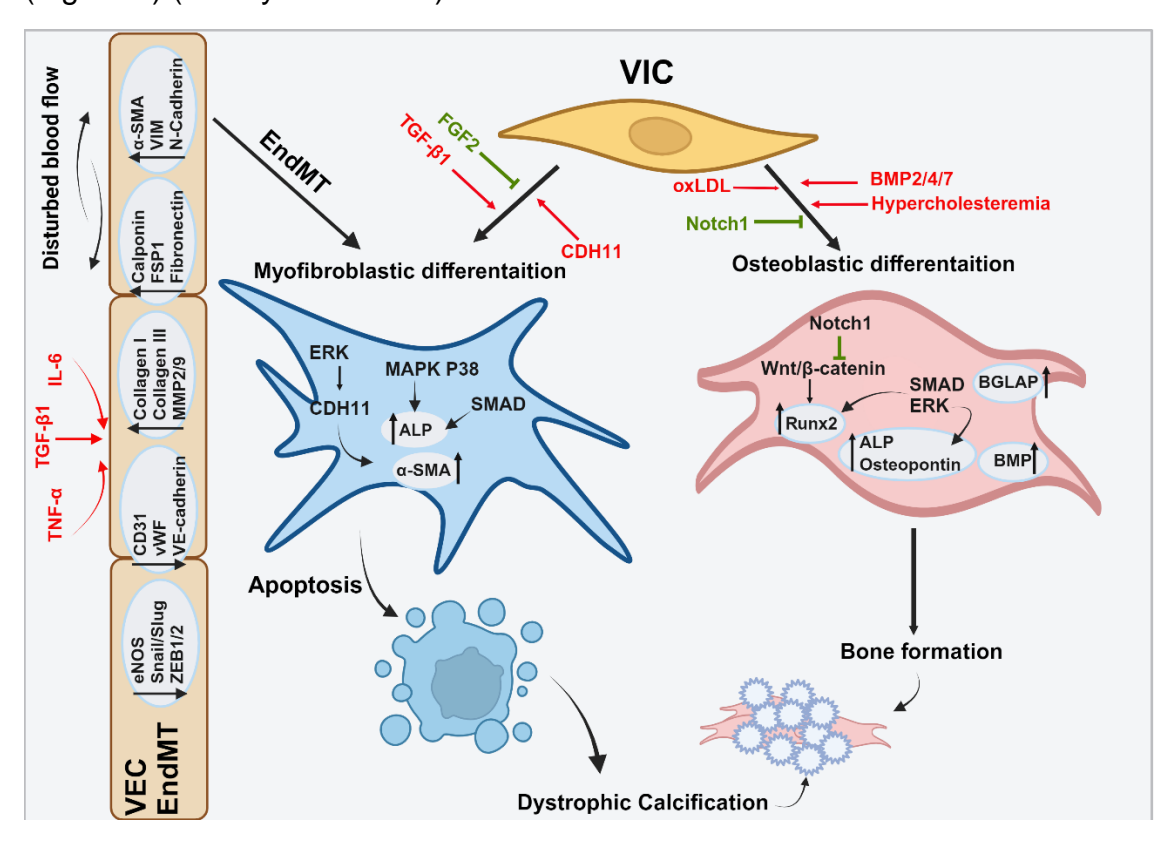


Figure 4. Mechanisms of EndMT and Calcification in AVS.

EndMT is triggered by disturbed blood flow and proinflammatory cytokines such as TGF- $\beta$ 1, TNF- $\alpha$  and IL-6. Under EndMT, VECs differentiate into myofibroblast-like VICs. VICs undergo myofibroblastic differentiation and osteoblastic differentiation leading to dystrophic calcification and biomineralization, respectively (Picture designed using BioRender).

#### 1.2.5.2. Calcification in AVS

Under pathological conditions in AVS, VICs differentiate into either myofibroblast or osteoblast-like cells. Progressive calcification of valves in AVS occurs through two main mechanisms: dystrophic calcification and biomineralization (Figure 4).

Dystrophic calcification involves passive deposition of hydroxyapatite in degraded ECM. In this process, myofibroblastic differentiation of VICs which can be induced by TGF-β1 and inhibited by fibroblast growth factor (FGF) 2 plays a key role. TGF-β1 enhances nodule formation and increased alkaline phosphatase (ALP) activity through two primary pathways: canonical pathway via small mothers against decapentaplegic (SMADs) or non-canonical pathway involving mitogen-activated protein kinase (MAPK) and its relevant pathways such as p38 signaling pathway and extracellular signal-regulated kinase1/2 (ERK1/2). Activation of ERK1/2 by TGF-β1 enhances the expression of cadherin-11 (CDH11) and its binding to ACTA2 (Figure 4) (Rutkovskiy et al. 2017). Myofibroblastic VICs undergo apoptosis leading to the formation of hydroxyapatite resulted from the binding of Ca²+ and phosphate ions in apoptotic bodies. Hydroxyapatite crystals interact with ECM and further function as nucleation sites or scaffolds for more deposition of hydroxyapatite crystals and mediate diffuse/dystrophic calcification (Figure 4) (Simionescu et al. 2003). Microscopic calcified nodules are found near areas of inflammation and LDL deposition, suggesting a potential link (Laird et al. 2006).

Biomineralization, on the other hand, is resulted from osteogenic differentiation of VICs secreting extracellular vesicles (EVs) which are rich in calcium and ectonucleotidase, producing inorganic phosphate ions and form calcium-phosphate crystals. Crystals grow in EVs, eventually causing the vesicles to rupture and deposit within ECM (Laird et al. 2006). The progression of calcification is influenced by factors such as decreased levels of fetuin-A, an inhibitor of ectopic calcification, and increased serum calcium and phosphate levels. Concurrent dystrophic calcification and biomineralization can result in the formation of massive mineral deposits in ECM, characterized by polymorphic shapes and complex mineral compositions. (Figure 4) (Di Minno et al. 2017). Presumably, myofibroblast can also be differentiated into osteoblastic VICs; however, the existing evidence is rather controversial (Simionescu et al. 2003). Osteogenic differentiation of VICs is accompanied by an increase of osteogenic markers including runt-related transcription factor 2 (RUNX2), bone morphogenetic protein (BMP), ALP, osteocalcin or bone gammacarboxyglutamate protein (BGLAP), and osteopontin (Figure 4) (Kostyunin et al. 2019). Differentiation of VICs into osteoblasts involves several signaling pathways and is largely orchestrated by RUNX2. Wingless and Int-1 (Wnt)/β-catenin is one of the active signaling pathways which directly stimulates RUNX2 expression (Figure 4) (Kostyunin et al. 2019). It has been shown that oxidized LDL and hypercholesterolemia induce the secretion of WNT3 from VECs into the inner parts of valve followed by binding to the LDL receptor-related protein 5 (LRP5) leading to the accumulation and nuclear translocation of β-catenin and promotes the expression of RUNX2 and proliferation of VICs (Kostyunin et al. 2019). Notch signaling pathway is a potent repressor of osteogenic differentiation through the inhibition of β-catenin nuclear translocation, and inhibition of NOTCH1 enhances aortic valve calcification (Figure 4) (Hutcheson et al. 2013). In addition, compelling studies show that BMP2/4/7 induces osteogenic differentiation of VICs through interaction with ERK1/2 and SMADs by significantly increasing ALP, RUNX2, and osteopontin (Figure 4) (Nishimura et al. 2012).

## 1.3. Extracellular Vesicles (EVs) as Regulators of Cardiovascular Disease

#### 1.3.1. Biogenesis of EVs

Extracellular vesicles (EVs) are released by cells into the extracellular space and contain different type of cargoes. They play a crucial role in protecting their cargo from extracellular nucleases and proteinase and facilitating their transfer to the distant recipient cells, enabling efficient intercellular communication (Yáñez-Mó et al. 2015). The cargo composition of EVs is determined by their cellular origin and vary based on environmental factors and the physiological or pathophysiological state of parent cells. Therefore, cells under different conditions release distinct EVs with unique molecular signatures, resulting in significant heterogeneity among EV populations (van Niel et al. 2018). EVs are categorized based on their size, content, and biogenesis into three different subtypes: apoptotic bodies, large EVs (IEVs), also known as ectosomes, microvesicles or shedding vesicles, and small EVs (sEVs), also known as exosomes. Importantly, the current methods for EV isolation yield complex mixtures and do not allow precise purification of each subtype. While some proteins have been assigned as specific markers for each subpopulation, more specific markers for each subtype are needed (Choi et al. 2013: Kalra et al. 2013). Nevertheless, there are distinct characteristics associated with each subpopulation (Figure 5):

- 1. Apoptotic Bodies: These are the largest EVs (>1 μm in diameter) and originate from apoptotic cells. Apoptotic bodies contain fragmented DNA and externalized phosphatidylserine as well as cellular cytokines and miRNAs (Mittelbrunn and Sánchez-Madrid 2012).
- 2. IEVs: Initially defined by their intermediate size (100 nm to 1 μm), and mainly characterized as vesicles directly shed from the plasma membrane. Their lipid composition resembles that of the plasma membrane, and they carry DNA, proteins, mRNAs, small RNAs such as miRNAs and long-non coding RNAs (IncRNAs), which can be taken up by neighboring cells (Mittelbrunn and Sánchez-Madrid 2012).
- 3. sEVs: The smallest EVs (30-100 nm) are generated from early endosome and later from intraluminal vesicles of multivesicular bodies (MVBs). These MVBs are fused to the plasma membrane and release their contents into the extracellular space (Simons and Raposo 2009). sEVs are enriched for endosomal sorting complex required for transport (ESCRT) machinery, tetraspanins (CD9, CD63, CD81, CD82), heat-shock proteins, ceramide, cholesterol and sphingolipids. Similar to

IEVs, sEVs carry DNAs, proteins, and RNAs and can be taken up by recipient cells (Mittelbrunn and Sánchez-Madrid 2012).

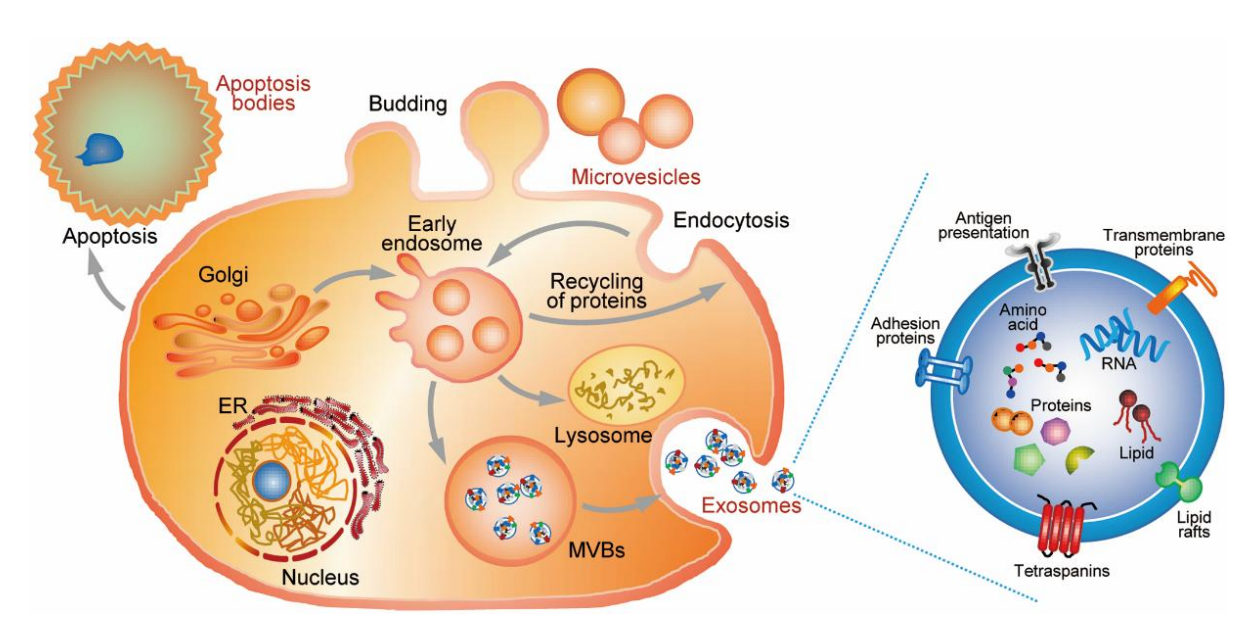


Figure 5. Biogenesis of extracellular vesicles (EVs).

EVs are typically categorized into apoptotic bodies, large EVs (microvesicles) and small EVs (exosomes). Large EVs/ microvesicles are simply embedded from the cell membrane and small EVs/ exosomes are generated from multivesicular bodies (MVBs) which are formed during endosomal maturation (Picture adapted from Xue et.al) (Xue and Yam 2022).

EVs employ different mechanisms to transfer their cargoes into the recipient cells; by binding directly to cell-surface receptors in recipient cells or fusing their membrane with the target cell membrane, facilitated by phosphatidylserine (PS) on the EV surface, or by endocytosis, pinocytosis, or phagocytosis (Jansen et al. 2017a).

#### 1.3.2. Role of EVs in AVS and other cardiovascular diseases

EVs play crucial roles in various physiological and pathological processes, including blood coagulation, inflammation, cellular communication, tumorigenesis, and cardiovascular biology. Initially EVs were thought of as a way that cells use to dispose cellular waste; lately, however, EVs have been found to play essential roles in both cardiac repair and disease progression. They function either locally or systematically via the bloodstream. Once EVs are released into the bloodstream, they interact with cardiac cells, such as CMs, ECs, fibroblasts, and immune cells, influencing either homeostasis or disease progression by transferring micro-molecules to recipient cells (Gan et al. 2020; Liu et al. 2019).

ECs release EVs in response to endothelial injury. Accumulation of EVs in atherosclerotic lesions is associated with key biological processes including inflammation, proliferation, thrombosis, calcification, and vasoactive responses, potentially driving the initiation and progression of cardiovascular diseases (Boulanger et al. 2006). The increased level of

IEVs released from leukocytes has been reported in asymptomatic patients with subclinical atherosclerosis (Chironi et al. 2006). Atherosclerotic plaques contain a significant number of IEVs, primarily derived from lymphocyte and monocyte-macrophage cells, associated with unstable plaques and increased risk of atherothrombosis (Rautou et al. 2011). Furthermore, increased plasma levels of endothelial cell-derived IEVs has been identified as a novel biomarker of endothelial dysfunction associated with carotid artery disease and high-risk lesions in cardiovascular disease (Rautou et al. 2011; Bernal-Mizrachi et al. 2004). In coronary artery disease (CAD), coronary calcification, and acute coronary syndrome (ACS), both platelet-derived IEVs and endothelial cell-derived IEVs are elevated (Mallat et al. 2000; Simak et al. 2006; Jayachandran et al. 2008).

In diseased heart valves, cellular crosstalk via EVs including VECs, platelets, leukocytes, and VICs play critical roles to either promote or prevent endothelial dysfunction, valvular inflammation, and subsequent calcification, which is primarily dependent on EV content (Jansen et al. 2017b). Under physiological conditions, EVs derived from parent cells contain high levels of biological contents that inhibit calcification, including fetuin-A and matrix Gla protein, as well as anti-osteogenic microRNAs (miRNA-30, miRNA-125-b, miRNA-143, miRNA-145, and miRNA-155) (Jansen et al. 2017b). Calcifying EVs released by VICs are enriched with minerals and calcify within the extracellular matrix of the valve, contributing to microcalcifications and macrocalcifications (Krohn et al. 2016). Several factors such as annexin, alkaline phosphatase, extracellular calcium and phosphate levels influence the nucleation and growth of calcifying EVs, ultimately leading to massive calcification and valve dysfunction (Krohn et al. 2016). The release of calcium-containing EVs may show cellular mechanisms to prevent intracellular calcium overload and subsequent cell injury. In severe degenerative AVS, there is a significant increase in circulating IEVs originating from endothelial, platelet, and leukocyte sources compared to controls (Diehl et al. 2008). Platelet-derived IEVs can bind to the circulating monocytes, and form conjugates expressing CD11bb, facilitating monocyte adhesion and transmigration through the endothelial cell layer (Klinkner et al. 2006). The activation of leukocytes and the release of leukocyte-derived IEVs contribute to a pro-inflammatory state and thereby release of endothelial-derived IEVs, creating a vicious circle that mediates the progression of valve endocardium dysfunction (Klinkner et al. 2006). These findings are aligned with microscopic observations indicating that dense inflammatory infiltrates primarily composed of macrophages in calcific valves (Coté et al. 2013). Interestingly, co-culture experiments of VECs and VICs have shown that VICs inhibit the osteogenic differentiation of VECs via EndMT, while VECs decrease VIC activation, highlighting the importance of intra-valvular communication in regulating cellular functions and phenotypes related to a rtic valve calcification (Coté et al. 2013).

#### 1.4. MicroRNAs and Post-transcriptional Regulation in AVS

#### 1.4.1. miRNA biogenesis and molecular mechanism

miRNAs constitute a class of non-coding RNAs (ncRNAs) with the length of approximately 21-24 nucleotides and play a crucial role in gene expression in a wide range of organisms,

including animals, plants, and unicellular eukaryotes (Economou et al. 2015). miRNAs interact with mRNAs by binding to specific sites within the mRNA molecules, leading to translational repression or mRNA degradation (Economou et al. 2015). miRNAs play a significant role in cell fate determination, cell death, cancer development, animal development, cell differentiation, apoptosis, and physiological homeostasis (Bartel 2004). While most miRNAs are located within cells, circulating miRNAs or extracellular miRNAs found in biological fluids and can be transported to the target cells via EVs (Sohel 2016).

In mammals, miRNA biogenesis involves multiple steps occurring in the nucleus and cytoplasm (Figure 6). In the nucleus, primary(pri)-miRNAs, which are transcribed by RNA polymerase II/III, fold into hairpin structures and undergo several modifications. The microprocessor complex, including DGCR8--Drosha, recognizes and cleaves pri-miRNAs and generates a ~60-70bp stem-loop known as precursor(pre)-miRNAs which is exported to the cytoplasm by exportin 5 (Figure 6). In the cytoplasm, Dicer processes pre-miRNAs into ~19-25bp mature miRNA duplexes. One strand of the mature miRNA is retained in Argonaute proteins to form the functional RNA-induced silencing complex (RISC), while the other strand known as a passenger strand is degraded. RISC complex degrades mRNA through binding to the 3'UTR of mRNA or represses the protein translation (Figure 6) (Filipowicz et al. 2008).

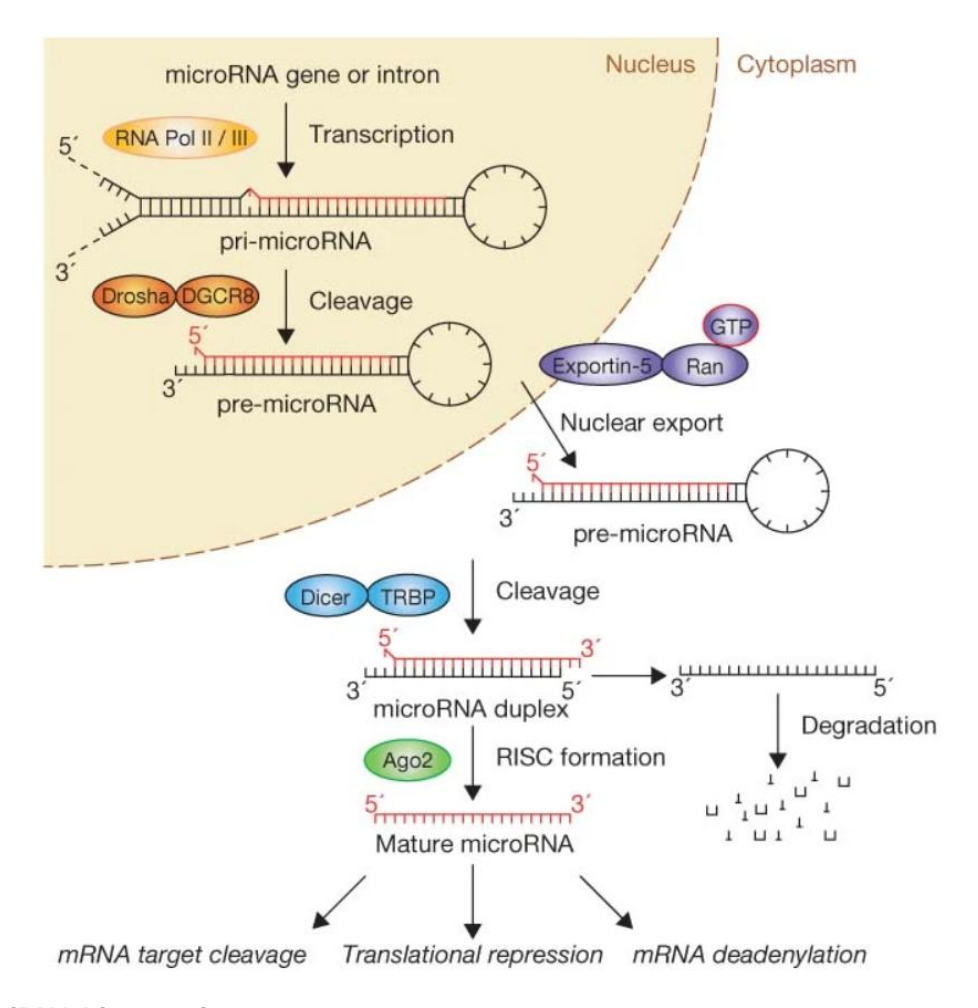


Figure 6. miRNA biogenesis.

pri-miRNA are transcribed by RNA polymerase II/III and cleaved by Drosha-DGCR8 in nucleus to generate pre-miRNA which is exported by Exportin 5 into the cytoplasm where the loop structure is cleaved off by Dicer to generate duplex miRNA. One strand is degraded and the another one form RISC together with Ago2 to silence mRNA through mRNA target cleavage, translation repression or mRNA deadenylation (picture adapted from Winter et.al) (Winter et al. 2009).

miRNAs regulate a wide range of biological processes through two main mechanisms: mRNA degradation and translation inhibition. mRNA degradation occurs through perfect or imperfect binding of miRNA to mRNAs. In mammals, miRNA in RISC binds imperfectly to the 3'UTR of mRNA due to the central mismatches in the 5' seed region (nucleotides 2–8) of guide miRNA in RISC and interacts with GW182 family proteins, recruiting CCR4-NOT complex to promote deadenylation and remove of the poly (A) mRNA resulting in mRNA degradation (Mathonnet et al. 2007). However, in plants miRNAs perfectly match the mRNA target and the miRNA guide strand mediates endonucleolytic cleavage of the mRNA between nucleotides 10 and 11 of the miRNA, leading to mRNA degradation (Bartel 2004). miRNAs inhibit protein translation at both the initiation and elongation stages. At the initiation stage, miRNAs interfere with the elF4F complex, which recognizes the m7G cap structure at the 5' end of mRNA, thereby inhibiting the assembly of the 80S ribosomal complex and subsequent translation initiation. Moreover, miRNAs can

modulate the activity of poly(A)-binding protein (PABP), which binds to the 3'UTR mRNA and influences translation efficiency (Filipowicz et al. 2008). miRNAs can also impact ribosome elongation during the post-initiation stage, causing ribosomes to prematurely dissociate from the 3'UTR mRNA, a phenomenon known as ribosome drop-off. These mechanisms collectively contribute to the repression or inhibition of protein translation without affecting mRNA stability (Filipowicz et al. 2008). The degree of translational repression depends on factors such as the number and precise positioning of miRNAs within the 3'UTR of the target mRNA (Fabian et al. 2010).

#### 1.4.2. Role of miRNAs in AVS and other cardiovascular disease

Recent studies have highlighted the involvement of miRNAs in various biological process and their potential applications in diagnostics and therapeutics of cardiovascular diseases such as atherosclerosis, coronary artery disease, and myocardial infarction (MI) (Economou et al. 2015). Studies have implicated the crucial function of specific miRNAs in heart development and their dysregulation in cardiomyopathies (Zhao et al. 2007; Chen et al. 2008). miRNAs have been detected not only in cardiac tissue but also in the bloodstream, indicating their role in intercellular communication (Economou et al. 2015). Initial investigations revealed dysregulated miRNAs in plasma of patients with coronary artery diseases, which can serve as potential diagnostic biomarkers (Fichtlscherer et al. 2010).

In patients with bicuspid aortic valve, the expression of miRNA-26a, miRNA-30b, and miRNA-195 is significantly decreased compared to aortic insufficiency (AI). These miRNAs act by targeting ALP1, SMAD1, SMAD3, SMAD5, RUNX2, and BMP2, which play essential roles in preventing aortic calcification (Nigam 2010). miRNA-30b has been found as a regulator of calcification in aortic valves by inhibiting BMP2-induced osteogenic differentiation of VICs and apoptosis by directly targeting RUNX2, SMAD1, and CASP3 (Caspase-3) (Zhang et al. 2014). The downregulated expression of miRNA-141 in bicuspid valves compared to tricuspid valves has been associated with calcification by regulating BMP2 (Yanagawa et al. 2012). miRNA-148a-3p and miRNA-214 have been reported as shear sensitive miRNAs in AVS, correlated to inflammation and calcification (Nader et al. 2020). Furthermore, increased expression of miRNA-143 has been observed in AVS directly targeting the matrix gla protein (MGP) involved in osteogenesis (Nader et al. 2020). In addition, dysregulated miRNAs involved in extracellular matrix regulation, such as miRNA-122-5p, miRNA-625-5p, miRNA-30e-5p, miRNA-21-5p, and miRNA-221-3p, have been identified in stenotic valves (Coffey et al. 2016). In bicuspid aortic valves, several miRNAs such as miRNA-26b-3p, miRNA-139-3p, miRNA-197-3p, miRNA-328-3p, miRNA-520g-3p, miRNA-561-3p, miRNA-573, and miRNA-1180-3p have been shown to mediate differential response of endothelial cells to oxidative stress, DNA damage, and apoptosis (Poggio et al. 2019).

In summary, miRNAs have significant regulatory roles in the development and progression of aortic valve disease, particularly in aortic valve calcification. Their dysregulation affects various molecular pathways involved in inflammation, osteogenesis, extracellular matrix remodeling, and endothelial dysfunction. Understanding the specific

roles of miRNAs in aortic valve disease can provide valuable insights into the pathogenesis of the condition and potentially lead to the development of novel diagnostic and therapeutic strategies.

#### 1.5. Aim of PhD Thesis

AVS is the most common type of valvular disease; despite advances in research, many aspects of its pathogenesis are still poorly understood. Recent evidence suggests that EVs may play a crucial role in cardiovascular diseases, particularly in AVS. However, the contribution of EV-derived miRNAs in AVS warrants further investigation. This study aims to address this gap in knowledge by investigating the active involvement of EVs and EV-associated miRNAs in the regulation of AVS via two main mechanisms including EndMT and calcification. The specific objectives are as follows:

- 1. Profiling EV-derived miRNAs in patients with AVS to identify potential candidates for further analysis.
- 2. Validating the identified EV-derived miRNAs to confirm their presence and establish their association with AVS.
- 3. Assessing the functional role of EV-derived miRNAs in EndMT model to understand their involvement in the pathological mechanisms of AVS.
- 4. Examining the functional role of EV-derived miRNAs in calcification model to elucidate their role in calcification processes observed in AVS.

By addressing these aims, the purpose of this study is to enhance our understanding of the role of EVs and EV-associated miRNAs in AVS, which could lead to novel therapeutic approaches for this prevalent valvular disease.

#### 2. Material and Methods

#### 2.1. Obtaining Human Aortic Valve Tissue

Human aortic valve samples for sequencing were obtained from patients undergoing AV replacement surgery for AVS and AI at the Heart Center Bonn, University Hospital Bonn, Germany. The study protocol was approved by the Ethics Committee of the University Hospital Bonn (approval number AZ 078/17), and informed consent was obtained from all patients.

Calcific aortic valve samples for primary VIC isolation were obtained from AV replacement surgeries for severe aortic valve stenosis at Brigham and Women's Hospital, Harvard Medical School, United States. The study protocol was approved by the Ethics Committee and informed consent was obtained from all patients.

The study was conducted in accordance with the ethical standards of Helsinki Declaration and the International Conference on Harmonization of Good Clinical Practice (Schmidt, Frewer 2007).

#### 2.2. Cell Culture Methods

#### 2.2.1. Materials in cell culture

- 2% Alizarin Red Stain, Life Line, CM-0058
- Alkaline Phosphatase Assay Kit, Abcam, ab83369
- Bambanker, GC LYMPHOTEC, 302-14681(CS-02-001)
- Bovine Serum Albumin (BSA), Fatty acid free, Sigma-Aldrich, A7030
- Cetylpyridinium Chloride Monohydrate, 40300072, bioWORLD
- Corning® Matrigel® Basement Membrane Matrix, LDEV-free, corning, 356234
- Collagenase Type II, Worthington-UK, LS004177
- Dexamethasone, Sigma-Aldrich, D4902
- DMEM (1x) Dulbecco's Modified Eagle Medium +4.5g/L D-glucose, +L-Glutamine, -Sodium Pyruvate, ThermoFisher Scientific, 11965
- Dimethylsulfoxide (DMSO), Carl Roth, A994.2
- EBM™-2 Endothelial Cell Growth Basal Medium-2, Lonza, CC-3156
- EGM™-2 MV Microvascular Endothelial SingleQuotsTM Kit, Lonza, CC-4147
- Exo-FBS HI, Exosome-depleted FBS Media Heat Inactivated, System Biosciences, Exo-FBSHI-250A-1
- Fetal bovine serum, Qualified, One Shot, Sigma-Aldrich, A3160802
- β–glycerol Phosphate, EMD Millipore, 3567s-506M
- Human recombinant TGF beta1, R&D Systems, 240-B-002
- Human Valvular Endothelial Cells (VECs), Lonza, 00225975
- L-ascorbic Acid, Sigma, A4S44
- L-Ascorbate Phosphate, Sigma, A8960
- Mitomycin C, Sigma-Aldrich, M4287M4287-2MG
- PBS PH7.4, Gibco, 10010023
- Paraformaldehyd (PFA), Roth, 0335.3
- PrestoBlue™ Cell Viability Reagent, Thermofisher, A13261

- PKH67 Green Fluorescent Cell Linker Kit for General Cell Membrane Labeling, Merck, PKH67GL
- Penicillin, Streptomycin (P/S), Biochrom AG, Berlin, A2213
- Recombinant Human BMP2 protein, Abcam, ab50099
- Recombinant Human IL-1β, Peprotech, 200-01B
- Recombinant Human TNF-alpha Protein, R&D System, 210-TA-020 / CF
- ReagentPack™ Subculture Reagents, Lonza, CC-5034
- Sodium Dihydrogen Phosphate, Sigma, 7558-80-7
- Sodium-L-ascorbate, Sigma-Aldrich, A4034
- Trypan Blue Solution, 0.4%, ThermoFischer Scientific, 15250-061
- Trypsin-EDTA (0.05 %), Gibco, 25300054

#### 2.2.2. Equipment in cell culture

- 100mm cell culture dish, Sarstedt, 83.1802.001
- 75cm<sup>2</sup> cell culture flask, Sarstedt, 83.3911
- 175cm<sup>2</sup> cell culture flask, Sarstedt, 83.3912.002
- Cell counting chamber, Invitrogen, C10283
- Culture-Insert 2 Well in μ-Dish 35 mm high, Lonza, 81176
- Cell scraper, Croning Falcon<sup>™</sup>, 353085
- Conical tubes15ml and 50ml, Sarstedt, 62.554.001, 62.548.004
- 0.22µm filter, VWR, 514-0061
- Cryogenic vials, Sarstedt, 72.379.992
- Eppendorf Centrifuge 5430, Eppendorf
- EnSpire™ multimode plate reader, PerkinElmer, USA
- Fluidic Unit, ibidi, 10903
- Hose clip, ibidi
- ibidi Pump System, ibidi, 10902
- Incubator, HERAcell® 150, Heraeus
- Laminar air flow, Herasafe<sup>™</sup>, Heraeus
- Microscope, LEICA DMIL, Leica Microsystems GmbH
- 0.5ml, 1.5ml, 2ml micro centrifuge tube, Sarstedt, 72,704,004, 72,690,001, 72,691
- 40µm Nylon mesh, Thermofischer, 22363547
- 6, 12 TPP plates, Techno Plastic Products, 92006, 92012
- Perfusion Set RED, 15 cm, ID 1.6 mm, Ibidi, 10962
- Pierce Protein Concentrator PES, 100k MWCO, Thermo Fischer, 88533
- PumpControl software, ibidi
- µ-Slide I Luer 0.4mm, ibidi, 80176
- Serological pipettes 5ml, 10ml, 25ml, Sarstedt, 86.1253.001, 86.1254.001,
- 86.1685.001)
- 6,12, 24, 96 well plates, Sarstedt, 86.1836.001, 83.3921.005, 83.3922, 83.3925.500

Table 2: Cell culture medium used for VIC experiments

VIC cell culture	Components
VIC culture medium	DMEM (+4.5g/L D-glucose,+L-Glutamine,- Sodium) supplemented with 10% fetal bovine serum (FBS) and 1% penicillin/streptomycin
Osteogenic medium (OM)	DMEM supplemented with 10% FBS, 10nmol/L dexamethasone, 10mmol/L β– glycerol phosphate, and 100μmol/L L- ascorbate phosphate
Pro-calcifying medium (PM)	DMEM with 5% FBS, 2 mmol/L sodium dihydrogen phosphate (NaH2PO4) and 50 µg/mL L-ascorbic acid

Table 3: Cell culture medium used for VEC experiments

VEC cell culture	Components
VEC culture medium	EBM™-2 Endothelial Cell Growth Basal Medium-2) supplemented with EGM™-2 MV Microvascular Endothelial SingleQuotsTM Kit
EndMT basic medium	EBM™-2 Endothelial Cell Growth Basal Medium-2 supplemented with BulletKit™ without VEGF, hydrocortisone, and GA-1000
EV experiments	EBM™-2 Endothelial Cell Growth Basal Medium-2) supplemented with EGM™-2 MV Microvascular Endothelial SingleQuotsTM Kit (without FBS) and 5% EV depleted FBS

#### 2.2.3. VIC isolation from human aortic valve

To isolate VICs from the aortic valve of patients with severe AVS, a sequential collagenase digestion approach was performed according to Goto et al.,2019 (Figure 7) (Goto et al. 2019). For this, explanted cusps were placed in 5ml of DMEM (Table 2) and immediately transported to the laboratory for cell isolation. After rinsing with sterile 1x phosphate buffered saline (PBS), the valve was cut into small pieces (1-2mm²). These pieces were then digested in a solution of 1mg/ml collagenase II in DMEM (Table 2) for 1h at 37°C with gentle agitation. The supernatant was discarded, and 1mg/ml fresh collagenase II solution was added. The digestion process continued with gentle agitation at 37°C for an additional 3h. The resulting cell suspension was filtered through a 40µm nylon mesh and centrifuged at 1,000 rpm for 5min. VICs were then seeded onto a T75 flask and cultured in the complete VIC culture medium (Table 2) (Figure 7).

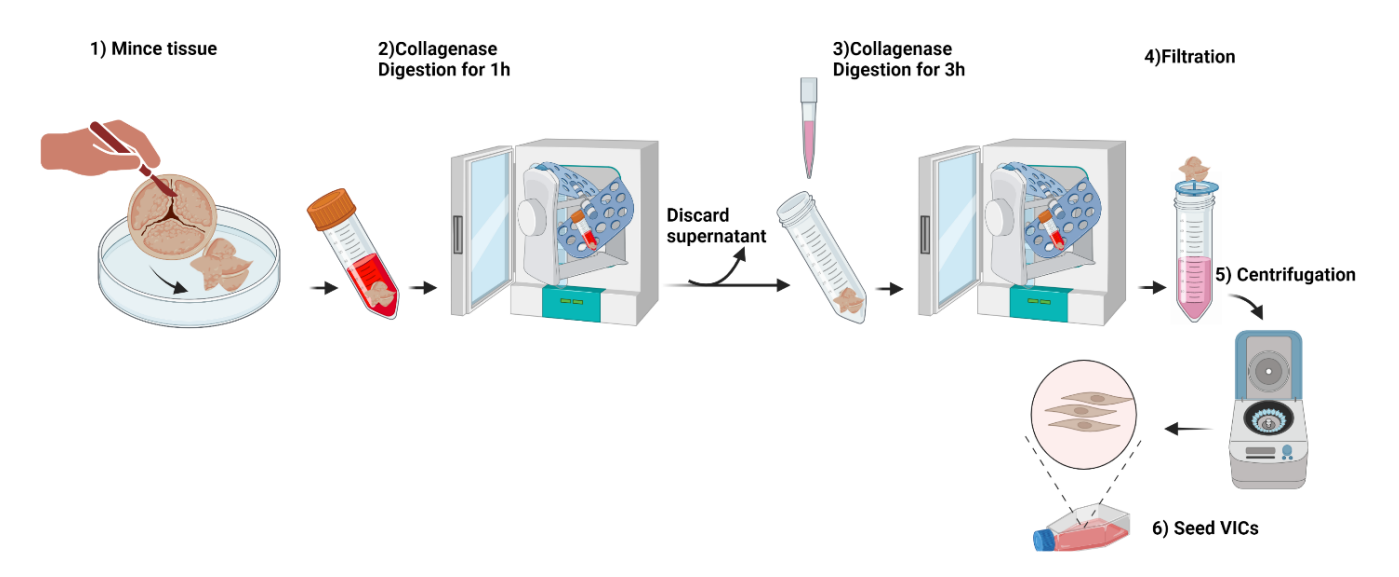


Figure 7. Schematic illustration of VIC isolation from calcific aortic valve.

VICs were isolated from calcific aortic valves after the surgery for aortic valve replacement. 1) The tissue was cut into small pieces 2) followed by 1h collagenase digestion in an incubator. 3) Supernatant was discarded. Subsequently, fresh collagenase was added to the remaining tissue, and it was incubated for 3h. 4) Cell suspension was filtered through a nylon mesh and 5) centrifuged. 6) VICs were plated in a T75 flask (Picture was designed with Biorender).

#### 2.2.4. Cell culture of commercial VICs and VECs

VICs and VECs were bought from Lonza (Switzerland) and cultured in VIC medium (Table 2) and endothelial cell medium (Table 3). Cells were maintained in a cell culture incubator at 37°C and 5% CO<sub>2</sub>. The medium was changed every two days to supply essential cell growth factors and supplements.

#### 2.2.5. VEC culture under the laminar flow

Ibidi pump system consisting of one fluidic unit with a mounted perfusion set, and  $\mu$ -slide was used to run pulsatile flow. This system provides unidirectional laminar flow running from one reservoir to the other one (Figure 8).

To culture VECs under the laminar flow, cells were seeded at a density of  $10^5$  cells/cm<sup>2</sup> on  $\mu$  slide and incubated at  $37^{\circ}$ C, and 5% CO<sub>2</sub> for 2h to ensure proper cell attachment and confluence. The ibidi pump system was installed based on manufacturer's instructions. Briefly, the perfusion set was connected to the fluidic unit. Each reservoir was filled with 6 ml medium (Table 3), and the pump was run to confirm the correct insertion of tubing. The flow rate was calibrated based on the manufacturer's instructions. The  $\mu$ -slide with seeded cells was connected to the perfusion set, and cells were cultured under the laminar flow for 24h (Figure 8), after which cells were harvested for RNA extraction.

Using the PumpControl software, the following parameters were utilized to create unidirectional pulsatile shear stress: 1) pressure: 40mbar 2) shear stress: 20 dyn/cm<sup>2</sup> 3)

flow rate: 23ml/min 4) shear rate: 3143 5) unidirectional switching time: 15s 6) oscillating switching time: 0.5s.

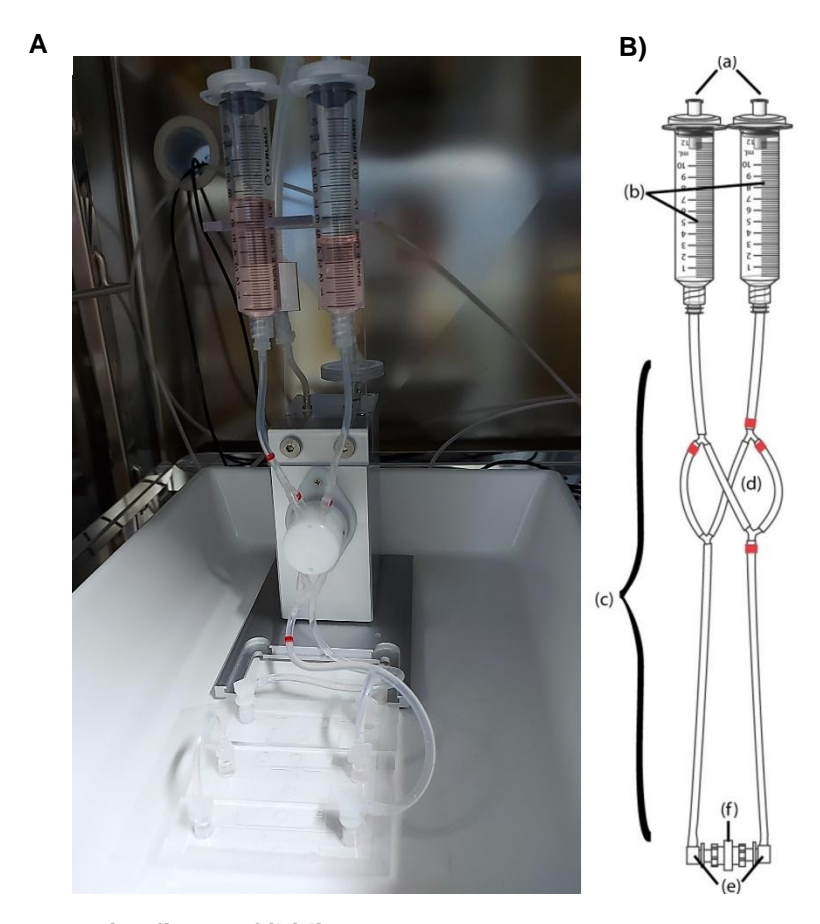


Figure 8. Representative figure of ibidi pump system.

A) ibidi pump system setup in an incubator for generating unidirectional flow B) Different parts of Perfusion Set: a) sterile air filters, b) syringe reservoir, c) tubing, d) branched tubes, e) luer adapters f) female luer coupler. (Picture B adapted from instruction manual of ibidi pump system).

#### 2.2.6. Trypsinization and cryo-preservation of VECs and VICs

Cells cultured at 80% confluency were passaged at a ratio of 1:3. For this, cells were washed once with PBS, harvested using ReagentPack™ Subculture Reagents from Lonza, and incubated at 37°C for 5 min. The cell suspension was subsequently resuspended in culture medium and centrifuged at 1,000 rpm for 10min. After centrifugation, cells could be either frozen and stored for a longer period of time or re-seeded for passaging. For cryopreservation, the cell pellet was re-suspended in growth medium containing 10% DMSO. Cryotubes were stored at -80°C at least for 1 day, and finally transferred to liquid nitrogen (-196°C) for long-term storage. All experiments were performed when cells reached 70% confluency, using cells at the fourth or fifth passage in 12-, 24-, or 48-well plates.

#### 2.2.7. Lentiviral transduction for immortalization and overexpression of miRNA

SV40 Large T antigen lentivirus was used to immortalize VECs. To generate immortalized VECs (I-VECs), cells were seeded in 600µl of endothelial cell medium (Table 3) and incubated at 37°C for 9h. Afterwards, cells were treated with the SV40 Large T antigen lentivirus at a concentration equivalent to 50ng/well. Next day, cell culture medium was filled up to 1 ml. Medium was changed every two days.

To overexpress miRNAs, third-generation lentiviral vectors (pRRLSIN) containing miRNA-150-5p, Let-7c-5p and miRNA-30b-5p was generated (section 2.5) and used. The same protocol was utilized to transduce VECs with the lentiviruses. The efficiency of transduction was assessed by tracking the green fluorescent protein (GFP) which was located in the downstream of CMV promotor and the expression levels of the miRNAs by qPCR.

#### 2.2.8. EndMT induction

To induce EndMT, VECs were plated on 12-well plates. TGF- $\beta$ 1, BMP2, IL-1 $\beta$  and TNF $\alpha$  were purchased and prepared based on manufacturer's instructions. After achieving confluency, cells were treated with the following concentrations of cytokines to induce EndMT: 10ng/ml TGF- $\beta$ 1, 50ng/ml BMP2, 10ng/ml IL-1 $\beta$  and 25ng/ml TNF $\alpha$  in VEC EndMT medium (Table 3). The culture medium was refreshed every two days, and EndMT was induced for a total period of 7 days.

Following the treatment period, total RNA was extracted from the cells for further experimental analysis and investigation of molecular changes associated with EndMT.

#### 2.2.9. Scratch assay to assess VEC migration

To assess the migratory capacity of VECs, cells were seeded on each side of Ibidi culture-insert 2 well at the density of 900 cells/ $\mu$ I in a total volume of 70 $\mu$ I (Figure 9). Next day, VECs were treated with 10 $\mu$ g/ml Mitomycin C to inhibit cell proliferation and incubated for 2h at 37 °C and 5% CO<sub>2</sub>. After incubation, the medium was discarded and replaced with fresh medium. The culture-insert was then gently removed creating cell-free scratch in the center of the well. The images of the scratch were captured at different time points of 0h, 6h and 12h. The extent of cell migration was quantified using image J software (ImageJ2, Rasband, W.S., U. S. National Institutes of Health, Bethesda, Maryland, USA).

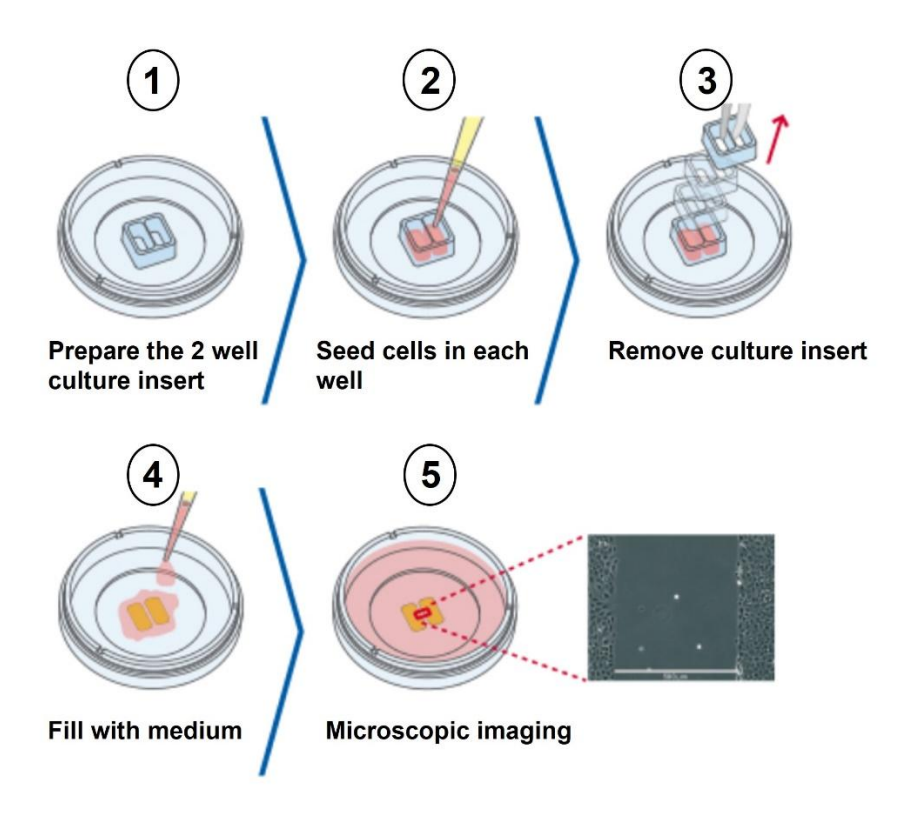


Figure 9. Representative figure of ibidi 2 well culture-insert. (Picture adapted from instruction manual of ibidi 2 well culture-insert).

#### 2.2.10. Tube formation assay

To assess the angiogenesis potential of VECs, a 96-well plate was pre-coated with 50µl of cold Matrigel per well and incubated at 37°C for 40min to allow for gelation. Subsequently, VECs were seeded at the density of 240 cells/ml in the total volume of 100µl in each well. Afterwards, the plate was incubated at 37°C and 5% CO₂ for 4h allowing the cells to form tube-like structures on the Matrigel. After incubation, the tube network formed by the VECs was imaged using inverted microscope to visualize the extent of tube formation. The length and number of tubes were quantified using Wimasis online image analysis tool (https://www.wimasis.com/en/).

#### 2.2.11. Cell proliferation

To measure the proliferation of both immortalized VECs and non-immortalized VECs, PrestoBlue cell viability reagent was utilized. PrestoBlue is a resazurin-based solution that undergoes rapid reduction by metabolically active cells, resulting in a color change from blue to red.

Cells were seeded in a 96-well plate at a density of 2000 cells/well. The following day, cells were treated with 10µl/well PrestoBlue and incubated for 2h in an incubator at 37°C and 5% CO₂. After the incubation period, the absorbance was measured in duplicates using EnSpire™ plate reader (λ570nm). Blank (cell growth medium and PrestoBlue

reagent) and background (wells with media) wells were measured in triplicates for proper baseline correction.

#### 2.2.12. Cellular uptake of IEVs

Immortalized VECs were cultured with EV-free medium for 24h, and the medium was collected for IEV isolation as mentioned in section 2.4.3. After IEV isolation, they were labeled with PKH67 dye (PKH67 Green Fluorescent Cell Linker Kit), a green fluorescent dye that binds to the lipid membrane of the vesicles. For this, recipient VECs were seeded onto a coverslip in a 24-well plate at a density of 25,000 cells per well. 100µg EVs were incubated with PKH67 dye solution following the manufacturer's instructions. In brief, Dye Solution was prepared in Diluent C by adding 4µL of the PKH67 ethanolic dye solution to 1ml Diluent C in a centrifuge tube and mixed thoroughly. EVs were added to 2x Dye Solution with the 1:1 ratio and incubated at RT for 10min. Labelling was stopped by adding PBS containing 1% bovine serum albumin (BSA). Following labelling, PKH67-labeled IEVs were centrifuged at 20,000 g for 45 min in 100µl of PBS to remove any unbound dye. Next, 8µg of PKH67-labeled EVs (see section 2.6.3) were added to the EV-free cell culture medium of VECs and incubated for 24h at 37°C with 5% CO<sub>2</sub>.

#### 2.2.13. Co-incubation of IEV with VECs and EndMT assay

For EV uptake experiments, freshly isolated EVs were used in order to preserve the integrity of EVs and incorporated miRNAs. VECs were plated on 24-well plates and allowed to reach 70% confluence. Next, following media was used for this experiment: 1) EndMT basic medium (Table 3) 2) EndMT basic medium supplemented with 25ng/ml TNF $\alpha$  and 3) EndMT basic medium supplemented with IEV (80µg/ml) (see section 2.6.3) and 4) EndMT basic medium supplemented with 25ng/ml TNF $\alpha$  and IEV (80µg/ml). The medium was changed every other day for 7 days.

#### 2.2.14. Osteogenic differentiation of VICs (calcification assay)

VICs were seeded on 48-well plates and treated with two distinct calcific media including osteogenic medium (OM) and pro-calcifying medium (PM) (Table 2). For controls, VICs were cultured in the basic VIC culture medium (Table 2). The culture medium was refreshed every two days.

#### 2.2.15. Alizarin red staining

To evaluate calcium deposition, VICs were cultured in OM and PM for 14 days and then stained using alizarin red stain. For staining, cells were gently washed with PBS and subsequently fixed using 10% paraformaldehyde (PFA). After 15min incubation at room temperature (RT), cells were washed three times with milli-Q water. Afterwards, 2% alizarin red solution was applied to stain the cells, followed by a 15min incubation at RT. To remove excess stain, cells were washed again with milli-Q water and the plate was left at RT for 24h to dry. To quantify alizarin red stain Cetylpyridinium chloride (CPC) was used. CPC elutes alizarin red from the calcium ions through its interaction with the negatively charged carboxyl groups of alizarin red (Gregory et al. 2004). 100mM CPC

was added to the dried alizarin red, followed by a 3h incubation at RT. The absorbance was subsequently measured at a wavelength of 540 nm using EnSpire™ multimode plate reader.

#### 2.2.16. Tissue non-specific alkaline phosphatase (TNAP) activity

Tissue non-specific alkaline phosphatase (TNAP) is a pivotal regulator of calcific mineralization, playing a crucial role in hydrolyzing pyrophosphate to phosphate. This hydrolysis leads to the inactivation of pyrophosphate, a calcification inhibitor, while simultaneously providing phosphate ions essential for the formation of hydroxyapatite crystals. To assess TNAP activity during calcification, VICs were seeded on a 12-well plate and cultured in NM, OM and PM for 7 days. TNAP activity was measured using alkaline phosphatase assay kit (Abcam, ab83369), according to the manufacturer's protocol. Briefly, 100µl ALP assay buffer was added to the cells and the mixture was incubated at 4°C for 30min. Subsequently, the cells were carefully harvested using a scraper and transferred into a new tube. To initiate the enzymatic reaction, 50µl of a 5mM pNPP (p-Nitrophenyl phosphate) solution was combined with 80µl sample. The reaction mixture was incubated at 37°C for 1h, resulting in the conversion of the pNPP substrate into the colored p-Nitrophenol (pNP) by the ALP enzyme. Afterward, the optical density (OD) of the reaction was measured at the wavelength of 405nm using EnSpire™ multimode plate reader. TNAP activity was normalized to protein concentration as measured by a BCA protein assay kit (see section 2.7.3.).

#### 2.3. Extracellular Vesicle Methods

#### 2.3.1. Materials

- Ampuwa, Fresenius Kabi, Bad Homburg, Germany
- EBM™-2 Endothelial Cell Growth Basal Medium-2, Lonza, CC-3156
- Exo-FBS HI, Exosome-depleted FBS Media Heat Inactivated, System Biosciences, Exo-FBSHI-250A-1
- Glutaraldehyde, Science Services, Munich, Germany
- innuSOLV RNA Reagent, Analytik Jena, 845-SB-2090100
- PBS PH7.4, Gibco, 10010023
- Penicillin, Streptomycin (P/S), Biochrom AG, Berlin, A2213
- Uranyl acetate, Science Services, Munich, Germany

#### 2.3.2. Equipment

- Crossbeam 550, Carl Zeiss, Oberkochen, Germany
- Conical tubes15ml and 50ml, Sarstedt, 62.554.001, 62.548.004
- Eppendorf Centrifuge 5430, Eppendorf
- Formvar/carbon-coated copper TEM grids, Science Services, Munich, Germany
- 31.5 mL, Open-Top Thinwall Polypropylene Konical Tube, Beckman Coulter, 358126.
- 5 mL, Open-Top Thickwall Polycarbonate Tube, Beckman Coulter, 355630.

- Tube rotator, American laboratory trading
- Ultracentrifuge, Beckman Coulter
- ZetaView® Basic NTA-PMX-120, Germany

#### 2.3.3. IEVs and sEV isolation from aortic valve tissue and cell culture medium

IEVs were isolated from the aortic valve by mechanical disruption. For this, explanted AV cusps were washed with PBS and placed into cell culture medium. The cusps were then cut into small pieces and incubated in a shaker incubator at 37°C for 4h. Following incubation, the supernatant was first pre-cleared by centrifugation at 300 g for 10min at 4°C to remove cell debris. Next, the supernatant was centrifuged at 20,000 g for 45min at 4°C to pellet IEVs. The supernatant obtained from IEV isolation was further centrifuged at 100,000 g for 1h at 4°C to pellet sEVs. The pelleted vesicles were washed with ice-cold PBS and centrifuged at 100,000g for 1h at 4°C. The pellet was re-suspended in 1ml innuSOLV RNA Reagent for RNA isolation.

For IEV isolation from the VEC culture medium, cells were cultured in basic endothelial cell medium supplemented with 10% EV depleted FBS (Table 3). Medium was collected, and above-described method for IEV isolation was used.

#### 2.3.4. Nano particle tracking analysis (NTA)

The size distribution and concentration of IEVs were determined using Zeta view (ZetaView® Basic NTA-PMX-120, Germany). IEVs were isolated from culture medium as described above and re-suspended in PBS and further diluted 1:1000 for the analysis. The measurement was performed based on the manufacturer's protocol. Each sample was recorded 4 times with 3 cycles at 11 positions using a minimum brightness of 25.

#### 2.3.5. Scanning electron microscopy (SEM)

EVs were isolated from the culture medium (section 2.3.3.) and dissolved in PBS. For electron microscopy, samples were bound to glow-discharged formvar/carbon-coated copper TEM grids (400 mesh) (Science Services, Munich, Germany). The loaded TEM grids were then incubated on drops of 1% glutaraldehyde (Science Services, Munich, Germany) for fixation, followed by eight washes with drops of filtered ultrapure distilled water (Ampuwa, Fresenius Kabi, Bad Homburg, Germany). After washing, the TEM grids were negatively stained with 2% uranyl acetate (Science Services, Munich, Germany) for 45-60s and air-dried. Images were acquired using a Crossbeam 550 (Carl Zeiss, Oberkochen, Germany) with a STEM detector at 30 kV acceleration voltage and 150 pA currents in imaging mode.

# 2.4. Immunological Methods

#### 2.4.1. Materials

- Anti-ACTA2 antibody, Abcam, ab7817
- Anti-CD31 antibody, Abcam, ab56299
- Anti-vWF antibody, Abcam, ab6994

- DAPI, InvitrogenTM, D1306
- Donkey anti-Rabbit IgG (H+L) Highly Cross-Adsorbed Secondary Antibody, Alexa Fluor™ 647, Abcam, A-31573
- Glycine, AppliChem, 131340
- Goat anti-Mouse IgG (H+L) Cross-Adsorbed Secondary Antibody, Alexa Fluor™ 555, Abcam, A-21422
- Immu-Mount™ ThermoFisher Scientific, 9990402
- Paraformaldehyd (PFA), Roth, 0335.3
- PKH67 Green Fluorescent Cell Linker Midi Kit, Sigma Aldrich, Midi67
- Triton®X-100, BDH Prolabo Chemicals,28817.295
- Tween-20, Sigma Aldrich, P2287

#### 2.4.2. Equipment

- Confocal microscope, Zeiss 5
- ImageJ software
- Menzel<sup>™</sup>, Microscope Coverslips, Thermo Fisher Scientific, 11778691
- Microscope cover glasses 14mm, Glaswarenfabrik Karl Hecht GmbH & Co. Sondheim, Germany, 41001114

#### 2.4.3. Immunofluorescence (IF) staining

For immunofluorescence staining, cells were washed with PBS (Table 4) and fixed with 4% PFA (Table 5) for 1h at 4°C. Subsequently, cells were washed with PBS and incubated with 0.25% TritonX-100 for 10min at RT to facilitate cell membrane permeabilization. Subsequently, cells were washed three times with PBS. To visualize cell nuclei, cells were incubated with 4′,6-diamidino-2-phenylindole (DAPI). Cells were blocked with 1% BSA-glycine-PBS-T (Table 6) for 30min at RT to minimize nonspecific binding. Afterwards, cells were incubated with specific primary antibodies in blocking solution for 2h at RT. Subsequently, cells were washed three times with PBS and incubated with secondary antibodies in 1% BSA-glycine-PBS-T blocking solution (Table 6) and DAPI for 1h at RT. Staining was analyzed using Immunofluorescence microscope and ImageJ software. Antibodies are listed in Table 7.

Table 4. PBS

Component	Amount	
NaCl	137nm	
Na <sub>2</sub> HPO <sub>4</sub>	8mM	
KH <sub>2</sub> PO <sub>4</sub>	1.4mM	
KCI	2.7mM	
Components were dissolved in H <sub>2</sub> O and pH was adjusted to 7.4		

#### Table 5. PFA 4%

Component	Amount
Paraformaldehyde	40gr
PBS	960ml

#### Table 6. BSA-glycine-PBS-T

Component	Amount
BSA	1% (w/v)
Glycine	22.52 mg/ml
Tween 20	0.1% (v/v)
PBS	Add components to PBS

Table 7. List of primary and secondary antibodies.

Antibody	Source	Dilution
Anti-CD31 antibody	abcam #ab56299	1:400
Anti-vWF antibody	Abcam # ab6994	1:100
Anti-ACTA2 antibody	Abcam #ab7817	1:100
Donkey anti-Rabbit IgG, Alexa Fluor 647	ThermoFisher # A-31573	1:200
Goat anti-Mouse IgG, Alexa Fluor 555	ThermoFisher # A-21422	1:500

# 2.5. Cloning and Lentiviral Vector Generation

#### 2.5.1. Materials

- Agarose, Merck, A9539
- Ampicillin sodium salt, Santa Cruz Biotechnology, 69523
- Agel-HF, New England BioLabs (NEB), R3552
- Calcium Acetate, Merck, 62-54-4
- DNA gel loading dye, Thermo Scientific<sup>™</sup>, R0611

- DMEM (1x) Dulbecco's Modified Eagle Medium +4.5g/L D-glucose, +L-Glutamine, -Sodium Pyruvate, ThermoFisher Scientific, 11965
- EcoRI-HF, New England BioLabs (NEB), R3101
- EcoR-V-HF, New England BioLabs (NEB), R3195
- Ethanol, Roth, 9065.4
- Ethylenediaminetetraacetic acid, Merck, 60004
- Fetal bovine serum, Qualified, Sigma-Aldrich, A3160802
- HBSS, Calcium, Magnesium, no phenol red, Gibco, 14025126
- illustra<sup>™</sup> GFX<sup>™</sup> PCR DNA and gel band purification kit, Cytiva, 28-9034
- NucleoBond Xtra Maxi EF, Maxi kit for endotoxin-free plasmid DNA, Macherey Nagel, 740424
- 2-Propanol, Roth, 6752.4
- Penicillin, Streptomycin (P/S), Biochrom AG, Berlin, A2213
- PspOMI-HF, New England BioLabs (NEB), R0653
- Pstl-HF, New England BioLabs (NEB), R3140
- Poly-L-lysine solution, Sigma, P4832-50ML
- Q5® High-Fidelity 2X Master Mix, New England Biolabs (NEB), M0492
- RNAseA, New England Biolabs (NEB), T3018L
- Sodium-dodecyl sulphate (SDS), Roth, 2326.2
- Sodium hydroxide, Merck, 106462
- Sall-HF, New England BioLabs (NEB), R3138
- T4 DNA Ligase, New England BioLabs (NEB), M0202
- Tris-Hydrochlorid, Merck, 10812846001
- Tris, Roth, AE15.3

#### 2.5.2. Equipment

- Gel casting chambers: RunOne™ Agarose Gel Casting Systeme, Embi Tec San Diego, CA, USA
- Incubator, AL01-07-100, Advantage Lab bvba, Schilde, Belgium
- Microwave, Severin, Sundern
- QuantityOne® Software, BioRad, München
- Spectrophotometer, NanoDrop 2000, ThermoFisher Scientfic
- Thermocycler, T1 Thermocycler, Biometra GmbH, Göttingen
- Thinwall Polypropylene Tube, 5ml and 30 ml, Beckman Coulter
- UV light transilluminator, GelDoc®XR, BioRad, München
- Ultracentrifuge, Beckman Coulter

#### 2.5.3. Preparation of insert DNA

For miRNA overexpression, PCR-based cloning was utilized. Briefly, PCR reaction was performed to amplify DNA of interest, which was later digested and cloned into the third-generation lentiviral vector (pRRLSIN). HEK-293 genomic DNA (gDNA) was used as a template to amplify miRNA-150-5p, Let-7c-5p, and miRNA-30b-5p. The primary miRNA was amplified using forward and reverse primers that initiate amplification from 200

nucleotides upstream and downstream of the seed region. These primers were designed to insert Nsil and Sall restriction sites (Figure 10).

The length of PCR products for each miRNA can be found in Table 8. The PCR components and PCR conditions are listed in Table 9 and Table 10, respectively.



Figure 10. A representative picture of primary miRNA structure.

Forward and reverse primers initiate the amplification of primary miRNA from upstream and downstream of flanking regions

Table 8. List of primers used to amplify miRNAs and the length of corresponding PCR product.

Gene	Forward (5´-3´)	Reverse (3'-5')	Length of PCR Product
miRNA-150-5p	CTTCATGCATCTCTACTGCCC CCAGCATAG	CACAGTCGACGAACAGGACA GGACACACGG	508 bp
Let-7c-5p	GTAGATGCATGGCAGGTTAGAT GGTCAGAAG	CATGGTCGACTGAACATGGA GTGACAACCC	550bp
miRNA-30b-5p	CAGTATGCATTAGTAGCGTGCC TGTAGTG	CACAGTCGACCTACTCCTAC TGCAACCATGC	533 bp

Table 9. PCR reaction mix.

Component	Amount
Q5 High-fidelity 2X master mix	12.5µl
10 μM forward Primer	1.25µl
10 µM reverse Primer	1.25µl
gDNA template	50ng
Nuclease free water	-
Total	25µl

Table 10. PCR program used for DNA Insert Amplification.

Step	Temperature (°C)	Time (s)	Repeat
------	---------------------	-------------	--------

Initial denaturation	98	30		Temperature (°C)	Time (s)	Repeat
Denaturation	98	15		98	15	
Annealing	60	15	5X	70	15	32X
Extension	72	30		72	30	
Final extension	72	10				

Agarose gel electrophoresis was performed to visualize and identify the insert DNA. Agarose was dissolved in 1x TAE buffer (Table 11) and heated in microwave for 2min. Ethidium bromide (800ng/ml) was added and poured into the casting chambers, left to solidify at RT. Loading dye (1:6) was added to the PCR samples, subsequently loaded on agarose gel and run at 100V for 1h. DNA bands were visualized under UV detector and evaluated using QuantityOne® software (BioRad). The bands of interest were cut and purified using GFX™ PCR DNA and Gel Band Purification Kit (Cytiva, 28-9034) according to the manufacture's protocol. Briefly, the agarose bands were mixed with capture buffer and incubated at 60°C for 30min. Next, dissolved agarose was transferred to a new assembled GFX MicroSpin column and collection tube and incubated at RT for 1min followed by centrifugation at 16000 g for 30s. Afterwards, the flow-through was discarded and DNA was washed using 500µl wash buffer followed by centrifugation at 16000 g for 30s. The collection tube was discarded, and DNA was eluted in 20µl DNAase free water.

Table 11. 50X TAE buffer

Component	Amount
EDTA	50mM
Tris	2M
Acetic acid	1M

#### 2.5.4. Digest insert DNA and vector

The insert DNA and 1µg vector were separately digested using the appropriate restriction enzymes provided in Table 12 and incubated for 1h at 37°C. The mixture was purified using GFX™ PCR DNA and Gel Band Purification Kit according to the manufacture's protocol to remove impurities and unwanted bands. Briefly, the mixture was mixed with 500µl capture buffer and transferred to the assembled GFX MicroSpin column and collection tube, followed by DNA purification and elution, see section 2.5.3. The concentration of DNA was measured using Nanodrop Spectrophotometer 2000 (ThermoFisher Scientific).

Table 12. Restriction digestion reaction

Component	Amount
DNA insert/Vector	Whole DNA/1µg
10X Cut smart buffer	2.5µl
Pstl-HF	1μΙ
Sall-HF	1μΙ
Nuclease free water	-
Total	25µl

#### 2.5.5. Ligation of insert DNA into the vector

To ligate the insert DNA into the plasmid, 50ng of vector was used, and the ligation was performed with a 1:3 molar ratio of vector to insert (Table 13). The 1:3 ratio was calculated using NEBioCalculator (<a href="https://nebiocalculator.neb.com/#!/ligation">https://nebiocalculator.neb.com/#!/ligation</a>). Afterwards, the ligation reaction was incubated overnight at 16°C. An empty vector as a control was used.

Table 13. Ligation reaction.

Component	Amount
Plasmid	50ng
PCR Product	-
10X T4 DNA Ligase Buffer	2μΙ
T4 DNA Ligase	1μΙ
Nuclease free water	-
Total	20μΙ

#### 2.5.6. Bacteria transformation

XL1 Blue competent *E. coli* (90µl) were thawed on ice, and 10µl of ligation mixture was added to the competent cells. The bacterial mixture was incubated on ice for 20min to allow the bacteria to take up the vector. The heat shock method was used to facilitate vector uptake by bacteria. In this method, the bacterial mixture was placed in 42°C water for 45s, followed by immediate incubation on ice for 2min. The transformed bacteria were mixed with 900µl LB medium (Table 14) and cultured in shaker incubator at 37°C, 225 rpm for 1h to allow for the recovery and expression of antibiotic resistance. Afterwards, the transformed bacteria were centrifuged at 3,000 rpm for 5min, and the pellet was re-

suspended in 250µl LB medium. Afterwards, transformed bacteria was plated on LB agar plates containing ampicillin and incubated in a shaker incubator overnight at 37°C.

Next day, multiple colonies were picked from each plate and transferred into the 5ml LB medium supplemented with 100µg/ml Ampicillin and incubated in the shaker incubator overnight at 37°C.

Table 14. LB Medium

Component	Amount
Tryptone	10gr
NaCl	10gr
Yeast extract	5gr
H2O	950ml
Adjust pH to 7 and fill up to 1L with H2O	

#### **2.5.7. Miniprep**

A single colony was carefully picked from each plate and transferred into the 5ml LB medium supplemented with 100µg/ml Ampicillin and incubated overnight at 37°C to allow bacterial growth and plasmid amplification.

Next day, 1ml of bacterial culture was pelleted by 3,500 rpm centrifugation for 10min followed by resuspension in 250 µl of resuspension buffer (Table 15). To lyse the bacteria and release the plasmid DNA, 250µl lysis buffer was added and incubated at RT for 3min (Table 15). Next, 250µl of neutralizing buffer was added to neutralize the lysis buffer (Table 15) and incubated on ice for 15min followed by centrifugation for 15min at 4°C, 13,000 rpm. The supernatant was transferred to new tube, and plasmid DNA was precipitated by adding 0.7 (v/v) isopropanol (100%). The mixture was incubated at -20°C for 20min and centrifuged for 10 min at 4 °C, 14,000 rpm. The supernatant was discarded and the DNA pellet was washed two times with 70% ethanol. Afterwards, the pellet was air-dried and dissolved in 30µl of sterile water.

Table 15. Miniprep buffers

Buffer	Component	Amount
	Tris-HCl, pH 8,0	50mM
Resuspension Buffer	EDTA	10mM
	RNAseA	100µg/ml
Lysis Buffer	NaOH	200mM
	SDS	1%

Neutralizing Buffer	Calcium Acetate, pH 5,5	3M

#### 2.5.8. Verification of plasmid integrity via restriction digestion and sequencing.

Due to the possibility of mutations in PCR-based cloning, it is essential to verify the integrity of the DNA insert after cloning and transformation. To achieve this, plasmids from the miniprep were digested using appropriate restriction digestion enzymes (Table 16, 17, and 18) and incubated at 37°C for 1h. The digested plasmids were loaded onto a 1% agarose gel. After the confirmation of DNA fragments on the gel, plasmids containing the expected insert bands were sequenced by Microsynth company to ensure the sequence of DNA insert.

Table 16. Restriction digestion for miRNA-150-5p

Component	Amount	miRNA-150-5p	Vector
Plasmid	1µg		
10X Cut smart buffer	2.5µl		
PspOMI-HF	1µl	919bp	7132bp
Agel-HF	1µl		- 1
Nuclease free water	-		
Total	25μΙ		

Table 17. Restriction digestion for Let-7c-5p

Component	Amount	Let-7c-5p	Vector
Plasmid	1µg		
10X Cut smart buffer	2.5µl		
EcoRI-HF	1µl	792bp	7259bp
Nuclease free water	-		
Total	25µl		

Table 18. Restriction digestion for miRNA-30b-5p

Component	Amount	miRNA-30b-5p	Vector
Plasmid	1µg		
10X Cut smart buffer	2.5µl	868bp	7183bp
Agel-HF	1µI		

EcoR-V-HF	1µl
Nuclease free water	-
Total	25µl

#### 2.5.9. Maxiprep

The maxiprep method was used to produce larger amount of plasmids for lentivirus production. The remaining bacteria from the miniprep which were used for maxiprep (section 2.5.8) were transferred into a larger flask containing 250ml LB medium supplemented with 100µg/ml Ampicillin, and incubated in a shaker incubator at 37°C overnight.

Next day, bacteria were pelleted via centrifugation at 4500 g, 4°C and for 15min. Subsequently, the plasmids were extracted using NucleoBond® Xtra Maxi EF kit, following the manufacturer's instructions. Briefly, DNA pellet was suspended in 12ml suspension buffer followed by cell lysis by 12 ml lysis buffer and incubation at RT for 5min. The lysate was neutralized with 12 ml neutralizing buffer and loaded on NucleoBond® Xtra column filter which was equilibrated by equilibration buffer. The lysate was washed with 10ml FiL-EF buffer. Afterwards, NucleoBond® Xtra column filter was discarded. The lysate was washed with 90 ml ENDO-EF buffer and next with 45 ml Wash-EF buffer. Plasmids were eluted by 15ml elution buffer. Subsequently, the eluted DNA was precipitated using 10.5 ml isopropanol and passed through a NucleoBond® Finalizer using a syringe. The DNA was washed with 70% ethanol. The flow-through was discarded, and NucleoBond® Finalizer was air dried by gently pressing air through it with a syringe. The plasmid DNA was eluted from the NucleoBond® Finalizer using 1ml H<sub>2</sub>O. Finally, the concentration of the extracted DNA was measured using a nanodrop spectrophotometer (ThermoFisher Scientfic).

#### 2.5.10 Lentivirus production

To produce lentiviruses, HEK293T cells were plated on poly-L-lysine-coated dishes and cultured in DMEM supplemented with 10% FBS and 1% penicillin/streptomycin at 37°C and 5% CO₂ overnight. For the transfection of HEK293 cells, a total of 175μg of pMDL (gag/pol), 68μg of RSV-Rev, and 95μg of CMV-VSV, along with 270μg plasmid of interest, were used for 12 plates (15 cm each) through the calcium phosphate-based transfection. Afterwards, cells were incubated at 37°C and 3% CO₂ overnight, followed by changing medium in the next day. The supernatant was collected from the cell culture medium, and ultracentrifuged at 19,400 rpm and 17°C for 2h. The resulting pellets were firstly dissolved in Hank's Balanced Salt Solution (HBSS) and then layered on 20% sucrose. Next, the supernatant was ultracentrifuged at 21,000 rpm and 17°C for 2h. The supernatant was carefully discarded, and the pellet was dissolved in HBSS. The viruses were further incubated in a thermal shaker for 45min at 16°C and 1,400 rpm. Finally, the supernatant was aliquoted and stored at -80°C for future use.

#### 2.6. Protein Methods

#### 2.6.1. Materials

- Diethyl pyrocarbonate (DEPC), Carl Roth, K028.1
- Ethylenediaminetetraacetic acid, Merck, 60004
- Nonidet® P 40 Substitute (NP-40), Fluka BioChemika, Cat. No. 74385
- Pierce<sup>™</sup> BCA Protein-Assaykit, Thermo Fisher, 23250
- Protease inhibitor cocktail, Complete® EDTA-free Roche, Mannheim, 11873580
- Sodiumchlorid (NaCl), Roth, 3957.1
- Sodium-dodecyl sulphate (SDS), Roth, 2326.2
- Tris-Hydrochlorid, Merck, 10812846001
- Tri-NAtriummonovanadat (NaF), Roth, 0735.2

#### 2.6.2. Equipment

- Eppendorf Centrifuge 5430, Eppendorf
- Spectrophotometer, NanoDrop 2000, ThermoFisher Scientfic

#### 2.6.3. Protein isolation and quantification

Cells were rinsed with PBS, and a minimal volume of PBS was then added. Subsequently, cells were harvested using a scraper and collected in tubes. Following centrifugation for 5 min at 500 g, the pellet was collected and lysed by RIPA buffer (Table 19). The mixture was vortexed for 10s and placed on ice for 2min. This step was repeated 5 times.

For EVs, RIPA buffer was added to the isolated EVs (see section 2.3.3.), followed by the same procedure as mentioned above.

The protein concentration was measured by Nano BCA Kit following the manufacturer's instruction. Briefly, working solution was prepared by mixing 1 part of Reagent B with 50 parts of Reagent A. Subsequently, 1µl of protein lysate was diluted in 8 µl working solution and incubated at 37°C for 30min. Then, the concentration of protein was measured using a Nanodrop Spectrophotometer (ThermoFisher Scientfic) at 595nm with a BSA standard.

Table 19. RIPA buffer.

Component	Amount
NaCl	150mM
Tris-HCI (pH:7.5)	50mM
Sodium Deoxycholate	0.5%(w/v)
NP-40	1%(v/v)
Sodium dodecyl sulphate (SDS)	0.1%(w/v)
EDTA	0.1mM

All substances were dissolved in Millipore H2O, filtered and stored at 4°C, and the following substances were added to the RIPA buffer freshly before use			
NAF	10mM		
Na <sub>3</sub> VO <sub>4</sub> 1mM			
Complete®EDTA free 40µl/ml			

#### 2.7. RNA Methods

#### 2.7.1. Materials

- Diethyl pyrocarbonate (DEPC), Carl Roth, K028.1
- Ethanol, Roth, 9065.4
- ExiLENT SYBR Green master mix, 203421
- hsa-miR-150-5p, Thermo Fischer Scientific, ID=000473
- hsa-let-7c-5p, Thermo Fischer Scientific, ID=000379
- hsa-miR-30b-5p, Thermo Fischer Scientific, ID=000602
- hsa-miR-486-5p, Thermo Fischer Scientific, ID=001278
- hsa-miR-486-3p, Thermo Fischer Scientific, ID= 002093
- hsa-miR-342-5p, Thermo Fischer Scientific, ID= 002147
- hsa-let-7g-3p, Thermo Fischer Scientific, ID= 002118
- human miRNA PCR panel I+II, Qiagen
- innuSOLV RNA Reagent, Analytik Jena, 845-SB-2090100
- miRCURY LNA Universal RT microRNA PCR, 203301
- 2-Propanol, Roth, 6752.4
- ProtoScript® II First Strand cDNA Synthesis Kit, New England Biolabs (NEB), E6560
- SYBR® Green PCR Master Mix, Thermo Fischer Scientific, 4309155
- Trichlormethan/Chloroform, Roth, 6340.1
- Transcriptor First Strand Synthesis Kit, Roche, 04379012001
- TaqMan® MicroRNA Reverse Transcription Kit, Thermo Fischer Scientific, 4366597
- TagMan™ Universal Master Mix II, with UNG, Thermo Fischer Scientific, 4440040

#### 2.7.2. Equipment

- ABI 7900HT Sequence Detection System (SDS) software, Applied Biosystems
- Autoclave, VX-150, Systec GmbH, Linden
- Centrifuge, Eppendorf, 5415R
- PCR tube 1.5 mL, Sarstedt, 72706
- Real-time PCR machine, Applied Biosystems<sup>®</sup> StepOnePlus™ System, ThermoFisher Scientific
- Real-time PCR machine, HT7900, Applied Biosystems
- QuantityOne<sup>®</sup> Software, BioRad, München
- Spectrophotometer, NanoDrop 2000, ThermoFisher Scientfic
- Thermocycler, T1 Thermocycler, Biometra GmbH, Göttingen

#### 2.7.3. Isolation of RNA

For RNA isolation from cells or EVs innuSOLV RNA Reagent was used as the lysis buffer. Briefly, 1ml of innuSOLV RNA Reagent was added to the cells/EVs. The lysates were then transferred to a reaction tube, and 200µl of cold chloroform was added to each sample. After vigorous shaking for 15s, the samples were incubated for 5min at RT and centrifuged at 4°C and 13,000 rpm for 20min. Following centrifugation, the mixture separates into three distinct layers: the upper phase contains RNA, while the two lower phases contain DNA, proteins and lipids. The upper phase was transferred to a new tube and 500µl cold isopropanol was added to precipitate RNA followed by centrifugation at 4°C and 13,000 rpm for 10min. Afterwards, the supernatant was discarded, and the RNA pellet was washed three times with 75% EtOH (in DEPC-H<sub>2</sub>O). The RNA pellet was airdried and dissolved in 15-20µl DEPC-H<sub>2</sub>O. The concentration of isolated RNA was quantified using a Nanodrop Spectrophotometer (ThermoFisher Scientific).

#### 2.7.4. RNA isolation from aortic and ventricular sides of aortic valve

RNA samples from each side of the valve were obtained from the research group of Prof. Bernd Fleischmann at the Institute of Physiology I, University of Bonn. The RNA isolation procedure was conducted by his PhD students Adrian Brandtner and Alexander Brückner.

For side specific RNA isolation, human aortic valves were obtained from patients who underwent AV replacement surgery for AVS and AI at the Heart Center Bonn, University Hospital Bonn, Germany. Explanted valves were thoroughly rinsed with PBS and placed between two glass coverslips and was firmly pressed with a cold aluminum rod for 3–5 s. This procedure led to the freezing of endothelial cells from both sides onto the coverslips. Afterwards, each cover slip was subjected to innuSOLV RNA Reagent to lyse the cells (Figure 11) (Simmons et al. 2004).

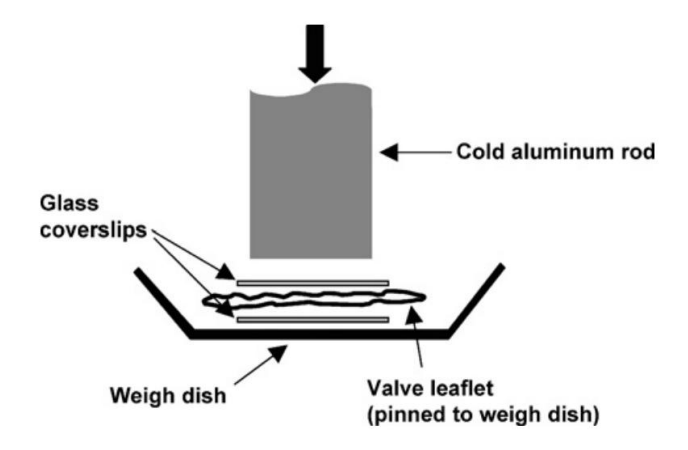


Figure 11. Side specific cell and RNA isolation from VECs (Figure adapted from Simmons et al. (Simmons et al. 2004).

The aortic valve was sandwiched between two glass coverslips. VECs from aortic and ventricular sides were frozen on the coverslips by applying pressure using cold aluminum rod for 3-5s. The coverslips were removed and used for RNA isolation.

#### 2.7.5. qPCR (SYBR green)

#### 2.7.5.1. cDNA synthesis

A total of 1000ng RNA was used to synthesize cDNA using the Protoscript® II First Strand cDNA Synthesis Kit following the manufacturer's instructions. cDNA was diluted 1:20 (50ng) in DEPC-H<sub>2</sub>O. The thermocycler program is detailed in Table 20.

Table 20. cDNA synthesis program

Step	Time (s)	Temperature (°C)
1	300	25
2	3600	42
3	300	80
4	hold	4

#### 2.7.5.2. Quantitative real-time polymerase chain reaction (qRT-PCR)

qRT-PCR reaction mix was prepared using 4µl cDNA, 0.5µl forward primer (10pmol/ml), 0.5µl reverse primer (10pmol/ml), and 2x SYBR Green master mix. GAPDH as an internal control was used to normalize gene expression. The list of primers can be found in Table 21. The primers were designed from exon-exon junctions using Primer3web version 4.1.0 (https://primer3.ut.ee/), and the specificity of each primer was determined using Primer-Blast NCBI.

(https://www.ncbi.nlm.nih.gov/tools/primerblast/index.cgi?GROUP\_TARGET=on).

qRT-PCR was conducted on the HT7900 instrument (Applied Biosystems) with the amplification program found in Table 22. A melting curve was generated at the end of each qPCR run to assess the specificity of PCR amplification.

Table 21. List of primers

Gene	Forward (5´-3´)	Reverse (5´-3´)
VWF	GTCGGTCGGGCTTCACTTAC	TCCTTCACTCGGACACACTC
ACTA2	CTGGACGCACAACTGGCATC	GACAATCTCACGCTCAGCAG
VIM	CAAGTTTGCTGACCTCTCTG	CCAGGGACTCATTGGTTCC
SLUG	CAGACCCTGGTTGCTTCAAG	GAGCCCTCAGATTTGACCTG
RUNX2	GAGTGGACGAGGCAAGAGT	GCGGTCAGAGAACAACTAG
ALPL	CGAGATACAAGCACTCCCAC	GGCTCGAAGAGACCCAATAG
OPG	CGCTCGTGTTTCTGGACATC	CACACGGTCTTCCACTTTGC
SPP1	CATCACCTGTGCCATACCAG	ACTGGAATTGAACTCTGTGTGC

GAPDH GATCATCAGCAATGCC	CCTG CATCCACAGTCTTCTGGGTG
------------------------	---------------------------

Table 22. qPCR thermal program

Step	Time (s)	Temperature (°C)	
1	600	95	Number of Cycles
2	15	95	40
3	60	60	40
	Melting curve		
6	1	95	
7	15	65	
8	-	95	

#### 2.7.6. TaqMan qPCR

#### 2.7.6.1. cDNA synthesis

A total of 10ng/µl RNA was utilized to synthesize cDNA using TaqMan™ MicroRNA Reverse Transcription Kit and 5x specific RT primers, following manufacturer's instructions (Table 23). In Taqman qPCR, the stem-loop primer was used to elongate miRNA length during the reverse transcription (RT) (Figure 12). In this method, stem-loop primer binds to miRNA, and RT enzyme synthesizes the complementary sequences from 3'to 5'end. Subsequently, specific forward primer (FP) and universal reverse primer (URP) amplify the targeted miRNA (Figure 12) (Gautam et al. 2016). The thermocycler program and list of Taqman primers can be found in Tables 24 and 25, respectively.

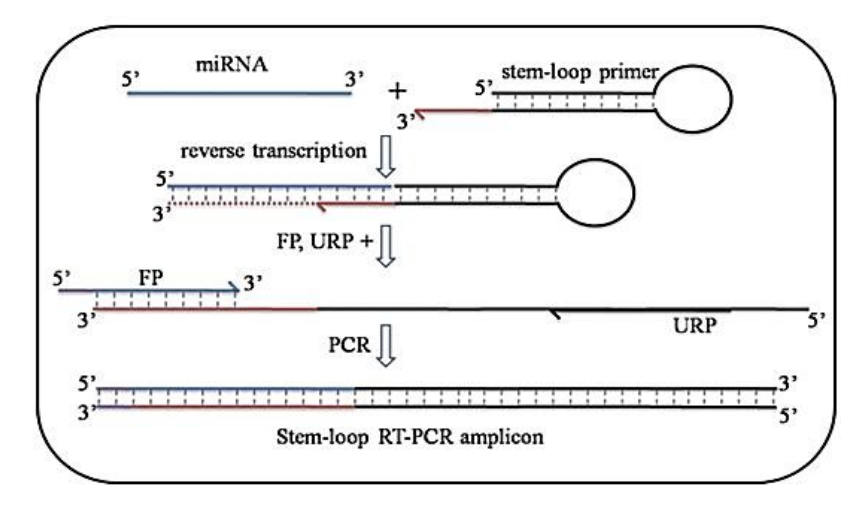


Figure 12. Stem-Loop RT PCR.

The stem-loop primer anneals to the mature miRNA, and the first strand cDNA is polymerized using a forward primer (FP) and a universal revere primer (URP). (Picture adapted from Gautam et al. (Gautam et al. 2016)).

**Table 23. cDNA components** 

Component	Amount (μΙ)
100mM dNTP	0.15
multiscribe reverse transcriptase 50u/µL	1
10x RT Buffer	1.5
Rnase Inhibitor 20u/µL	0.19
Rnase free water	6.41
20x RT-Primer	0.75
Total	10

Table 24. cDNA synthesis program

Step	Time (s)	Temperature (°C)
1	900	16
2	900	42
3	300	85
4	hold	4

Table 25. List of RT and PCR primers

miRNA Name	miRBase Accession Number	Mature miRNA Sequence
hsa-miR-150	MI0000479	UCUCCCAACCCUUGUACCAGUG
hsa-let-7c	MI0000064	UGAGGUAGUAGGUUGUAUGGUU
hsa-miR-30b	MI0000441	UGUAAACAUCCUACACUCAGCU
hsa-miR-486-5p	MI0002470	UCCUGUACUGAGCUGCCCCGAG
hsa-miR-486-3p	MI0002470	CGGGGCAGCUCAGUACAGGAU
hsa-miR-342-5p	MI0000805	AGGGGUGCUAUCUGUGAUUGA
hsa-let-7g*	MI0000433	CUGUACAGGCCACUGCCUUGC

#### **2.7.6.2. TagMan PCR**

The RT products were added to the PCR mixtures containing TaqMan™ Universal Master Mix II, with Uracyl N-glycosylase (UNG) and primers specific for PCR reaction, according to the manufacturer's instruction. The PCR primers and thermal protocol can be found in Tables 25 and 26, respectively.

Table 26. qPCR thermal program.

Step	Time (s)	Temperature (°C)	
1	600	95	Number of Cycles
2	15	95	40
3	60	60	40

#### 2.7.7. miRNA array

miRNA expression analysis was performed using a custom-made human miRNA PCR panel I+II containing 372 mature microRNAs in panel I and 380 mature microRNAs panel II. In this panel, three reference genes (SNORD38B, SNORD49A and U6 snRNA), five RNA spike-in control (UniSp2, UniSp4, UniSp5, UniSp6 and cel-miR-39-3p) and one interplate calibrator (UniSp3 IPC) were used. Reference genes with the stable expression across different cells or tissues were used for normalization of the miRNAs. RNA spike-ins (synthetic control templates) were used to assess the RNA isolation quality, cDNA synthesis reaction efficiency, and PCR amplification. After PCR, the RNA spike-ins are detected, and their values are compared with the samples to identify outliers.

100ng RNA was used to synthesize cDNA using miRCURY LNA Universal RT microRNA PCR according to the manufacturer's instructions. The RT program can be found in Table 27.

Table 27. cDNA synthesis program.

Step	Time (s)	Temperature (°C)
1	3600	42
2	300	95
3	hold	4

The cDNA was further diluted at the ratio of 1:30 and mixed with ExiLENT SYBR Green master mix, according to the manufacturer's protocol. The PCR program is detailed in Table 28. At the same time, the melting curve was analyzed to confirm a single PCR product in each well. PCR was performed and further analyzed using the Applied Biosystems ABI 7900HT Real Time Thermo Cycler and Sequence Detection System (SDS) software.

Table 28. qPCR thermal program

Step	Time (s)	Temperature (°C)	
1	120	95	Number of Cycles
2	10	95	40
3	60	56	40

# 2.8. Next Generation Sequencing (NGS)

#### 2.8.1. Library preparation and miRNA deep sequencing

miRNA library preparation and sequencing were performed by Cologne Center for Genomics (CCG) at University of Cologne, Germany. The Small RNA-Seq Library Prep Kit from Lexogen was used for library preparation which is compatible with Illumina sequencing platforms. Briefly, adapters were ligated to the 3' and 5' of RNA samples for reverse transcription of RNA and cDNA generation followed by PCR to amplify small RNAs. The amplified libraries were then subjected to size selection using gel to isolate the desired fragment size range. The libraries were assessed using Agilent TapeStation to analyze the quantity and size distribution of DNA. Sequencing was performed on the Illumina NovaSeq 6000 using a S1 Cluster Cartrige v1.5 on one lane in single read mode with read length of 101 bases. Base-calling, data filtering, and index sorting were performed by Illumina's bcl2fastq2 (v2.20.0).

## 2.8.2. Library preparation and mRNA sequencing (transcriptomics)

Total RNA was extracted from VECs using innuSOLV RNA Reagent (section 2.7.3.) mRNA library preparation and 3'poly(A)-mRNA sequencing was performed by Dr. André Heimbach at the NGS Core Facility of the Medical Faculty at the University of Bonn, Germany. Briefly, mRNA sequencing libraries were prepared using the Lexogen QuantSeq 3'mRNA FWD Library Prep Kit which is compatible with Illumina sequencing platforms. The library preparation process began with mRNA purification by poly(A) capturing of mRNA molecules. Subsequently, reverse transcription was performed using random primers to generate cDNA followed by reverse transcription to generate double-stranded cDNA. The library was prepared by ligation of adapters and performing PCR. Quantification of the prepared libraries was conducted using Qubit. Library size distribution and quality were assessed using an Agilent TapeStation device. The prepared libraries were sequenced on the Illumina NovaSeq 6000 device at the average sequencing depth of 10 million reads per sample.

# 2.9. Bioinformatic Analysis

#### 2.9.1. miRNA and mRNA differential expression analysis (DEA)

Bioinformatics analysis of both miRNA sequencing and mRNA sequencing was performed by Dr. Andreas Bunes, Core Unit for Bioinformatics Data Analysis, Medical Faculty, University Bonn.

For miRNA sequencing analysis, the nf-core small RNA-Seq pipeline (Ewels et al. 2020), smrnaseq (version 1.0), was applied for the preprocessing of the reads and the quantification of the miRNAs using default parameters. This comprehensive pipeline includes initial adapter sequence removal using TrimGalore (version 0.6.2) and read alignments against miRBase (version 22.1) using bowtie1 (version 1.3.0). The statistical analysis was performed in the R environment (version 4.0.3) (Spiess 2013). The raw read counts for mature miRNAs were converted to counts per million (CPM) values and normalized by library size factors using the edgeR package (version 3.32.1) (Robinson et al. 2010). To ensure robustness, miRNAs with a CPM value less than 2 in fewer than 3 samples were considered as low-count miRNAs and subsequently excluded from the analysis. After the initial filtering, the pooled cut-off was applied across all samples. Differential expression analysis (DEA) between the AVS and AI samples were analyzed using the Deseg2 package (version 4.3.0) (Love et al. 2014). To address multiple testing, the Benjamini-Hochberg method was employed to calculate adjusted p-values, commonly known as the false discovery rate (FDR). Principal component analysis (PCA) was performed using the package FactoMineR (version 2.4) (Lê et al. 2008). For visualization, volcano plots and heatmaps were generated using the ggplot2 package (Wickham 2016) ComplexHeatmap package (Gu et al. 2016), respectively.

For transcriptomics analysis, the nf-core RNAseq pipeline (Ewels 2020) (version 3.11) was applied for the pre-processing and the quantification of the reads using default parameters. Initially, quality and adapter trimming were conducted using TrimGalore (version 0.6.5), followed by aligning the trimmed reads to the human genome (GRCh38) with STAR (version 1.3.0). The aligned data were further used as input for Salmon (Patro 2017) for pseudoalignment to estimate transcript abundances. The transcript-level quantifications were aggregated to obtain gene-level expression estimates. The DGE analysis was performed in the R environment (version 4.2.0) using the Bioconductor package DESeq2 (Love et al. 2014). Only genes with at least 3 samples, each with a minimum count of 50, were considered for the statistical analysis. Statistical contrasts were calculated for each pair of groups to identify differentially expressed genes. The Benjamini-Hochberg method was used to calculate multiple testing adjusted p-values for each contrast. Data visualizations, such as volcano plots and heatmaps were generated using R-packages ggplot2 (Wickham 2016) and ComplexHeatmap (Gu et al. 2016), respectively.

#### 2.9.2. Prediction of miRNA target genes

The target genes of significantly dysregulated EV-miRNAs (adj. p < 0.05) were identified using miRTarBase (http://mirtarbase.cuhk.edu.cn/). This database includes the target genes that are validated by experiments. In the current study, genes validated by at least 2 different experimental methods (e.g., Western blot, qPCR, immunofluorescence) were selected for further analysis (section 2.9.3., 2.9.4. and 2.9.5.).

#### 2.9.3. Gene ontology (GO) and pathway enrichment analysis

Freely available bioinformatics tools such as Enrichr (https://maayanlab.cloud/Enrichr/) and DAVID (http://david.abcc.ncifcrf.gov/) were used for GO and signalling pathway analysis. p < 0.05 was used as a significant threshold.

#### 2.9.4. Protein protein interaction (PPI) and gene regulatory network (GRN)

The NetworkAnalyst 3 tool was utilized to analyze Protein-Protein Interaction (PPI) and Gene Regulatory Network (GRN) for genes associated with signaling pathways with p < 0.1, as identified through KEGG analysis.

#### 2.9.5. miRNA-mRNA Prediction

The 3'UTR binding site of miRNA was predicted using online tools including Targetscan (www.targetscan.org), RNA22 v2 (https://cm.jefferson.edu/rna22/), Pictar (https://pictar.mdc-berlin.de/) and miRDB (https://mirdb.org/). For analysis using the RNA22 database, the 3'UTR sequences of genes were obtained from Biomart (Ensemble) (https://www.ensembl.org/info/data/biomart/index.html) while miRNA sequences were acquired from miRBase (https://www.mirbase.org/). In this analysis, the threshold of minimum free energy (MFE) < -15 was employed.

#### 2.9.6. Statistical analysis

Statistical analysis was performed using GraphPad Prism 6 software (GraphPad Software Inc., 2014). For the comparison of two groups, an unpaired (two-tailed) t-test was applied. When comparing multiple groups, one-way ANOVA and two-way ANOVA in combination with Tukey's post-hoc multiple comparisons test was used.

#### 2.9.7. Image modification

Pictures were designed and modified using BioRender (BioRender.com).

## 3. Results

# 3.1. Next Generation Sequencing of EV-miRNAs in AVS

# 3.1.1. High throughput miRNA sequencing identified dysregulated miRNAs in tissue-derived EVs in AVS

Here, I aimed to identify dysregulated EV-derived miRNAs in patients with AVS. For this, EVs were isolated from patients with AVS (n=10, age  $69 \pm 7.2$  years old) and - as control - patients with AI (n=5, age  $68.6 \pm 5.8$  years old) using mechanical disruption, and total RNA was extracted and sequenced using NGS. Table 29 summarizes the clinical characteristics of patients with AVS and AI. All patients in both groups had a three-leaflet aortic valve.

Table 29. Baseline patient characteristics.

Group	Age (years)	SEX	ВМІ	Other Medical history
AVS-1	62	F	23	
AVS-2	68	F	20,1	
AVS-3	61	F	26,08	Left Ventricular hypertrophy
AVS-4	73	М	37,04	Left Ventricular hypertrophy
AVS-5	79	М	>25	
AVS-6	72	М	30	Ventricular heart failure, coronary heart disease
AVS-7	70	М	31,9	Ventricular heart failure, coronary heart disease
AVS-8	61	М	27,7	Left ventricular failure, coronary heart disease
AVS-9	62	М	29,7	Peripheral aortic valve calcification, coronary heart disease
AVS-10	82	М	26,51	
Al-1	66	М	24,07	
Al-2	63	М	31,5	Aortic ectasia, carotid sclerosis, left ventricular dilatation
Al-3	64	М	32,65	Mixed ischemic cardiomyopathy, coronary heart disease
Al-4	79	M	N.A.	Coronary heart disease

AI-5	71	М	31,2	carotid sclerosis

Using NGS, a total of 733 miRNAs were identified in AVS-IEV and 733 miRNAs in AVS-sEV (Figure 13). Among them, 3 miRNAs were significantly upregulated in AVS-IEV. (log2FC>1, adj. p < 0.05) (Figure 13A). Besides, 6 miRNAs were significantly upregulated (log2FC>1, adj. p < 0.05) and 3 miRNAs were significantly downregulated in AVS-sEVs (log2FC<-1, adj. p < 0.05) (Figure 13B). Significantly dysregulated miRNAs in both groups are listed in Table 30. Furthermore, hierarchical heatmaps were generated to show the distinct expression patterns of the top 15 highly dysregulated miRNAs across the samples both IEV and sEV groups of study, (Figures 13C and D). To assess the overall variability and pattern of miRNA expression among EV samples, PCA analysis was performed. The results showed a partial clustering of AVS and AI samples in the group of IEVs and sEVs. However, there was also a degree of overlap, indicating variability within the groups (Figures 13E and F). Overall, these findings provide novel insights into the miRNA associated with IEVs and sEVs in AVS, highlighting distinct expression profiles and dysregulated miRNAs associated with AVS pathology.

#### Valve-derived Large EVs

#### Valve-derived Small EVs

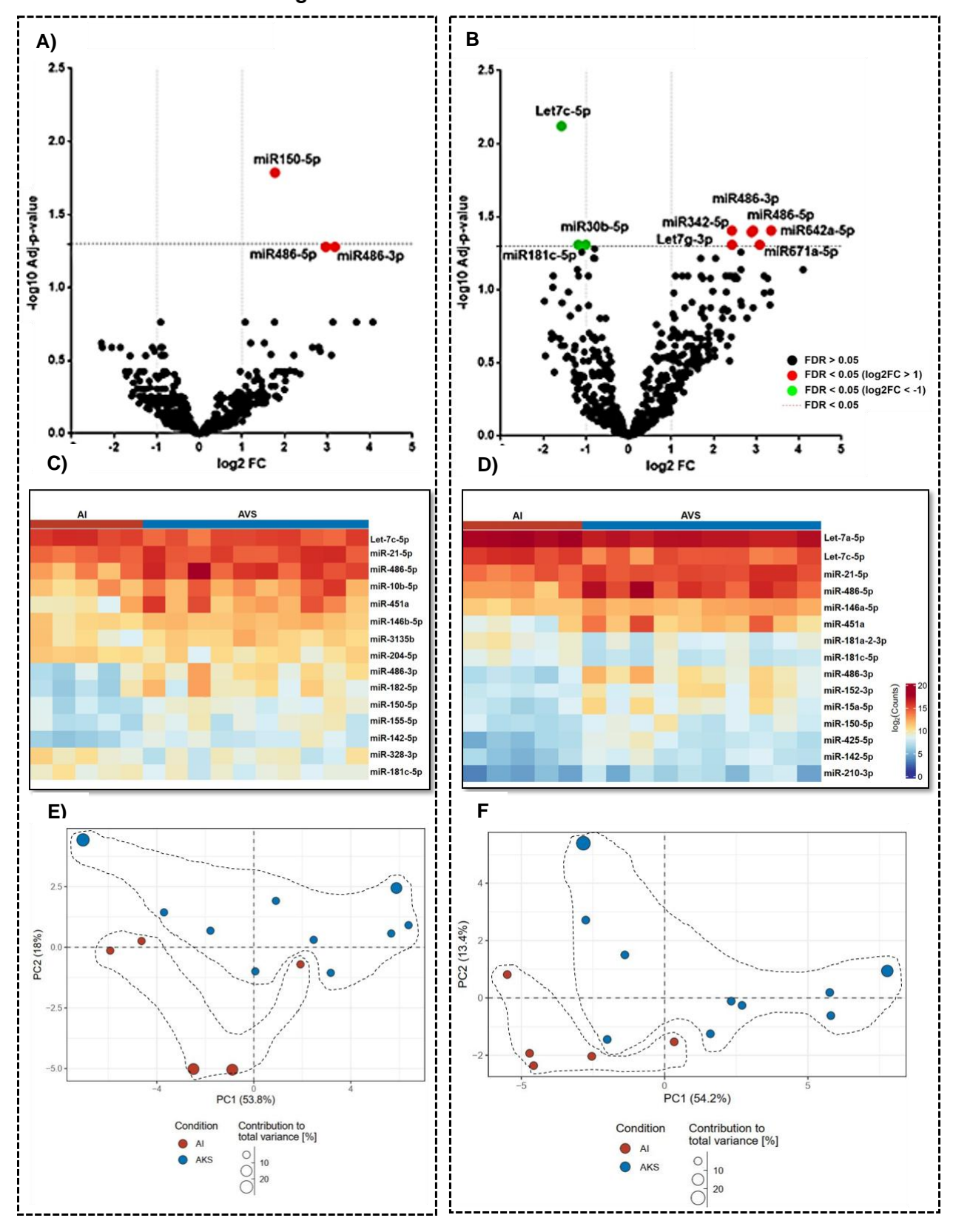


# Figure 13. Representative figure of sequencing data in IEV- and sEV-derived miRNAs in AVS compared to AI.

**A)** Volcano plot of differentially expressed miRNAs associated with IEVs in AVS compared to AI control. **B)** Volcano plot of differentially expressed miRNA associated with sEVs in AVS compared to AI control. **C)** Hierarchical clustering heatmap of gene expression profiles of the15 top highly expressed genes of AVS-IEVs compared to AI control. **D)** Hierarchical clustering heatmap of gene expression profiles of the 15 top highly expressed gens in AVS-sEVs compared to AI control. **E)** PCA analysis of miRNAs associated with AVS-IEVs **F)** PCA analysis of miRNA associated with AVS-sEVs. AVS (n=10) and AI (n=5). Cut-offs for differentially expressed miRNAs: |logFC|>1, adj. p < 0.05.

Table 30. List of significantly dysregulated miRNAs in EVs isolated from the aortic valve.

miRNA List	EV Source	Log2FC	Adj. p-value
miRNA-150-5p	IEV	+1.77	0.01
miRNA-486-5p	IEV	+2.97	0.05
miRNA-486-3p	IEV	+2.96	0.05
miRNA-671a-5p	sEV	+3.08	0.04
miRNA-642a-5p	sEV	+3.35	0.03
miRNA-486-5p	sEV	+2.92	0.03
miRNA-486-3p	sEV	+2.89	0.04
miRNA-342-5p	sEV	+2.42	0.03
Let-7g-3p	sEV	+2.42	0.04
Let-7c-5p	sEV	-1.57	0.007
miRNA-30b-5p	sEV	-1.00	0.04
miRNA-181c-5p	sEV	-1.17	0.04

#### 3.1.2. GO Analysis of differentially expressed EV-miRNAs

I have identified the target genes of dysregulated EV derived miRNAs (adj. p < 0.05) using miRTarBase. To understand the potential biological functions of these targets, I performed gene ontology and BioCarta pathway enrichment analysis (Figure 14). The results revealed enrichment of targeted genes in various functions (p< 0.05), including 108 molecular functions, 31 cellular components, and 532 biological processes. Notably, the target genes were primarily involved in the regulation of DNA-templated transcription and transcription by RNA polymerase II implicating their role in regulating cell proliferation (Figure 14A). Additionally, target genes of EV-miRNAs are associated with apoptotic processes emerged as another important aspect of the disease, suggesting that these miRNAs may modulate apoptotic pathways, affecting cell survival and tissue integrity.

Particularly, these target genes are enriched in positive regulation of miRNA transcription and cardiac epithelial to mesenchymal transition (EMT) (Figure 14A). In terms of cellular components, significant enrichment of the dysregulated miRNAs was associated with the intracellular membrane-bounded organelle, nucleus, and RISC-loading complex (Figure 14A). Molecular function analysis revealed that these genes contribute to the regulation of gene expression and post-translational modifications. Notably, the data showed that these genes regulate TGF- $\beta$  receptor binding, which is well-known as a mediator of AVS (Figure 14A).

I further extended the analysis to signaling pathway analysis to identify functional categories and canonical pathways affected by the targeted genes of EV-miRNAs (p < 0.05). I have identified 31 enriched canonical pathways. Among them, p53 signaling pathway, TGF- $\beta$  signaling pathway, hTert transcriptional regulation, first multivalent nuclear factor, cyclins and cell cycle regulation, peroxisome proliferators, MAP Kinase signaling pathway, IL-2 receptor beta chain in T cell activation, hypoxia-inducible factor in the cardiovascular system, p38 MAPK signaling pathway, and IL-10 anti-inflammatory signaling pathway were predicted to be among the top enriched pathways based on their p-values (Figure 14B).

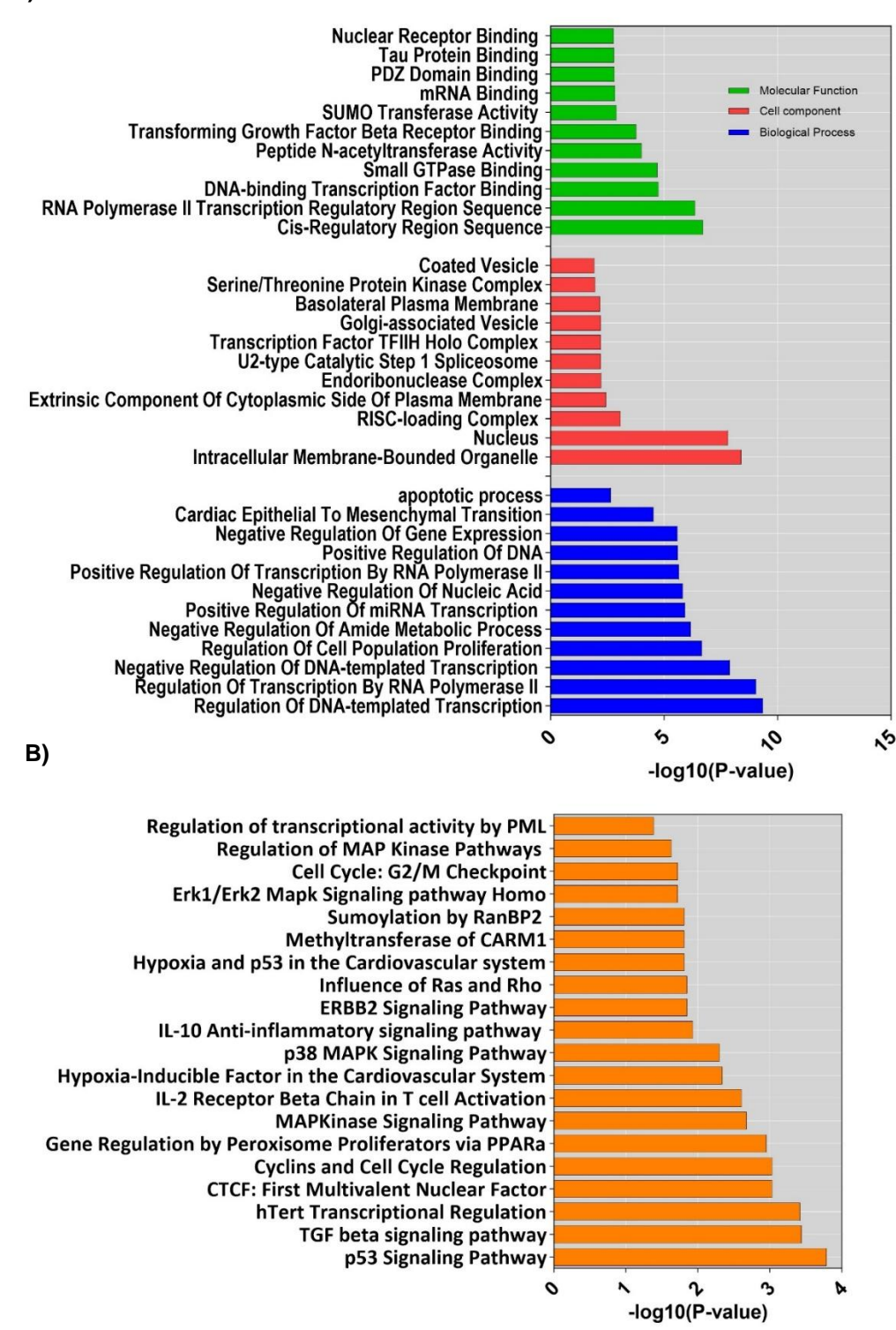


**Figure 14. Gene ontology (GO) and signaling pathway analysis of EV-miRNA target genes. A)** GO analysis of significantly dysregulated EV-derived miRNA target genes highlighting the top eleven enriched terms in biological processes, cellular components, and molecular functions. **B)** BioCarta pathway enrichment analysis of significantly EV-derived-dysregulated-miRNA target genes; higher -Log10 (p-value) indicates higher degrees of enrichment.

#### 3.1.3. Validation of dysregulated EV-miRNAs in AVS

Based on a literature review, I selected candidates for further validation and investigation of their roles in AVS and focused on those miRNAs that have impacts on cardiovascular diseases (Table 31). Among identified significantly dysregulated EV-miRNAs, miRNA-150-5p, Let-7c-5p, miR-30b-5p, miR-486-5p, miR-486-3p, miR-342-5p and Let-7g-3p mostly contributed to the different cardiovascular diseases (Table 31). Therefore, I focused on these 7 miRNAs for further validation.

Table 31. List of validated EV-miRNAs in cardiovascular diseases

miRNA List	Cardiovascular Disease
miRNA-150-5p	Atherosclerosis (Gong et al. 2018; Yin et al. 2021), Myocardial Infarction (MI)(Tang et al. 2015)
Let-7c-5p	Atherosclerosis (Qin et al. 2012), Coronary Artery Disease (CAD)(Faccini et al. 2017)
miRNA-30b-5p	AVS (Zhang et al. 2014), MI (Shen et al. 2015)
miRNA-486-5p	AVS (Patel et al. 2015), Carotid artery stenosis (Zhu et al. 2022), Cyanotic congenital heart disease (Zhu et al. 2022; Fan et al. 2019)
miRNA-486-3p	AVS (Patel et al. 2015), CAD (Wei et al. 2016)
miRNA-342-5p	CAD (Ahmadi et al. 2018), Atherosclerosis (Wei et al. 2013)
Let-7g-3p	Atherosclerosis (Mo et al. 2022)

Using Taqman qPCR, I validated distinct miRNA expression profiles in IEVs and sEVs isolated from the aortic valve of patients with AVS compared to AI control sample (Figure 15 and 16). The data indicated significantly increased expression of miRNA-150-5p in the AVS-IEVs compared to control samples. However, the expression level of miR-486-5p, miR-486-3p were not significantly changed in IEV group of study (Figure 15). Let-7c-5p and miRNA-30b-5p were significantly decreased in AVS-sEVs compared to AI-sEVs while the expression level of miR-486-5p, miR-486-3p, miR-342-5p, and Let-7g-3p were not significantly changed in this group of study (Figure 16).

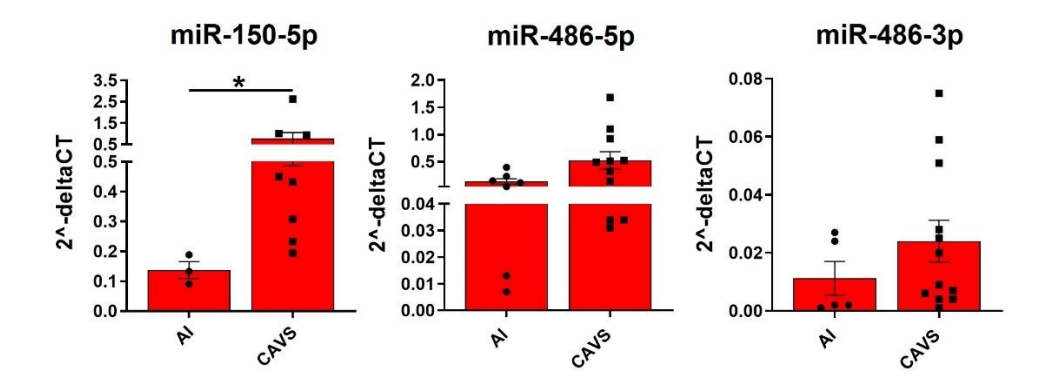


Figure 15. IEV-miRNA validation.

Taqman qPCR was conducted and normalized to the endogenous control U6 snRNA. Due to patient variabilities, some samples were identified as outliers, resulting in final sample sizes of AVS (Aortic Valve Stenosis; n=8-12) and AI (n=3-7). Statistical analysis was performed using Student's t-test. \*p < 0.05.

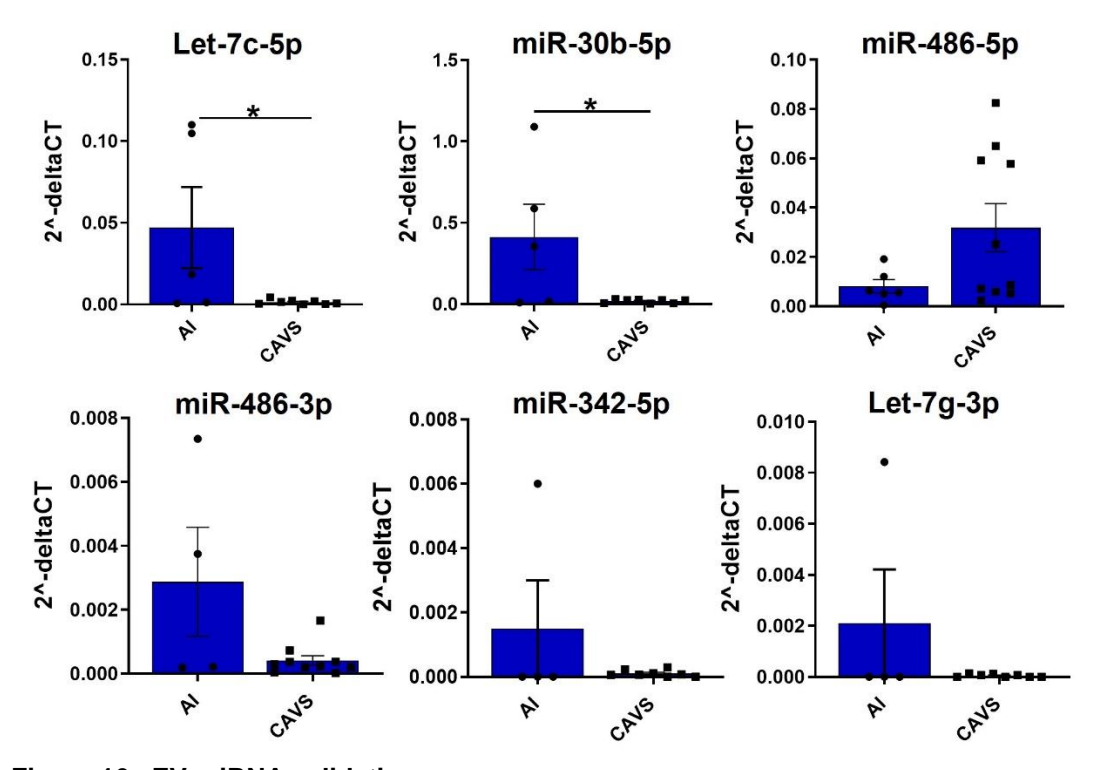


Figure 16.sEV-miRNA validation.

TaqMan qPCR was performed, and U6 snRNA was used for normalization (AVS=8-10 and Al=3-6). Statistical analysis was conducted using Student's t-test. \*p < 0.05.

#### 3.2. Effects of Candidate miRNAs in VECs

#### 3.2.1. Characterization of VECs and their assessments for VIC contamination

I characterized commercially purchased VECs from Lonza company to assess their endothelial identity and evaluate potential VIC contamination. To achieve this, Lonza

VICs were used as a control for comparison, and the expression levels of endothelial and VIC markers were examined using qPCR and immunofluorescence.

The microscopic picture showed a flattened and cobblestone-like morphology for VECs and an elongated fibroblastic morphology for VICs (Figure 17A). The qPCR data demonstrated high expression level of endothelial markers such as *PECAM1/CD31* and *VWF* and lower expression level of *ACTA2* in VECs compared to VICs (Figure 17B). To further validate the qPCR data, Immunofluorescence staining was performed showing positive fluorescent signal for vWF and CD31 and the absence of ACTA2 in VECs, while VICs showed positive signals for ACTA2 and an absence of vWF and CD31(Figure 17C).

Taken together, these data indicated that VECs were effectively isolated from the human aortic valve. Therefore, VECs could be reliably utilized for further experiments.

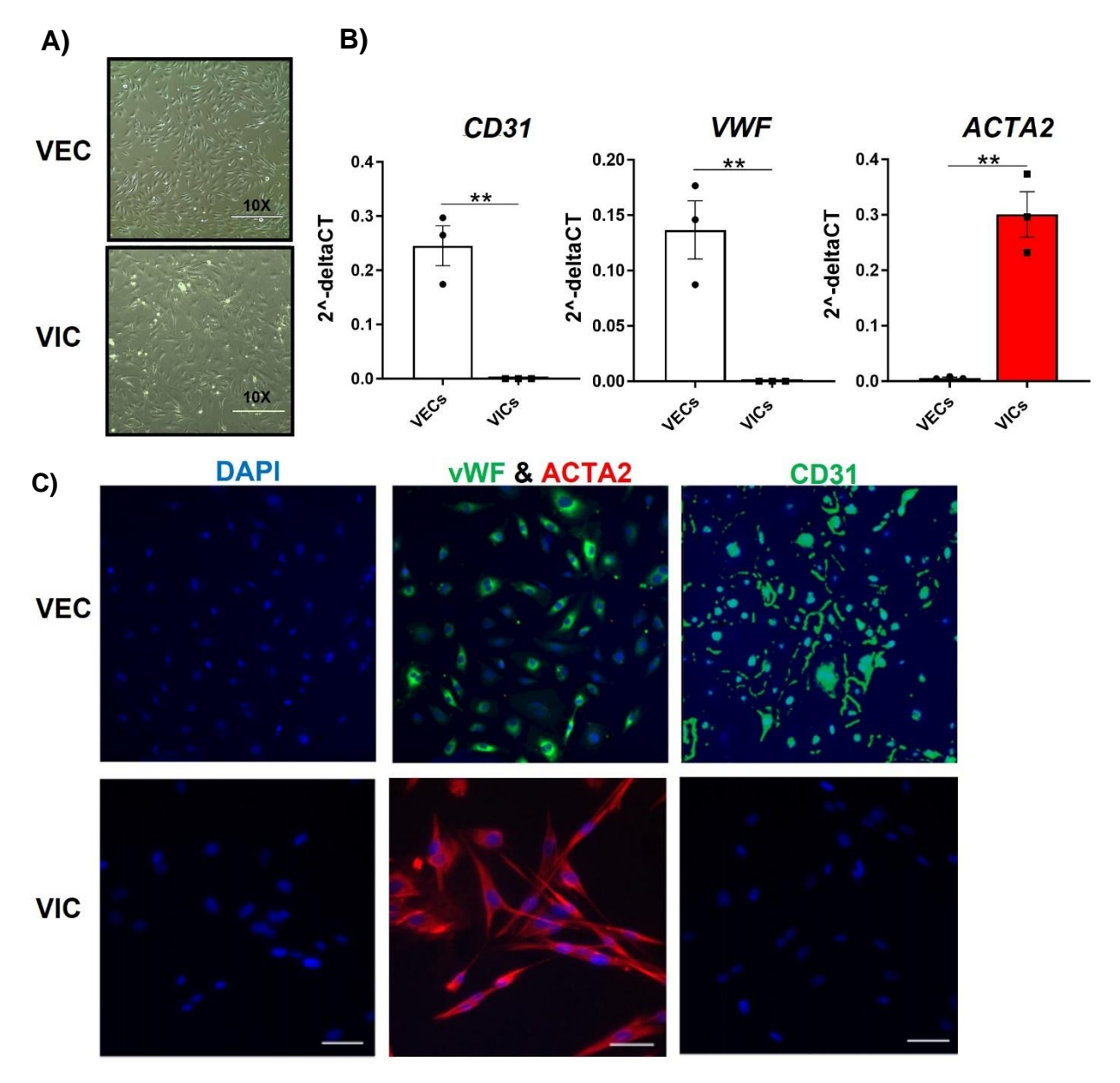


Figure 17. VEC Characterization.

**A)** The morphology of VECs and VICs under the microscope showed a flattened and cobblestone-like morphology for VECs and a fibroblastic morphology for VICs. **B)** qPCR validation of VEC showed higher expression of *CD31* and *VWF* and decreased expression level of *ACTA2* in VECs compared to VICs (n=3). **C)** Representative immunofluorescence staining of VECs showed the positive fluorescent signal for CD31 and vWF and the absence of ACTA2 in VECs, while VICs were positive for ACTA2 and negative for CD31 and vWF; DAPI (blue), vWF (green), ACTA2 (red), and CD31 (green), (n=3). \*p < 0.05, \*\*p < 0.01, \*\*\*p < 0.001, analyzed by Student's t-test.

#### 3.2.2. TNF $\alpha$ is the potent inducer of EndMT in VECs

To investigate the underlying mechanisms of AVS, EndMT model in VECs was established by treating VECs with several cytokines including TGF- $\beta$ 1, BMP2, IL-1 $\beta$  and TNF $\alpha$  to assess their potency. For this, VECs were treated with 10ng/ml TGF- $\beta$ 1, 50ng/ml

BMP2, 10ng/ml IL-1 $\beta$  and 25ng/ml TNF $\alpha$  for 7 days and the cell culture medium was changed every other day.

The microscopic results showed VECs treated with IL-1 $\beta$  and TNF $\alpha$  acquired a prominent spindle-shaped phenotype, indicative of EndMT induction (Figure 18). In contrast, the morphology of VECs treated with TGF- $\beta$ 1 and BMP2 did not show changes compared to untreated control cells (Figure 18).

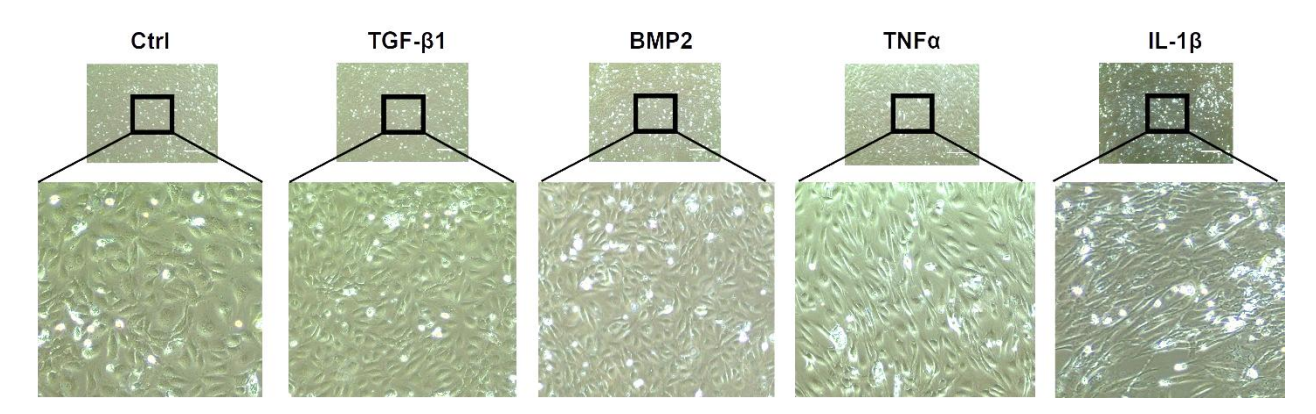


Figure 18. Morphology of VECs in EndMT model. VECs were treated with 10ng/ml TGF- $\beta$ 1, 50ng/ml BMP2, 10ng/ml IL-1 $\beta$  and 25ng/ml TNF $\alpha$  for 7 days. VECs treated with TNF $\alpha$  and IL-1 $\beta$  showed a mesenchymal morphology compared to the control cells in the EndMT model. Other cytokines did not change the morphology of VECs (n=3).

To further validate these observations, I analyzed the gene expression pattern of specific EndMT markers including vWF, ACTA2, SLUG and VIM in VECs (Figure 19). The qPCR data showed that TNF $\alpha$  decreased the expression level of endothelial marker *VWF* and increased the expression levels of mesenchymal markers such as *ACTA2* and *VIM* and EndMT indicator *SLUG*, representing a robust induction of EndMT (Figure 19). IL-1 $\beta$  treatment resulted in the decrease of *VWF* and a significant increase of *SLUG*, while the expression level of *ACTA2* and *VIM* were not significantly changed (Figure 19). BMP2 treatment had no impacts on EndMT markers. Furthermore, TGF- $\beta$ 1 treated cells showed an upregulation of *VIM*, without significant changes in the expression levels of other EndMT markers including *VWF*, *ACTA2* and *SLUG* (Figure 19). Taken together, these data showed that only TNF $\alpha$  can induce EndMT in VECs, but not IL-1 $\beta$ , BMP2 or TGF- $\beta$ 1 as evidenced by both morphological changes and gene expression alterations of EndMT markers (Figure 18 and Figure19). Therefore, TNF $\alpha$  was used to induce EndMT for further investigation of miRNAs in this study.

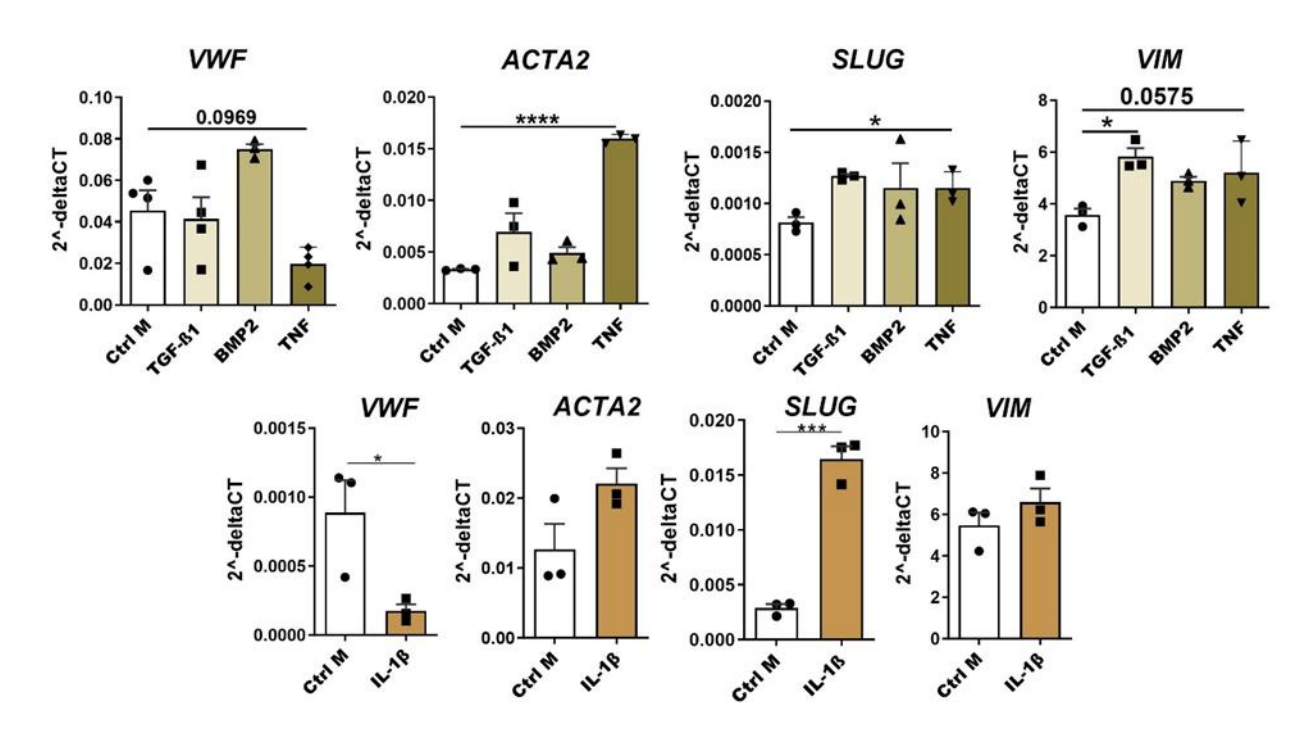


Figure 19. Gene expression levels of EndMT Markers treated with 10ng/ml TGF- $\beta$ 1, 50ng/ml BMP2, 10ng/ml IL-1 $\beta$  and 25ng/ml TNF $\alpha$  for 7 days.

VECs treated with TGF- $\beta$ 1 demonstrated an upregulation of *VIM* and no changes in the expression level of *VWF*, *ACTA2* and *SLUG*. BMP2 had no impacts on EndMT markers. VECs treated with TNFα showed the downregulation of *VWF* and the upregulation of *ACTA2*, *SLUG* and *VIM*. Similarly, IL-1 $\beta$  resulted in the downregulation of *VWF* and the increase of *SLUG* while had no effects on *ACTA2* and *VIM* (n=3). \*p < 0.05 \*\*p < 0.01, \*\*\*\*p < 0.001, \*\*\*\*\*p < 0.0001 as indicated, determined by one-way ANOVA and Student's t-test.

#### 3.2.3. hsa-miRNA-150-5p reduces EndMT in VECs treated with TNFα

The sequencing analysis and following Taqman qPCR revealed that IEV-miRNA-150-5p, sEV-Let-7c and sEV-miR-30b-5p were significantly dysregulated in patients with AVS. To clarify the role of these miRNAs in EndMT, I investigated whether the overexpression of these miRNAs can influence EndMT in VECs. Therefore, VECs were treated with lentivirus to overexpress miRNA-150-5p, Let-7c and miR-30b-5p, and validated their overexpression by qPCR (Figure 20). As a negative control, VECs were also transduced with the same lentivirus vector without miRNA, showing no significant effects on the expression levels of miRNA candidates (Figure 20).

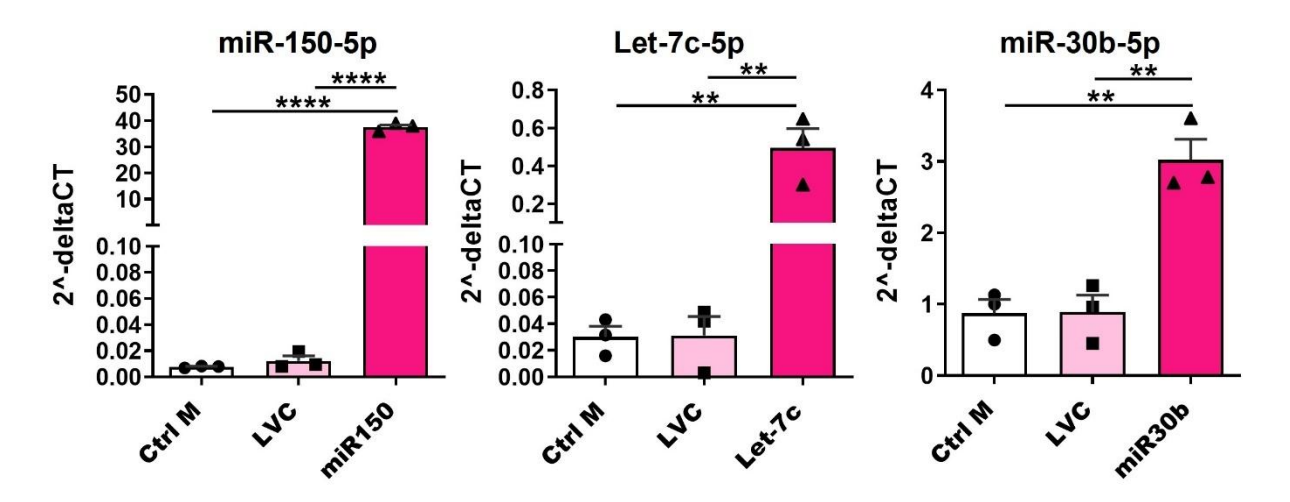


Figure 20. Validation of miRNAs overexpression in VECs after transduction. The qPCR analysis showed the overexpression of miRNA-150-5p, Let-7c-5p and miRNA-30b-5p in VECs transduced with lentiviruses (n=3). \*p < 0.05 \*\*p < 0.01, \*\*\*p < 0.001, \*\*\*\*p < 0.001 as indicated, determined by one-way ANOVA.

After confirming the miRNA overexpression in VECs, cells were treated with TNF $\alpha$  for 7 days to induce EndMT.

The overexpression of miRNA-150-5p in VECs treated with TNF $\alpha$  resulted in a significant increase in *VWF* and a reduction in the expression levels of *ACTA2*, *SLUG*, and *VIM* compared to non-transduced cells and control vector (Figure 21). These findings suggest that miRNA-150-5p might reduce EndMT in VECs. Furthermore, VECs transduced with Let-7c-5p showed a significant increase in the expression level of *ACTA2*, while it had no significant effects on the expression levels of *VWF*, *SLUG* and *VIM*. Similarly, miR-30b-5p significantly reduced the expression level of *VIM* but had no impacts on the other EndMT markers in VECs treated with TNF $\alpha$  (Figure 22). In line with the gene expression analysis, the phase contrast images of VECs treated with TNF $\alpha$  showed that VECs transduced with the lentivirus overexpressing miRNA-150-5p exhibited a cobblestone-like morphology, reflecting endothelial characteristics. However, VECs transduced with Let-7c-5p and miR-30b-5p maintained a spindle-like mesenchymal morphology, similar to control cells (Figure 23).

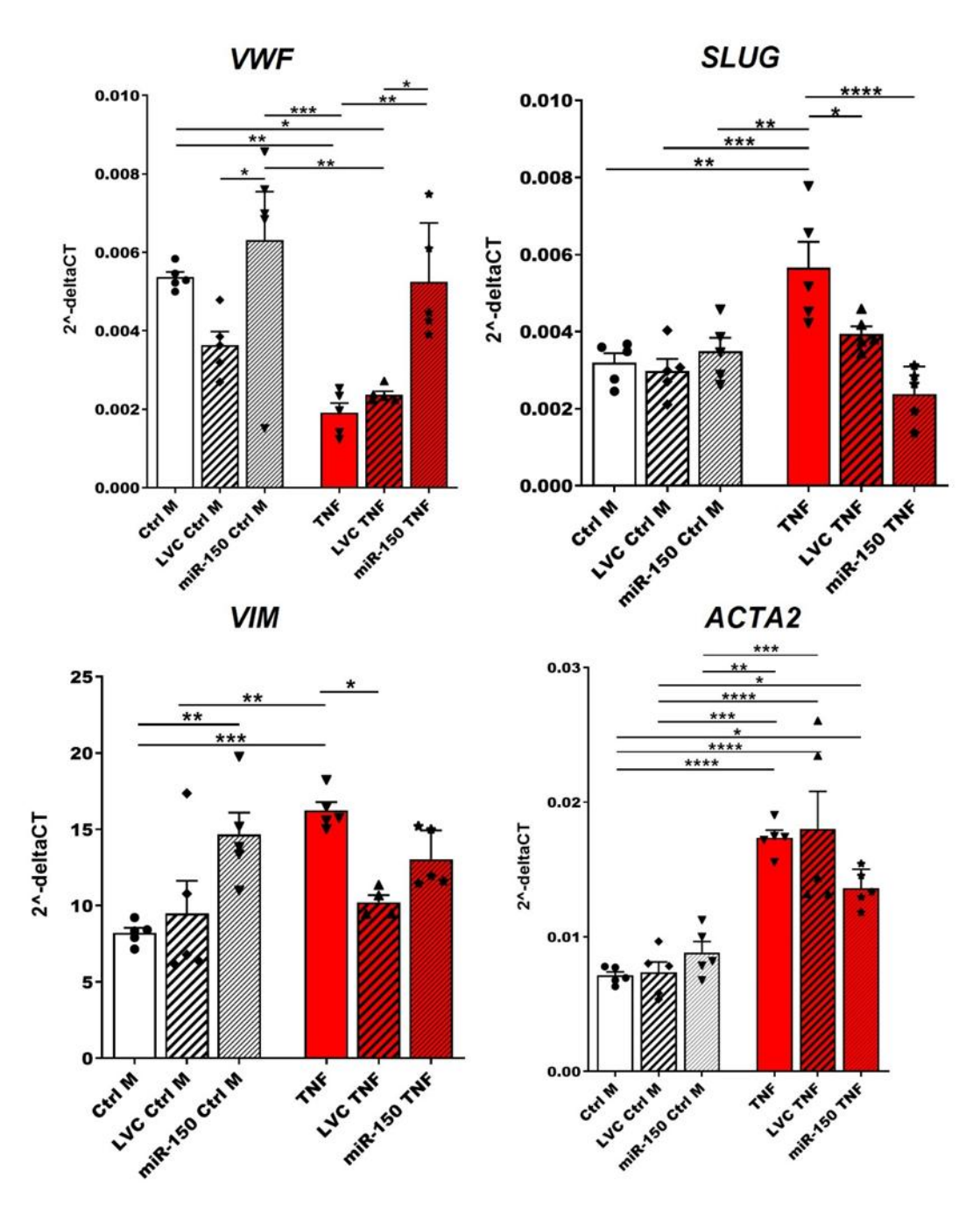


Figure 21. EndMT markers in VECs overexpressing miRNA-150-5p and treated with TNFα. VECs transduced with the lentivirus overexpressing miRNA-50-5p showed that this miRNA significantly increased the expression level of VWF and reduced the expression levels of ACTA2, SLUG and VIM in VECs (n=5). \*p < 0.05, \*\*p < 0.01, \*\*\*p < 0.001, one-way ANOVA.

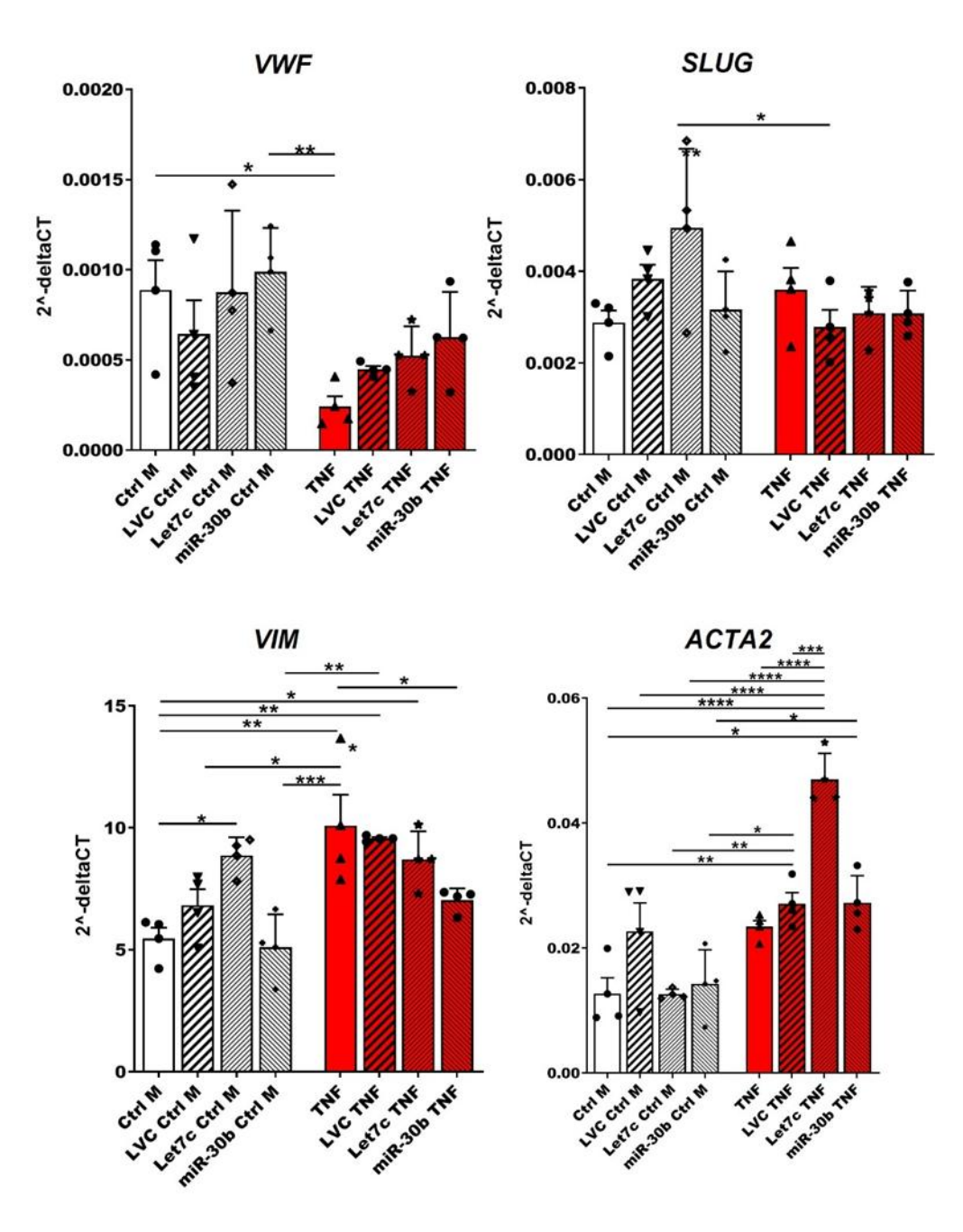


Figure 22. EndMT markers in VECs overexpressing Let-7c-5p and miRNA-30b-5p and treated with TNF $\alpha$ .

VECs transduced with Let-7c-5p showed increased expression levels of *ACTA2*, but had no effects on *VWF*, *SLUG* or *VIM*. MiRNA-30b-5p significantly reduced the expression level of *VIM*, but had no significant effects on *VWF*, *SLUG* and *ACTA2* in VECs (n=4). \*p < 0.05, \*\*p < 0.01, \*\*\*p < 0.001, one-way ANOVA.

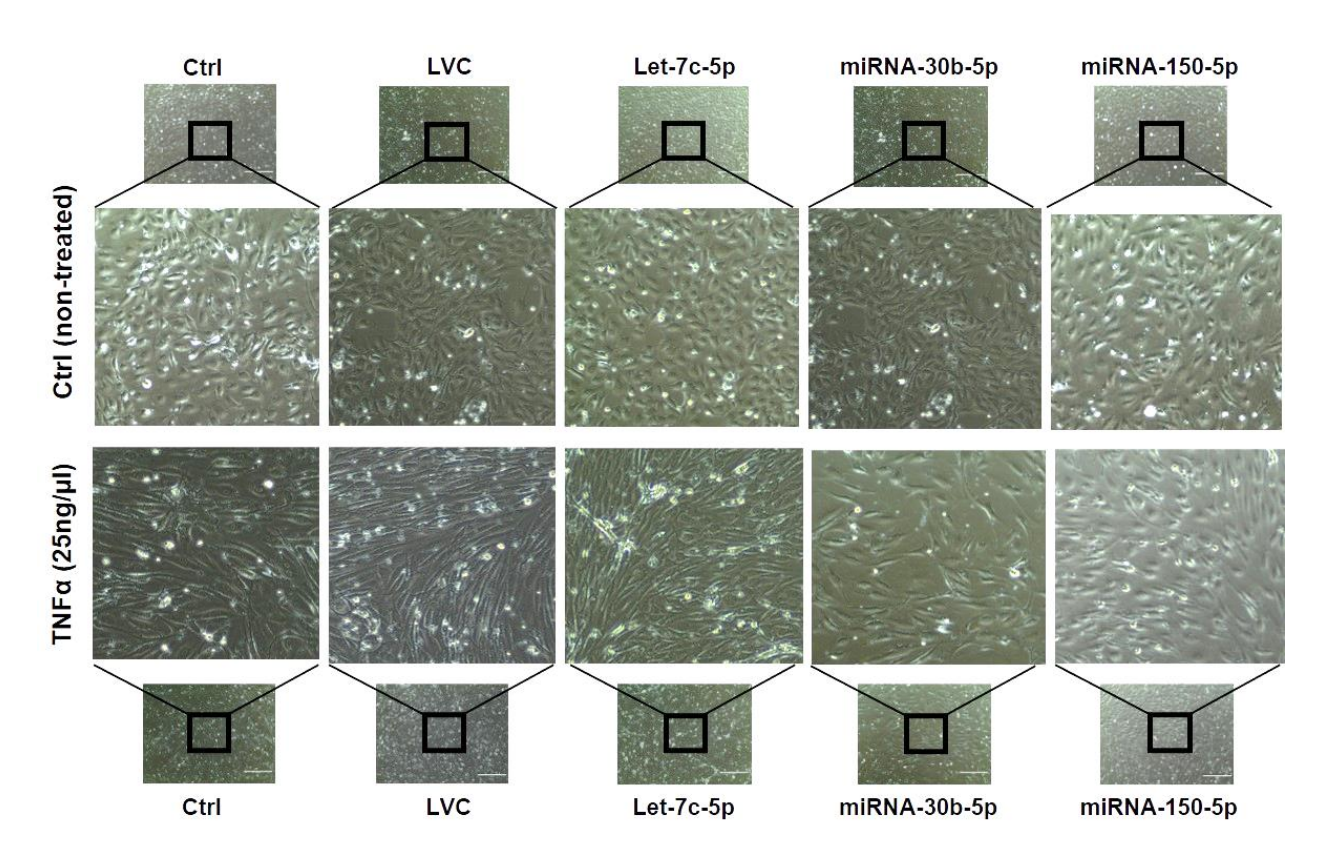


Figure 23. Microscopic images of VECs overexpressing miRNA-150-5p, Let-7c-5p, and miR-30b-5p after and before the TNFα treatment to induce EndMT (n=3).

#### 3.2.4. hsa-miRNA-150 increases tube formation in VECs

Next, the functional effects of miRNA-150-5p on VECs through tube formation and migration assay were investigated, as normal endothelial function is characterized by a quiescent cell phenotype with non-proliferative and non-migratory behavior, along with angiogenic capability. To assess the role of miRNA-150-5p in tube formation, I performed Matrigel-based tube formation assay using VECs transduced with the lentivirus overexpressing miRNA-150-5p to assess if this miRNA plays a role in tube formation capabilities of VECs. Compared to control cells, miRNA-150-5p enhanced the angiogenesis as evidenced by an increase of the number and the length of tubes compared to the control cells (Figure 24).

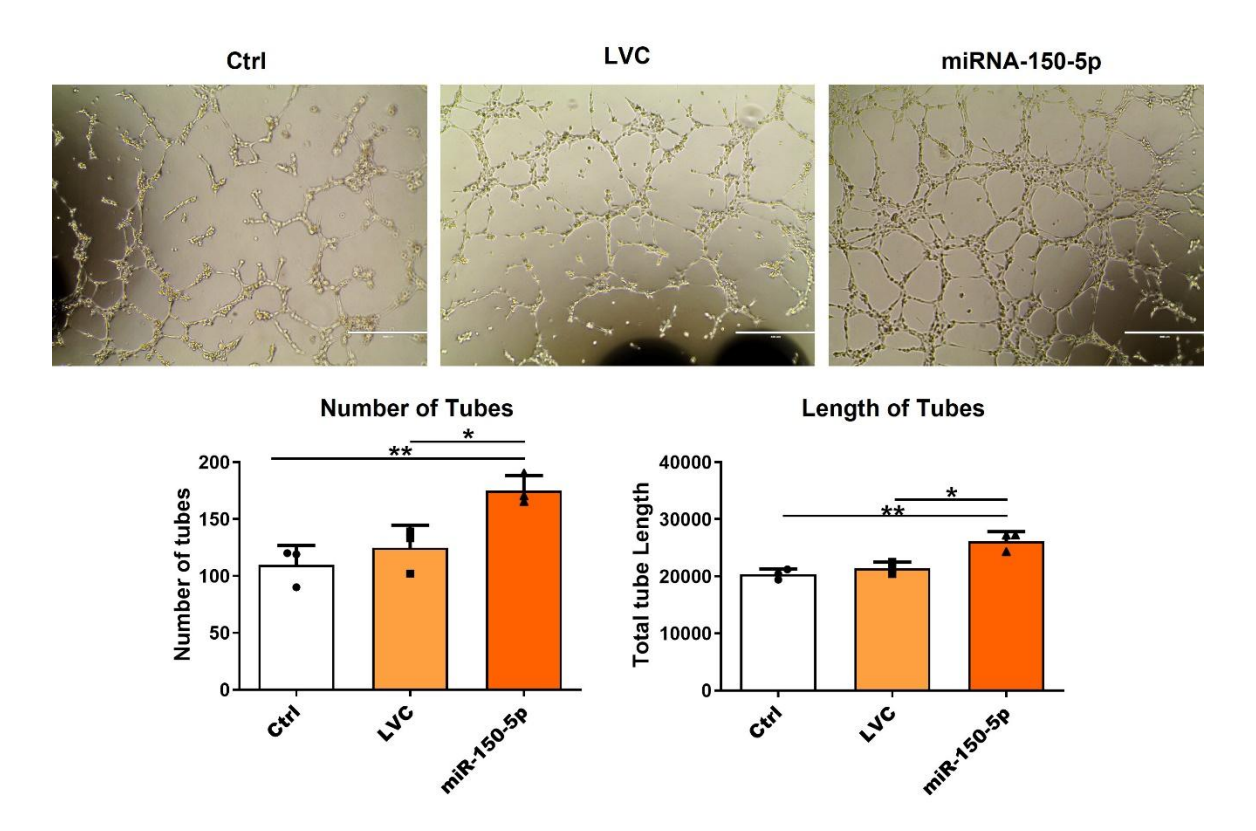


Figure 24. Effects of miRNA-150-5p on tube formation of VECs. VECs were allowed to form tube-like structures on a collagen gel for 4h. Microscopic pictures and quantified data showed an increased number of tubes and their length in VECs transduced with the lentivirus overexpressing miRNA-150-5p compared to LVC and non-transduced VECs (n=3).  $^*p < 0.05$ ,  $^*p < 0.01$ , one-way ANOVA.

### 3.2.5. hsa-miRNA-150-5p inhibits cell migration in VECs

As EC dysfunction and resulting enhanced cell migration are implicated in pathophysiology of AVS (Kovacic et al. 2019), I further explored the effects of miRNA-150-5p on VEC migration using a wound healing assay at different time points (0h, 6h, and 12h). Particularly, miRNA-150-5p significantly decreased the VEC migration compared to cells transduced with LVC and non-transduced control cells (Figure 25). These results suggested that miRNA-150-5p plays an important role in maintaining the endothelial phenotype, enhancing angiogenesis, and modulating cell migration.

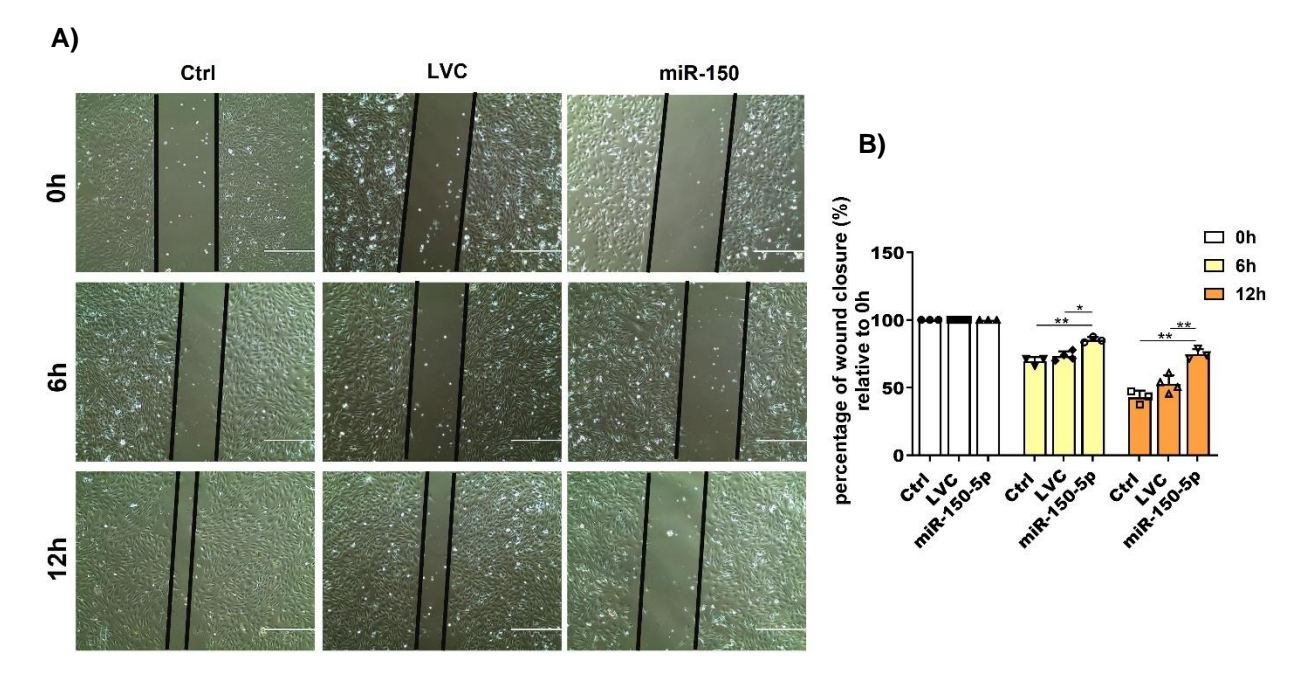


Figure 25. Effect of miRNA-150-5p on migration ability of VECs. A) Representative images of VECs transduced with the lentivirus overexpressing miRNA-150-5p and scratch assay at 0h,6h and 12 h (n=3). B) Wound closure was quantified at 0h, 6h and 12h (n=3).  $^*p < 0.05$ ,  $^{**}p < 0.01$ , one-way ANOVA.

# 3.2.6. hsa-miRNA-150-5p is expressed in VECs isolated from both aortic and ventricular sides of aortic valve

The aortic valve endothelium exhibits heterogeneity, primarily attributed to distinct blood flow patterns experienced on its two sides. The ventricular side is exposed to higher laminar flow, while the aortic side experiences low oscillatory shear stress. These differential flow patterns have the potential to influence the morphology and the gene expression of VECs on the aortic and ventricular sides (Deb et al. 2021). Concerning this heterogeneity, I investigated the expression level of miRNA-150-5p in both sides of the aortic valve. For this, aortic valves were obtained following surgical operation, and the RNA was isolated from both sides using methods described in chapter 2.7.4. (Simmons et al. 2004). The list of patients is provided in Table 32.

Table 32. Baseline patient characteristics.

Group	Side	Type of valve	Age (years)	SEX	Other Medical history
AVS-1	Valvular side	Bicuspid	53	М	Hypertension, Hyperlipidemia
AVS-2	Valvular side	Tricuspid	72	М	Hyperlipidemia, Diabetes
AVS-3	Valvular side	Tricuspid	68	М	Nicotine abuse, Atrial fibrillation
AVS-4	Aortic side	Tricuspid	58	М	Hypertension
AVS-5	Aortic side	Tricuspid	68	М	Nicotine abuse, Atrial fibrillation

AVS-6	Aortic side	Tricuspid	68	М	Hypertension, Hyperlipidemia, Diabetes

These data revealed that miRNA-150-5p is expressed from both aortic and ventricular sides of aortic valve with no statistically significant differences observed between these two sides (Figure 26).

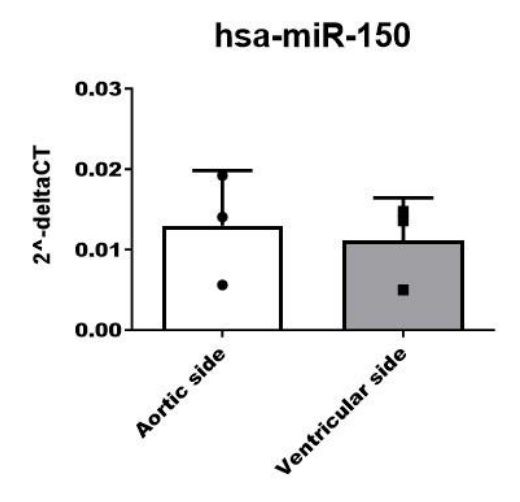


Figure 26. qPCR analysis of miRNA-150-5p expression on aortic and ventricular sides of the aortic valve showing the similar expression level of miRNA-150-5p in both regions (n=3). Statistical analysis was performed using Student's t-test.

### 3.2.7. hsa-miRNA-150-5p expression is increased under laminar shear stress

Fluid shear stress plays a crucial role in stabilizing endothelial quiescence, where areas with disturbed flow promote a less stable, activated, and dysfunctional endothelial phenotype, making them more susceptible to inflammation and disease. (Kant et al. 2022). Therefore, I exposed VECs to laminar flow and investigated the expression pattern of shear sensitive genes and miRNA-150-5p.

For this, I cultured VECs under shear stress levels of 20dyn/cm<sup>2</sup> for 24h using ibidi pump system. The microscopic picture revealed the parallel alignment of VECs to the direction of flow compared to control VECs cultured without flow (Figure 27).

## **Static**

### **Laminar Shear Stress**



Flow Direction: -->

Figure 27. representative microscopic picture of VECs cultured under laminar flow and static condition.

VECs exposed to laminar flow at 20dyn/cm<sup>2</sup> for 24h (right picture) aligned in the direction of flow compared to VECs cultured in static condition (left picture) (n=3).

Afterwards, I analyzed the expression level of shear sensitive genes including Krueppellike factor (*KLF*) 2, *KLF4* and *VCAM-1*. The qPCR analysis showed the overexpression of *KLF2* and *KLF4* known as protective genes for ECs against inflammation under the laminar flow and downregulation of their target genes *VCAM-1*, reflecting the protective effects of laminar flow in VECs (Ohnesorge et al. 2010b) (Figure 28).

Furthermore, miRNA profile of VECs was investigated under static and laminar flow conditions using a miRNA array. The miRNA array data revealed that miRNA-150-5p is among the top highly upregulated miRNAs in VECs exposed to 20dyn/cm² shear stress, which was further validated by Taqman qPCR (Figure 29). These findings suggest that miRNA-150-5p might play a protective role in preserving VEC function under the laminar flow.

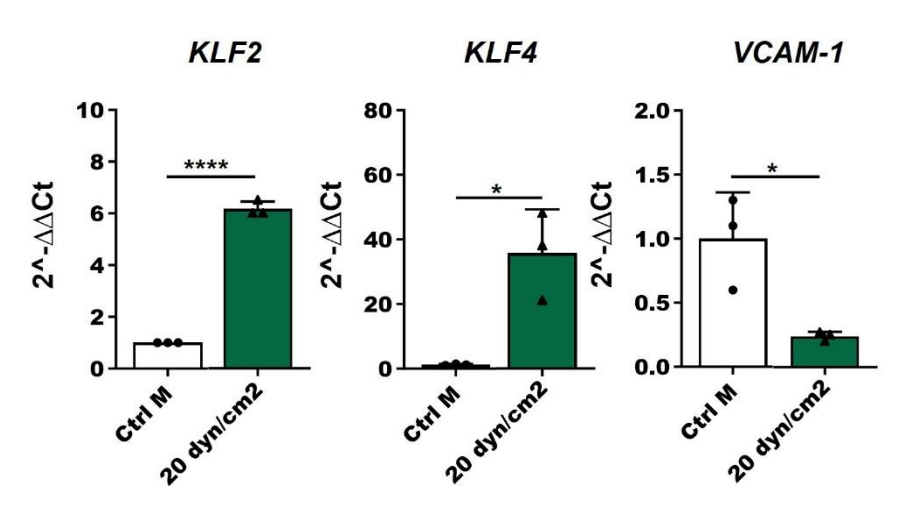
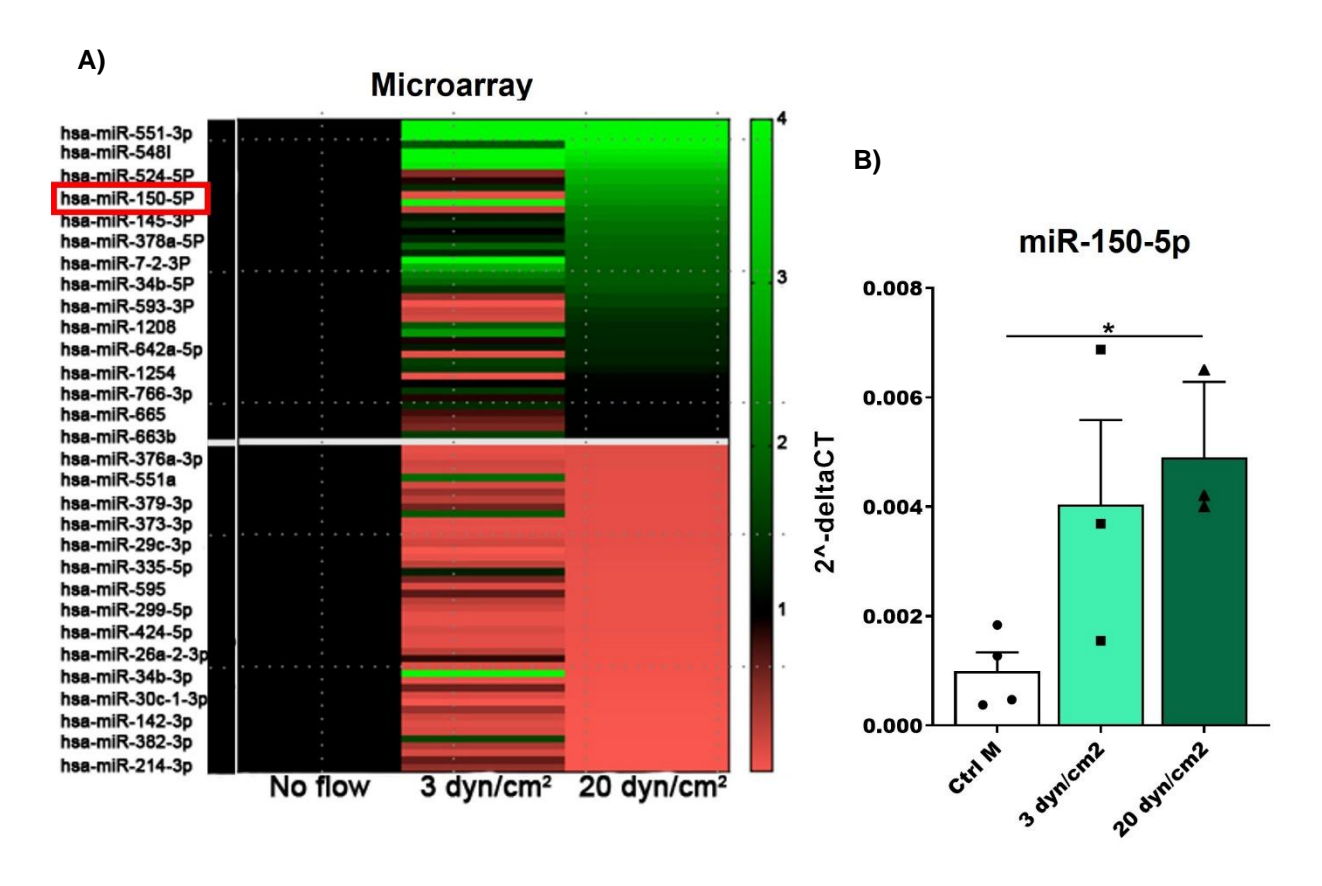


Figure 28. Gene expression pattern of shear sensitive genes in VECs exposed to laminar flow 20 dyn/cm<sup>2</sup> for 24h.

RT-qPCR showed increased expression level of shear sensitive genes such as KLF2 and KLF4 and decreased expression level of their target gene VCAM-1 (n=3). \*p < 0.05, \*\*p < 0.01, \*\*\*p < 0.001, \*\*\*\*p < 0.0001, Student's t-test.



**Figure 29.** miRNA profiling in VECs exposed to laminar flow compared to control cells. **A)** Heatmap depicting differently expressed miRNAs in VECs cultured under the laminar flow rates of 3.6dyn/cm² and 20 dyn/cm² indicated the increased expression level of miRNA-150-5p (n=3). **B)** Validation of miRNA-150-5p overexpression in VECs cultured under 3.6dyn/cm² and 20dyn/cm² shear stress flow (n=3). \*\*p < 0.01, one-way ANOVA.

### 3.2.8. Co-incubation of Large EVs containing miRNA-150-5p with VECs

#### 3.2.8.1. Immortalization of VECs

To explore the crosstalk between cells via EVs in the context of AVS, I extended my investigations into EV studies. For these experiments, I generated Lonza immortalized VECs (I-VECs) as a source of EVs, enabling us to obtain a higher yield of EVs. Immortalization of VECs was performed by transducing the cells with the SV40 large T-antigen lentivirus. Microscopic pictures revealed a cobblestone-like morphology for I-VECs, similar to non-immortalized VECs (Figure 30A). qPCR data showed a significantly higher expression level of Large T antigen in I-VECs compared to the non-immortalized cells (Figure 30B). Besides, the proliferation assay using PrestoBlue indicated that I-VECs exhibited a higher proliferation rate starting from day 5 compared to non-immortalized VECs (Figure 30C). This successful immortalization of VECs allowed us to produce a larger quantity of EVs, which was crucial for the subsequent EV uptake experiments.

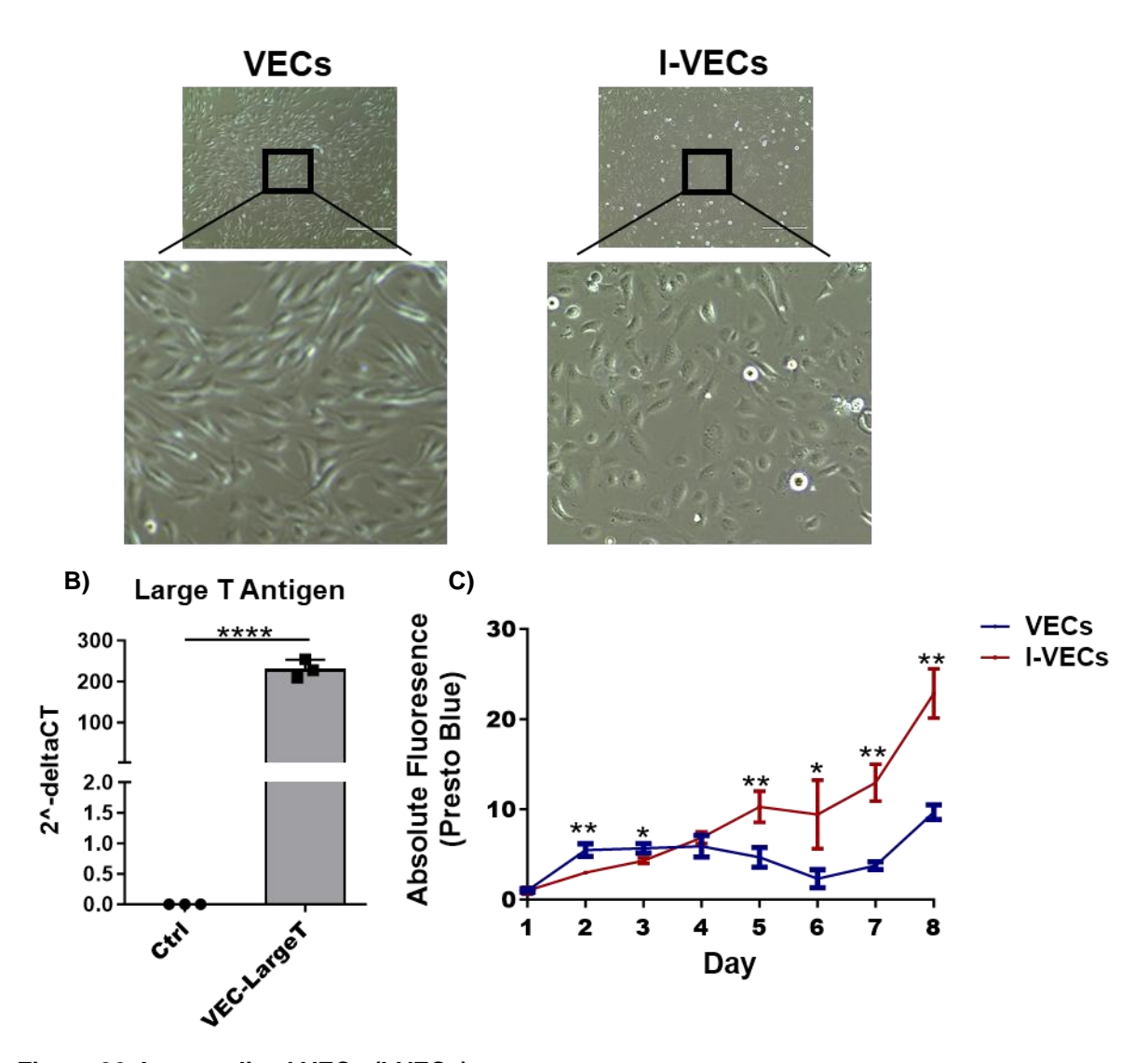
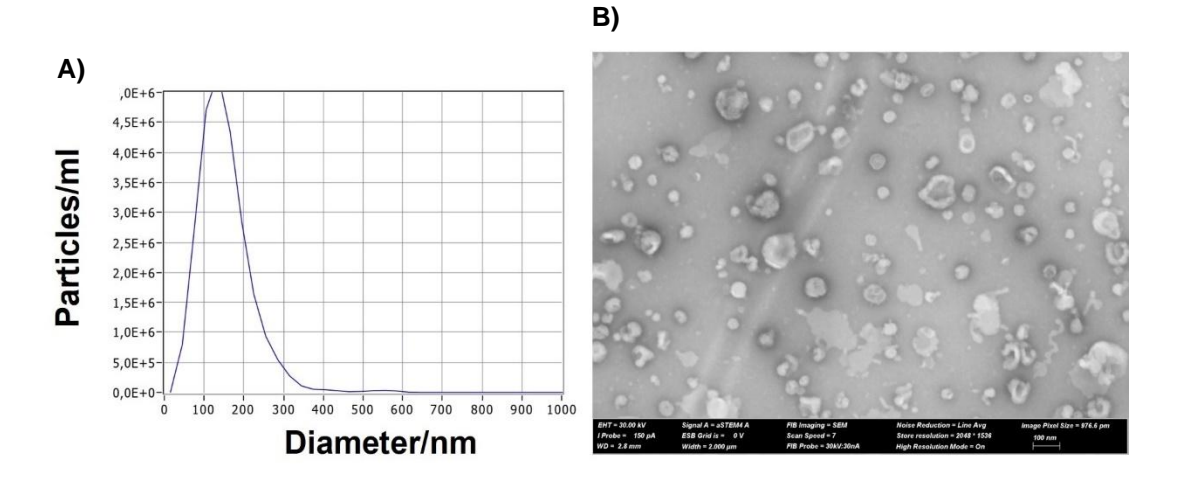


Figure 30. Immortalized VECs (I-VECs).

**A)** Representative microscopic image of non-trasnduced VECs (left) and immortalized VECs (I-VECs) (right), demonstrating the cobblestone-like morphology of both cell types. **B)** The expression level of large T antigen in immortalized VECs following transduction with SV40 Large T antigen lentivirus. C) The proliferation rate of I-VECs compared to the VECs measured by PrestoBlue proliferation assay. Statistical significance is indicated by \*p < 0.05, \*\*p < 0.01, \*\*\*p < 0.001, \*\*\*\*p < 0.0001 based on Student's t-test (n=3).

#### 3.2.8.2. IEV characterization

I-VECs were cultured in EV-depleted culture medium, and the medium was collected for IEV isolation. Serial centrifugation was performed to isolate IEVs as described in chapter 2.3.3. IEVs were subsequently resuspended in PBS and characterized by NTA and SEM. The NTA analysis provided insights into the size distribution of IEVs. The results showed that IEVs had an average size of 129 nm (Figure 31A). Furthermore, SEM depicted the presence of IEVs isolated from the culture medium of I-VECs (Figure 31B).



**Figure 31.** Characterization of IEVs isolated from immortalized VECs. **A)** Size distribution analysis of IEVs using NTA. **B)** SEM of IEV purified from the culture medium of I-VECs (n=3).

### 3.2.8.3. IEV-miRNA-150-5p is taken up and reduces EndMT in recipient VECs

To investigate the role of IEVs in intracellular communication, I aimed to co-incubate IEVs containing miRNA-150-5p with VECs in EndMT model. For this, I-VECs were transduced with the lentivirus to overexpress miRNA-150-5p and collected the medium for the IEV isolation. Subsequently, IEVs were labeled with PKH67 dye, a green fluorescent dye that binds to the lipid membrane of the vesicles. Afterwards, VECs were treated with IEVs for 24h, and uptake efficiency was assessed through fluorescence microscopy. The results revealed that EVs were taken up by recipient cells, as evidenced by the presence of labeled EVs within the VECs (Figure 32A). Besides, the qPCR analysis of the recipient VECs represented the increased expression level of miRNA-150-5p in recipient VECs (Figure 32B). These data confirmed that miRNA-150-5p was efficiently packaged into the IEVs and transferred sufficiently into the recipient VECs.

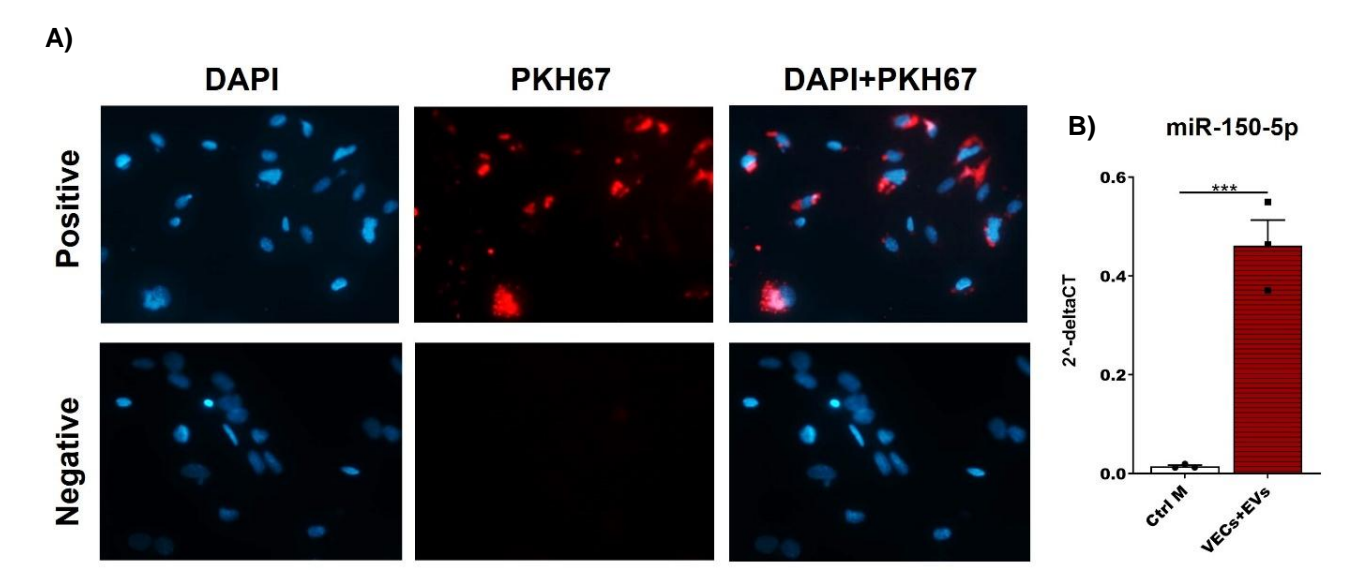


Figure 32. IEV uptake in VECs.

**A)** Representative fluorescence microscope images of VECs co-incubated with IEVs containing miRNA-150-5p for 24h, showing the uptake of IEVs by recipient VECs (n=3). IEVs were labeled with PKH67, a green fluorescent dye used for EV membrane labeling, to visualize their uptake. **B)** The qPCR analysis of miRNA-150-5p in VECs treated with IEVs derived from immortalized VECs, demonstrating a significant increase of miRNA-150-5p in recipient VECs (n=3). \*\*\*p < 0.001, Student's t-test.

After showing that miRNA-150-5p was transferred via IEVs into the recipient VECs, I assessed the impacts of IEVs-miRNA-150-5p on EndMT. For this, VECs were co-treated with IEVs containing miRNA-150-5p and TNF $\alpha$  to induce EndMT. This investigation revealed that the expression level of *VWF* was significantly increased in VECs treated IEVs-miRNA-150-5p while the expression level of *ACTA2*, and *VIM* was significantly reduced. The expression level of *SLUG* remained unchanged (Figure 33). These finding were in line with previous results (chapter 3.2.3.) in which transduced VECs with miRNA-150-5p reduced EndMT in VECs (Figure 21).

These findings strongly suggested that IEV-miRNA-150-5p could efficiently transfer into the VECs and mitigate the process of EndMT, indicating a protective role for VECs.

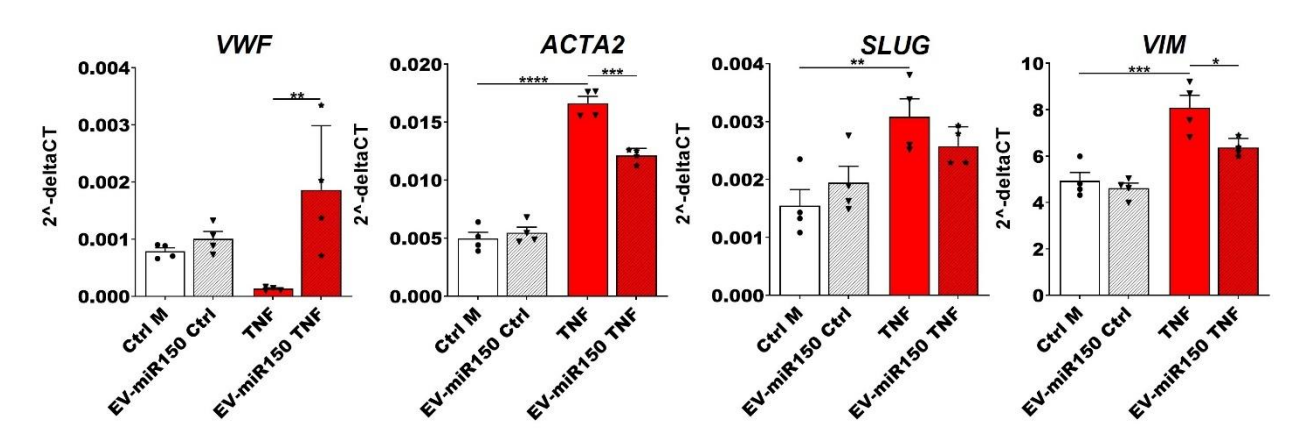


Figure 33. EndMT markers in VECs treated with IEVs containing increased level of miRNA-150 (n=4). Relative mRNA expression levels of EndMT markers including VWF, ACTA2, SLUG and VIM in VECs after the co-incubation of IEVs containing miRNA-150-5p with VECs in EndMT model. IEV-miRNA-150-5p significantly increased VWF and decreased ACTA2 and VIM. IEV-miRNA-150-5p showed no effects on SLUG (n=3). \*p < 0.05, \*\*p < 0.01, \*\*\*p < 0.001, one-way ANOVA.

### 3.2.9. Next generation sequencing of hsa-miRNA-150-5p target genes in VECs

# 3.2.9.1. mRNA sequencing identified dysregulated genes in VECs overexpressing miRNA-150-5p

To identify the potential target genes of miRNA-150-5p in VECs, sequencing was performed in VECs transduced with lentivirus overexpressing miRNA-150-5p, VECs transduced with control lentivirus and non-transduced VECs.

In total 14070, 14687 and 13245 genes were identified in non-transduced VECs, LVC-VECs and miRNA-150-5p-VECs, respectively. I performed PCA analysis to assess the gene expression patterns of study groups (Figure 34A). The PCA analysis showed the variance of 54.4% for PCA1 and 12.6% for PCA2, showing clearly distinguished groups of this study (Figure 34A). Hierarchical clustering heatmap analysis also showed the distinct expression pattern of genes within miRNA-150-5p-VEC, LVC-VEC and non-transduced VECs. The top 20 highly expressed genes are illustrated in Figure 34B. The heatmap analysis also confirmed the similar gene expression pattern between LVC and non-transduced VECs (Figure 34B). I analyzed dysregulated genes by volcano plot. The analysis identified 104 significantly upregulated genes and 247 significantly downregulated genes (|logFC|>1 and adj. p < 0.05) in VECs transduced with miRNA-150-5p compared to VECs transduced with LVC (Figure 34C).

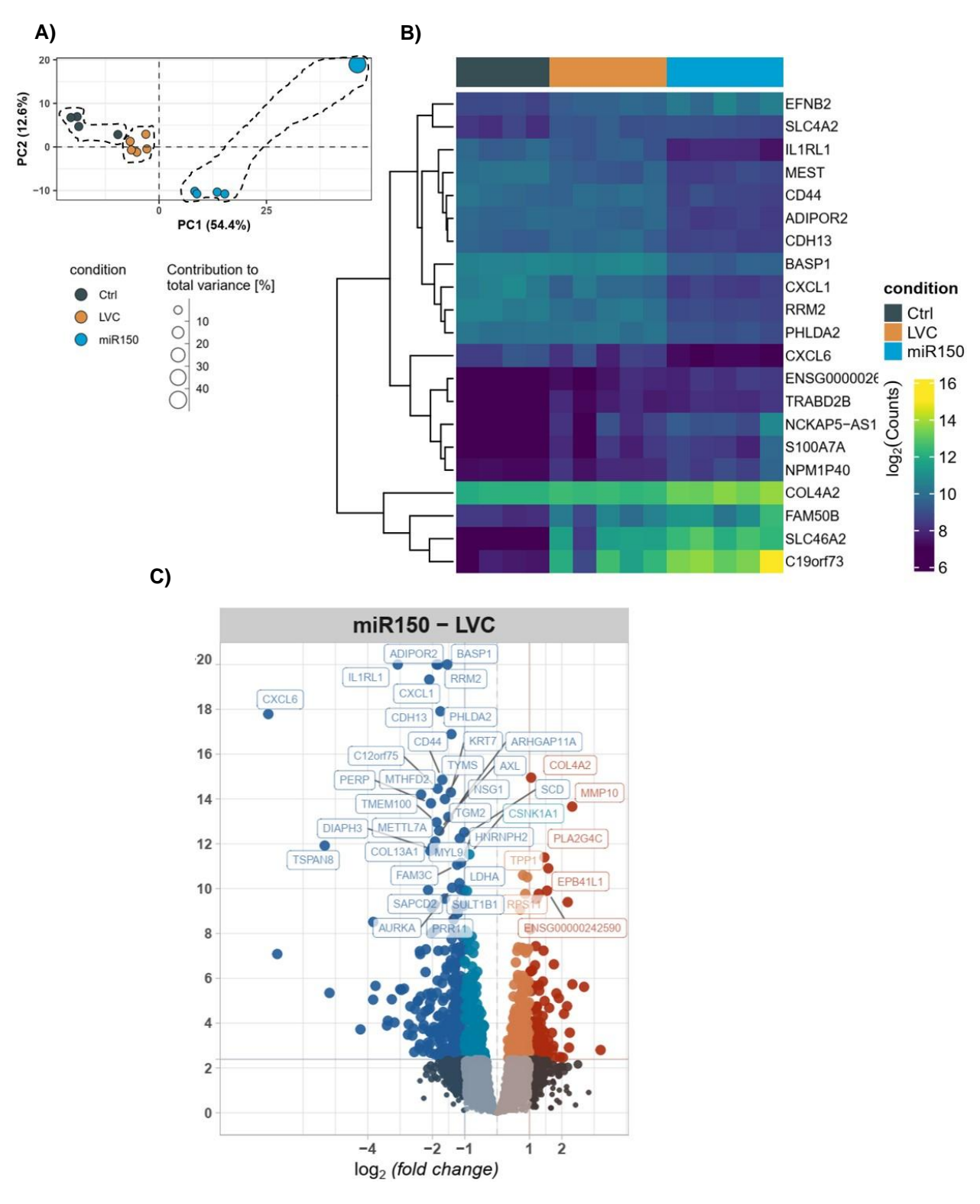


**Figure 34.** Representative figure of mRNA sequencing data in VECs overexpressing miRNA-150-5p. **A)** PCA analysis of genes identified in VECs overexpressing miRNA-150-5p. **B)** Hierarchical clustering heatmap gene expression profiles of 20 top highly expressed gens in control VECs, VECs transduced with LVC and VECs transduced with miRNA-150-5p. **C)** Volcano plot of differentially expressed genes in VECs overexpressing miRNA-150-5p compared to VECs transduced with LVC. |logFC|>1 and adj. p < 0.05.

### 3.2.9.2. GO analysis of differentially expressed miRNA-150-5p target genes

GO analysis was performed on significantly up- and downregulated genes (|log2FC|>1 and adj. p < 0.05) in VECs overexpressing miRNA-150-5p to gain deeper insights into their biological functions. For the upregulated genes, enrichment analysis of molecular functions revealed a significant enrichment in metalloendopeptidase activity, insulin like growth factor binding and protein tyrosine kinase binding (Figure 35). The involvement in the matrix remodeling and insulin like growth factor binding suggests that miRNA-150-5p regulates the composition and structure of the aortic valve as well as cell survival and proliferation, respectively. The analysis of cell component indicated a predominant presence of upregulated genes within collagen containing extracellular matrix, autolysosome and extracellular vesicles (Figure 35). Furthermore, biological process analysis showed that these upregulated genes are mainly involved in the extracellular structure organization, regulation of the ERK1 and ERK2 cascade, and the negative regulation of EMT (Figure 35). EMT is closely related to EndMT, and negative regulation of EMT aligns with the observed protective effect of miRNA-150-5p against EndMT in the previous experiments (section 3.2.3.). Additionally, KEGG signaling pathway analysis indicated that these genes contribute primarily to the RAS signaling, fluid shear sensitive and atherosclerosis and the VEGF signaling pathways (Figure 35). This suggests the pivotal role of miRNA-150-5p in valvular homeostasis, response to mechanical stress, and angiogenesis.

The molecular function analysis of downregulated genes showed that they mediate microtube and tubulin binding, metal ion binding, calcium ion binding and oxidoreductase activity (Figure 36). In the cellular component category, most genes were mainly found in spindle, microtubule cytoskeleton organization implicating their role in structural integrity of the aortic valve (Figure 36). Biological process analysis revealed that downregulated genes were positively regulate the cell cycle process and are involved in spindle and microtubule organization (Figure 36). Furthermore, KEGG signaling pathway indicated that downregulated genes were mainly involved in the cell cycle, ECM receptor interaction, P53 signaling pathways and AMPK signaling pathway suggesting their role in cell structural, apoptosis and metabolic regulation (Figure 36).

The data collectively provided valuable insights into potential mechanisms by which miRNA-150-5p exerts its protective effects in AVS. Further studies are warranted to functionally validate these findings. By elucidating the roles of these genes and pathways a deeper understanding can be gained regarding how miRNA-150-5p modulates VEC function and contributes to protective effects in AVS.

### Significantly Upregulated Genes

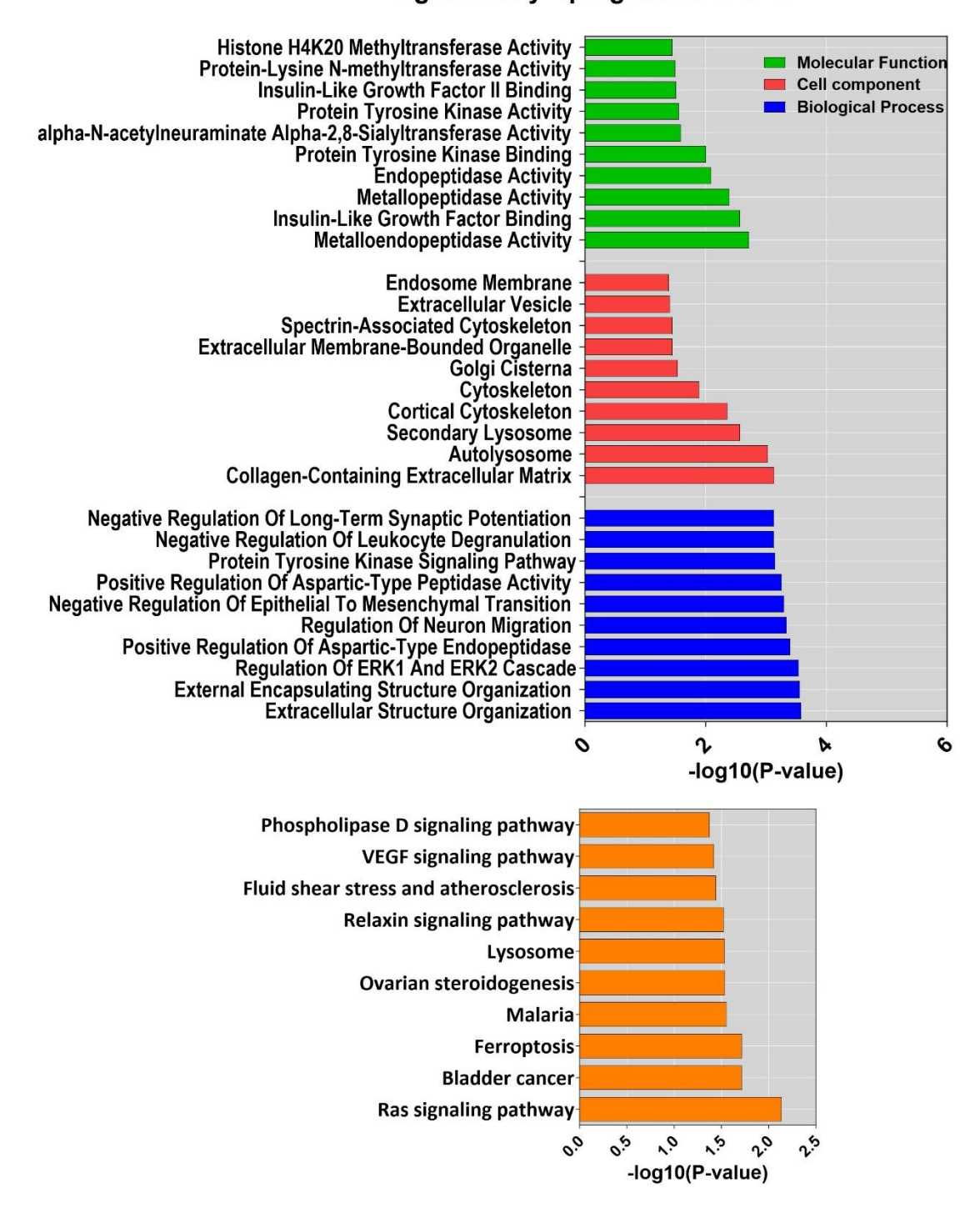


**Figure 35. Functional enrichment analysis of upregulated target genes of miRNA-150-5p. A)** GO analysis of upregulated target genes of miRNA-150 for the top 10 enriched GO terms in molecular function, cell component and biological process. **B)** KEGG pathway enrichment analysis of upregulated target genes of miRNA-150; higher -Log10 (p-value) indicates higher degrees of enrichment.

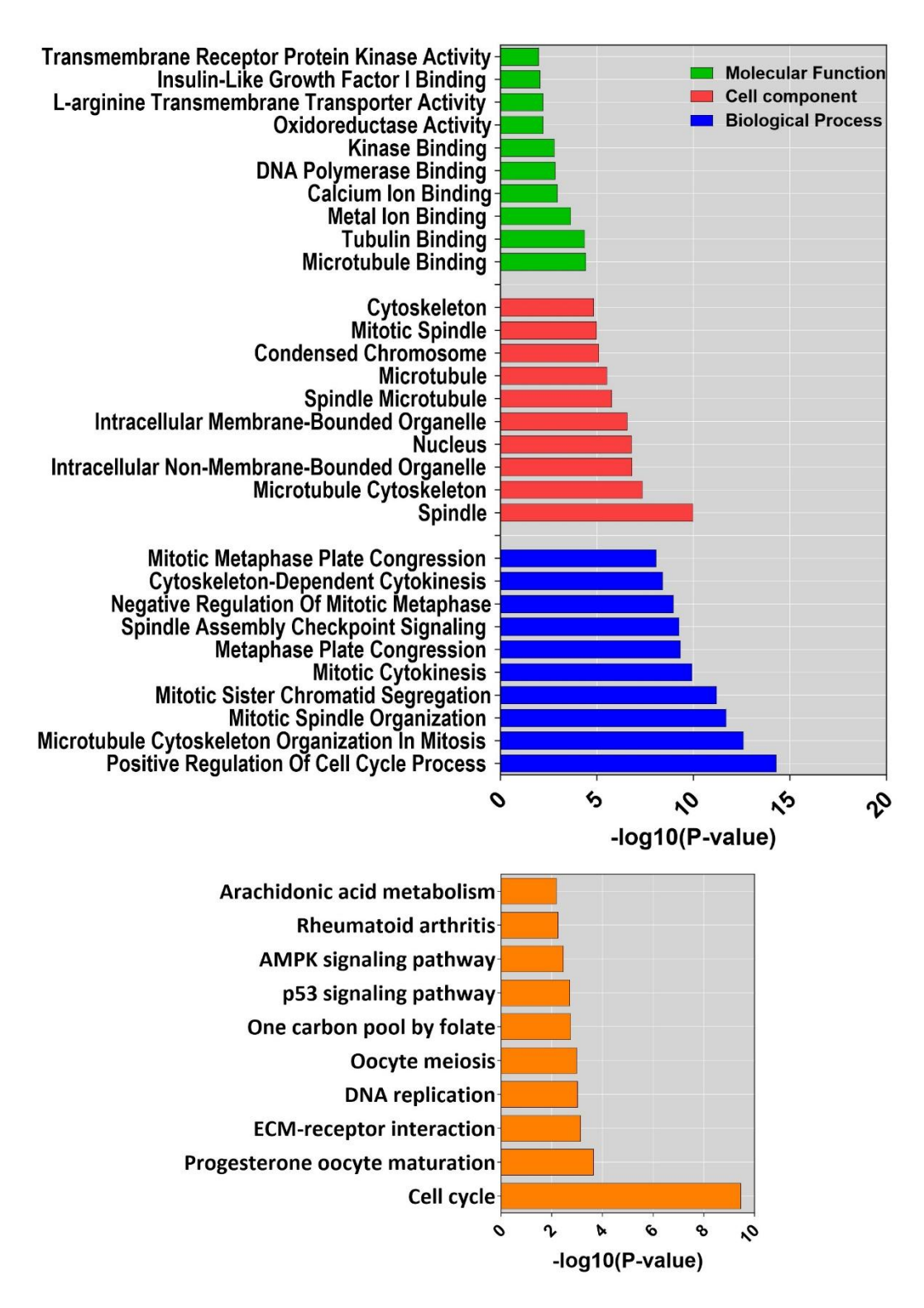


**Figure 36.** Functional enrichment analysis of downregulated target genes of miRNA-150-5p. **A)** GO analysis of downregulated target genes of miRNA-150 for the top 10 enriched GO terms in molecular function, cell component and biological process. **B)** KEGG pathway enrichment analysis of downregulated target genes of miRNA-150; higher -Log10 (p-value) indicates higher degrees of enrichment.

Next, I investigated the signaling pathways regulated by miRNA-150-5p in the context of EndMT. For this, I performed a literature review to list well-known signaling pathways relevant to EndMT. Afterwards, I compared these pathways with my identified KEGG signaling pathways (p < 0.1) of both upregulated and downregulated target genes of miRNA-150-5p. I found that the MAPK and VEGF signaling pathways were associated with EndMT in upregulated genes, and the ECM receptor signaling pathway and AMPK signaling pathway were relevant to EndMT in downregulated genes (Figure 37).

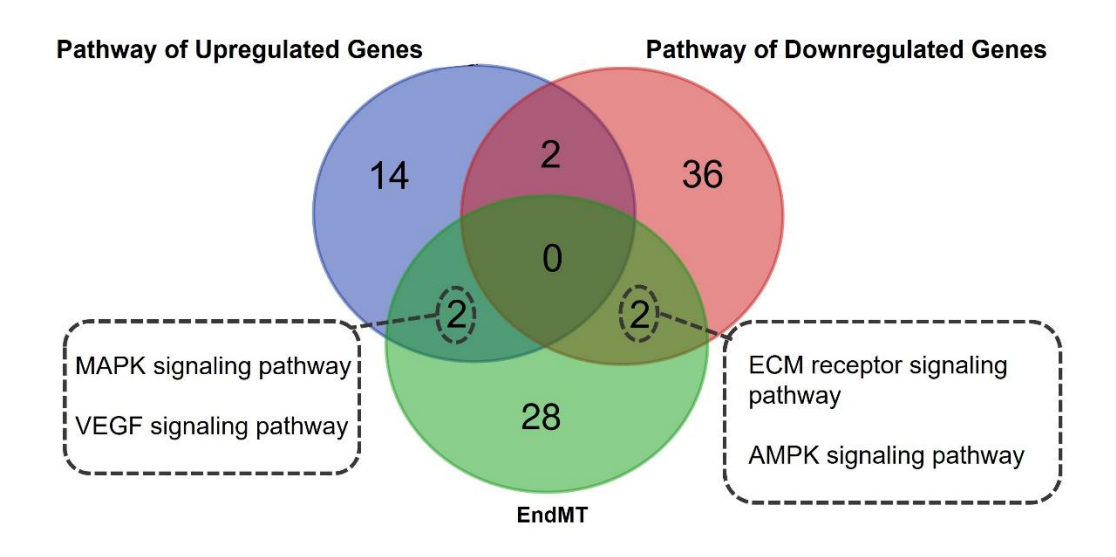


Figure 37. Venn diagram illustrating the signaling pathways associated with EndMT in both upregulated and downregulated target genes of miRNA-150-5p.

In the upregulated genes, the MAPK and VEGF signaling pathways demonstrated overlap with the well-established pathways associated with EndMT obtained from the literature. For the downregulated genes, the ECM receptor signaling pathway and AMPK signaling pathway displayed overlap with EndMT-relevant signaling pathways. The KEGG pathways are identified with a significance threshold of p < 0.1.

# 3.2.9.3. Protein-protein interaction (PPI) analysis and gene regulatory network (GRN) analysis

To gain deeper insight into the potential functional interactions of the genes associated with the signaling pathways identified by KEGG analysis (p < 0.1) (section 3.2.9.2.), I investigated the protein-protein interaction (PPI) and gene regulatory network (GRN) analyses using the NetworkAnalyst dataset. This analysis aimed to identify highly interacting genes (hub genes) within differentially expressed target genes.

The GRN analysis of upregulated genes revealed a total of 240 nodes, 499 edges and 15 hub genes (Figure 38A). Among genes with the highest interactions, *SHC2* (SHC adaptor protein 2) emerged as an EndMT-relevant gene involved in VEGF signaling pathway. Moreover, *EFNA1* (Ephrin A1) and *PLA2G4C* (Phospholipase A2 Group IVC)

were identified as EndMT-relevant genes associated with the MAPK signaling pathway (Figure 38A).

Additionally, the PPI analysis of upregulated genes revealed a total of 121 nodes, 29 edges and 8 hub proteins enriched by NetworkAnalyst (Figure 38B). Notably, among the top genes with the most interactions were SHC2 associated with VEGF signaling pathway, and EFNA1 and INSR (Insulin receptor) associated with the MAPK signaling pathway (Figure 38B).

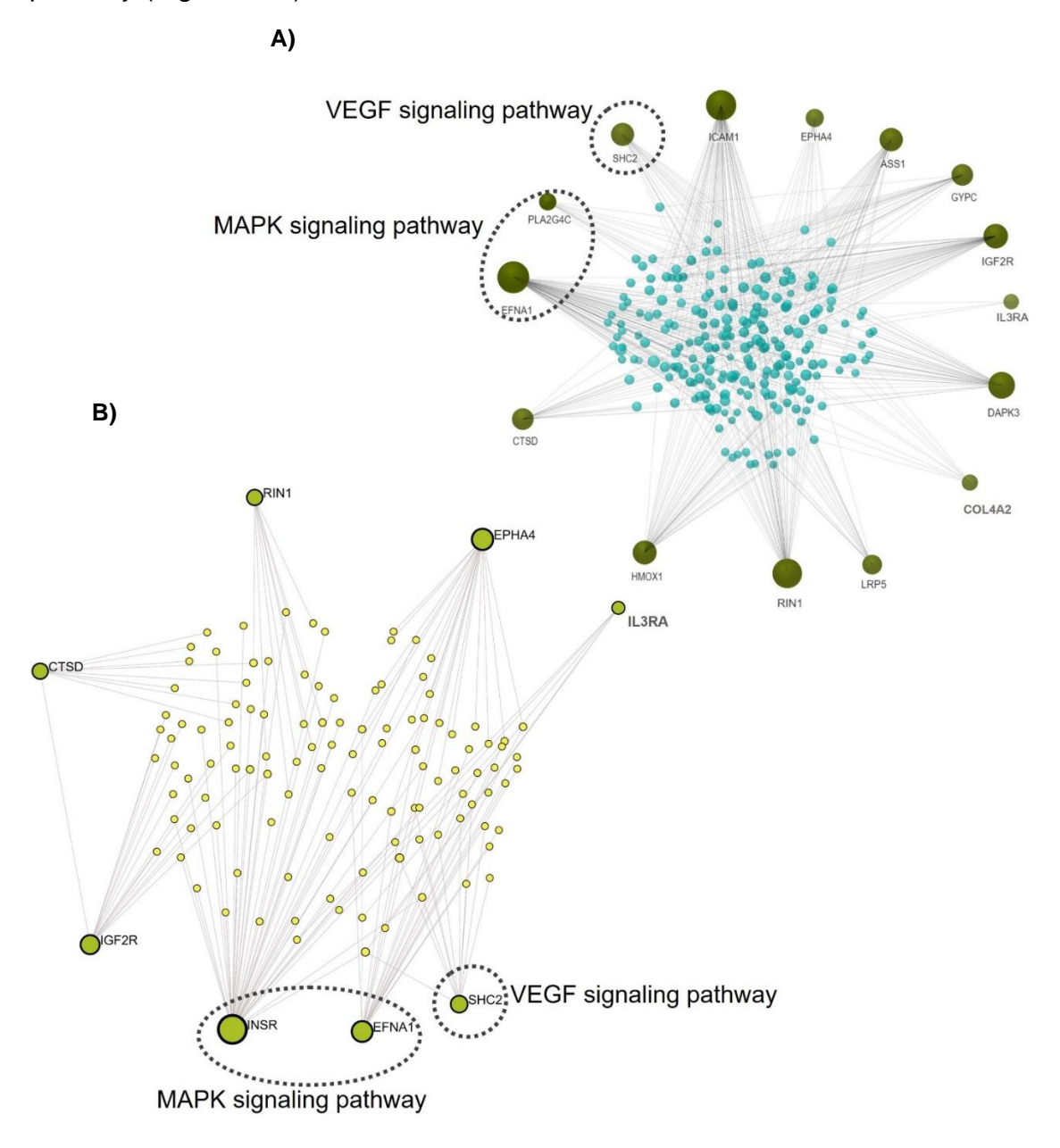


Figure 38. GRNs and PPIs analysis of upregulated target genes of miRNA-150-5p.

**A)** GRN analysis of significantly upregulated target genes of miRNA-150-5p. The network consists of 240 nodes, 499 edges and 15 hub genes. Genes corresponding to the VEGF signaling pathway and MAPK signaling pathways are highlighted within dotted circles. **B)** PPI network analysis of significantly upregulated

genes. The network comprises of 121 nodes, 29 edges and 8 hub proteins. Genes associated with the VEGF and MAPK signaling pathways are highlighted with dotted circles.

The GRN analysis of downregulated genes revealed a total of 349 nodes, 1591 edges, and 66 hub genes (Figure 39A). Among genes with the highest interactions, *COL1A1* (Collagen type I alpha 1 chain), *CD44*, *HMMR* (Hyaluronan Mediated Motility Receptor), *ITGA* (Integrin Subunit Alpha) 4, and *ITGA9* emerged as EndMT-relevant genes involved in ECM-receptor interaction. Moreover, *CCNA1* (Cyclin A), *CCNA2*, *ADIPOR2* (Adiponectin Receptor 2), and *SCD* (Stearoyl-CoA desaturase-1) were identified as EndMT-relevant genes associated with the AMPK signaling pathway (Figure 39A).

Additionally, the PPI analysis of downregulated genes revealed a total of 791 nodes, 1627 edges, and 46 hub proteins enriched by NetworkAnalyst (Figure 39B). Notably, among the top genes with the most interactions were COL1A1, COL1A2, ITGA4, ITGA9, and CD44, associated with ECM-receptor interaction, and CCNA1 and CCNA2, associated with the AMPK signaling pathway (Figure 39B).

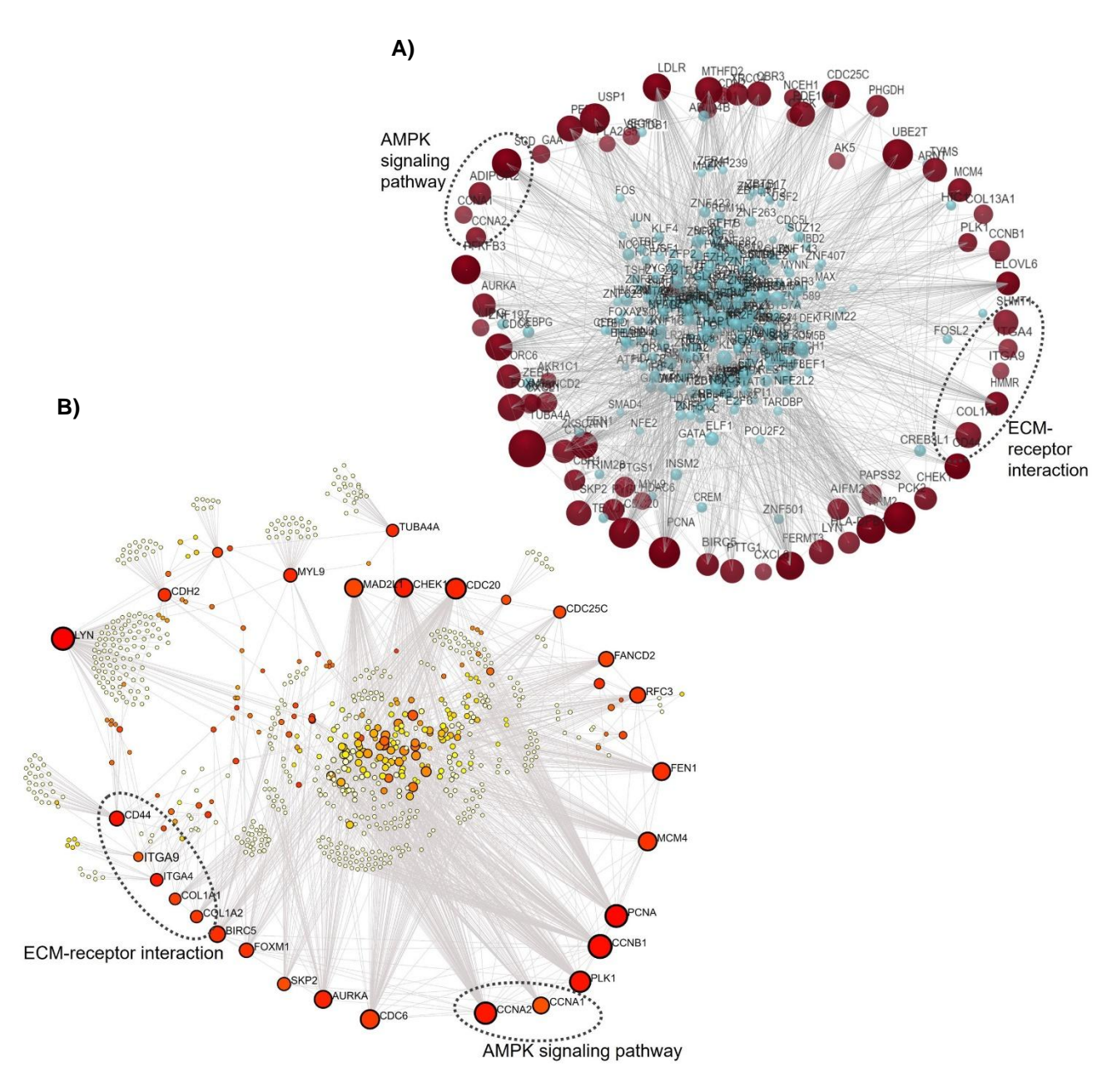


Figure 39. GRNs and PPIs analysis of downregulated target genes of miRNA-150-5p.

**A)** GRN analysis of significantly downregulated genes of miRNA-150-5p. The network consists of 349 nodes, 1591 edges and 66 hub genes. Genes corresponding to the ECM receptor interaction and AMPK signaling pathways are highlighted within dotted circles. **B)** PPI network analysis of significantly downregulated genes of miRNA-150-5p. The network comprises of 791 nodes, 1627 edges and 46 hub proteins. Genes associated with the ECM receptor interaction and AMPK signaling pathway are highlighted with dotted circles.

# 3.2.9.4. Identification of COL1A1 and ADIPOR2 as potential direct target genes of miRNA-150-5p in VECs

Next, I aimed to identify the potential direct target genes of miRNA-150-5p. Therefore, I assessed the potential binding sites within the downregulated target genes relevant to EndMT, as miRNAs bind to mRNAs resulting in mRNA degradation or translation inhibition. In this analysis, I focused specifically on genes that exhibited the highest interactions, as identified in the previous PPI and GRN analysis (chapter 3.2.9.3.) For this, the miRNA-mRNA hybridization within this subset of genes was evaluated using several miRNA target gene prediction tools such as Targetscan, RNA 22, Pictar and miRDB. To evaluate the hybridization, the pattern of miRNA-mRNA duplex binding and free energy were assessed. In this analysis, a threshold of minimum free energy (MFE) <-15 was used as a lower free energy value which corresponds to a more stable hybridization been the miRNA and mRNA (Table 33). The results revealed that the 3'UTR of COL1A1, and ADIPOR2 mRNA contained binding sites for miRNA-150-5p and notably, these binding sequences were conserved across different species (Table 33).

Table 33. miRNA-mRNA Hybridization and the pattern of binding site

Genes	Binding Position	MFE (kcal/mol)	Binding Pattern
COL1A1	896	-20.80	TGATGGGTGGGGTGGGGAGG     :        : GTGACCATGTTCCCAACCCTCT
ADIPOR2	525	-22.30	CATAGGGGTAAGGG-AGGGAGG   :    :         : GTGACCATGTTCCCAACCCTCT

In conclusion, i investigated highly interacting genes relevant to EndMT among downregulated target genes of miRNA-150-5p to identify the potential direct target genes of miRNA-150-5p. I identified COL1A1 and ADIPOR2 as potential direct target genes of miRNA-150-5p, supported by the presence of conserved miRNA-binding sites within their 3'UTRs. These findings provide valuable insights into the potential role of miRNA-150-5p in EndMT. Further studies are needed to elucidate its mechanisms.

#### 3.3. Effects of Candidate miRNAs in VICs

### 3.3.1. Primary VIC isolation from calcific aortic valve

Human primary VICs were isolated from the explanted aortic valve (Figure 40A), and the purity of isolation was assessed using RT-qPCR for VIC markers. Aortic endothelial cells

were used as a control for the comparison. The microscopic pictures of VICs showed elongated and spindle-shaped morphology (Figure 40B). Additionally, the qPCR data demonstrated the absence of endothelial markers such as *CD31* and *VWF* in the isolated VICs, while confirming a significantly elevated expression of *ACTA2* as a VIC marker (Figure 40C). Collectively, these data indicated that VICs were efficiently isolated from the human aortic valve and can be used for the further investigation.

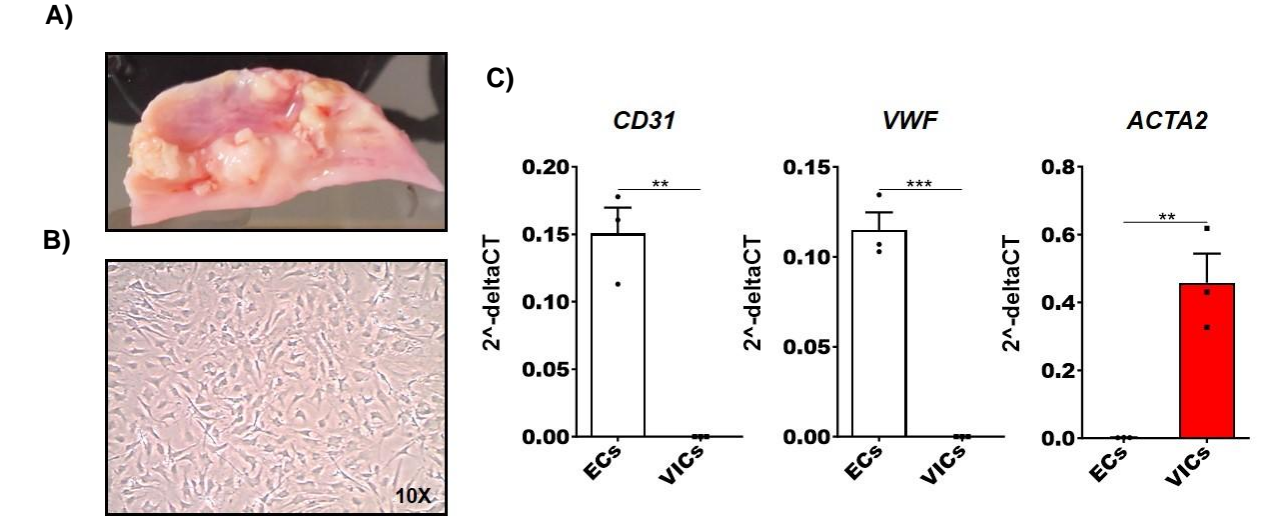


**Figure 40.** Characterization of isolated VICs from the calcific aortic valve. **A)** Morphology of the aortic valve explanted from patients with AVS. **B)** Representative light microscopy of isolated VICs from the valve **C)** qPCR validation of VICs showing the absence of endothelial markers including CD31 and VWF expression and elevated levels of ACTA2 in VICs, compared to aortic endothelial cells (n=3). \*p < 0.05, \*\*p < 0.01, \*\*\*p < 0.001, analyzed by Student's t-test.

### 3.3.2. miRNA-150-5p reduces calcification in VICs

As previously described (chapter 3.1.3), my investigation confirmed the dysregulation of three specific miRNAs in EV samples obtained from AVS patients including miRNA-150-5p, Let-7c-5p, and miRNA-30b-5p. Therefore, I aimed to identify their roles in calcification in VICs. However, the role of miRNA-30-5p was previously studied in calcification of VICs (Zhang et al. 2014). Therefore, I have exclusively focused on miRNA-150-5p and Let-7c-5p and their impacts in calcification.

To develop an *in vitro* calcification model, and thereby differentiate VICs into the osteoblast-like cells, VICs were subjected to two distinct calcifying media, osteogenic medium (OM) and pro-calcifying medium (PM), for 14 days. While OM contained organic phosphate such as glycerophosphate, PM was enriched with inorganic phosphate, which both are crucial for the mineralization by providing sites for calcium phosphate deposition on the extracellular matrix (Bäck and Michel 2021). Not all VICs isolated from calcified valves can be calcified using the OM or PM medium. This variability is likely due to the patient-to-patient differences. To identify the most suitable VICs for further investigation of candidate miRNAs, I assessed the VIC calcification obtained from different donors

(Figure 41). The calcium deposition was visualized using Alizarin red staining. VICs from six donors were treated with OM and PM. Among them, donors 1,2, and 3 were calcified in both OM and PM, whereas donors 4 and 6 showed calcification in OM, but a few calcified nodules was observed in PM (Figure 41). Donor 5 was not calcified in either OM or PM. Therefore, VICs from donors 1,2, and 3 were selected for subsequent experiments (Figure 41).

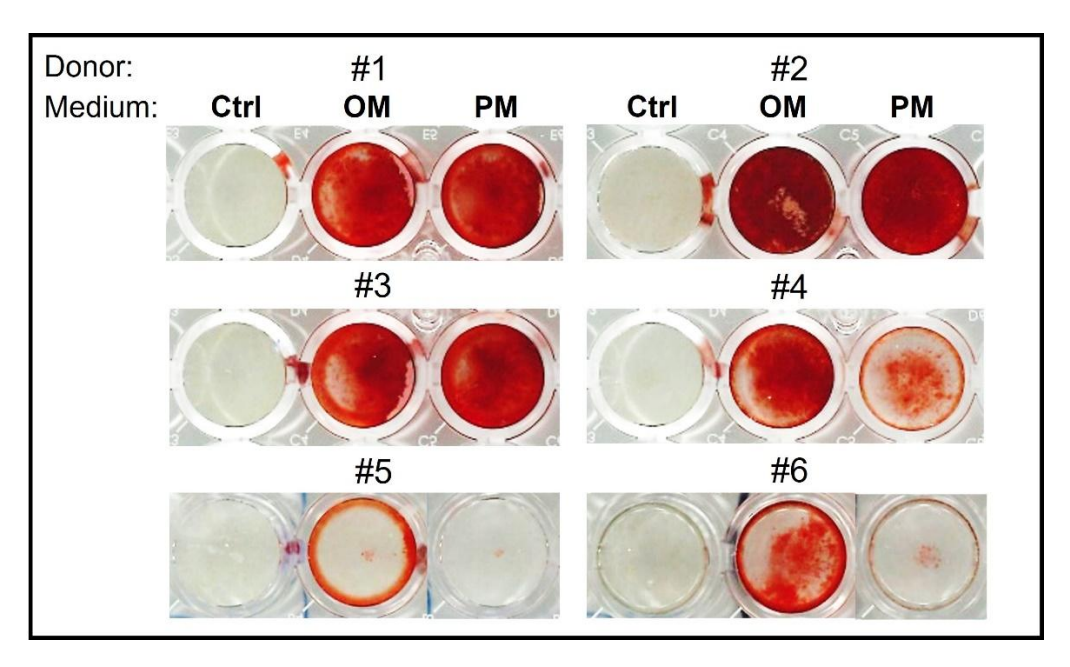


Figure 41. VIC calcification in 6 different patients with AVS.

Alizarin red staining of VICs isolated from 6 AVS patients cultured in the osteogenic medium (OM) and procalcifying medium (PM) for 14 days.

To determine the role of candidate miRNAs in calcification, VICs were transduced with the lentivirus to overexpress miRNA-150-5p and Let-7c-5p and cultured in both OM and PM for 14 days. After the transduction, the expression level of each miRNA was investigated using qPCR. The results revealed a significant upregulation of both miRNA-150-5p and Let-7c-5p in VICs as depicted in Figure 42. Importantly, Alizarin red staining showed that miRNA-150-5p significantly reduced the calcification in both OM and PM (Figure 43A). This finding was further validated by the quantification of alizarin red stain using cetylpyridinium chloride showing that miRNA-150-5p reduced mineralization intensity in VICs cultured in OM and PM (Figure 43B). Let-7c-5p exhibited no significant effects in the calcification of VICs in either OM or PM (Figure 43B).

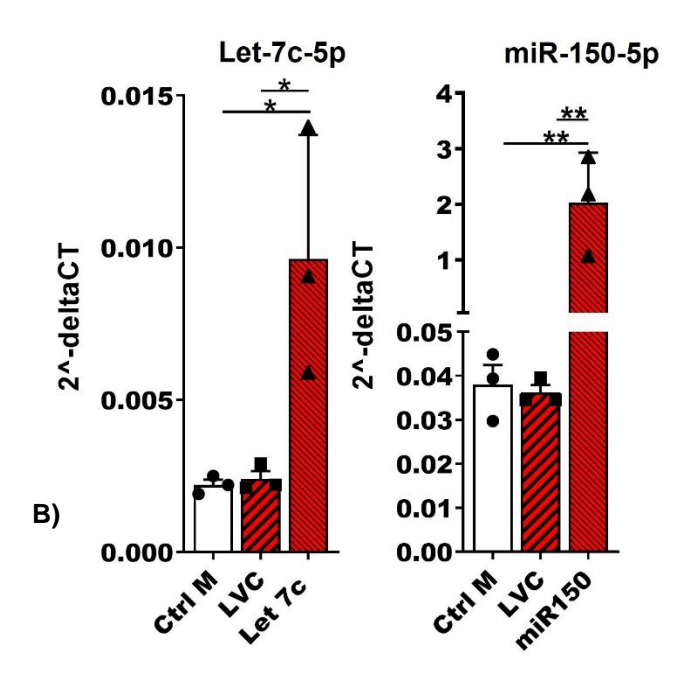


Figure 42. Validation of miRNA-150-5p and Let-7c-5p overexpression in VICs after transduction. The qPCR analysis of overexpressed miRNA-150-5p and Let-7c-5p after the lentiviral transduction in VICs (n=3). \* $^{*}p < 0.05$ , \* $^{*}p < 0.01$ , one-way ANOVA.

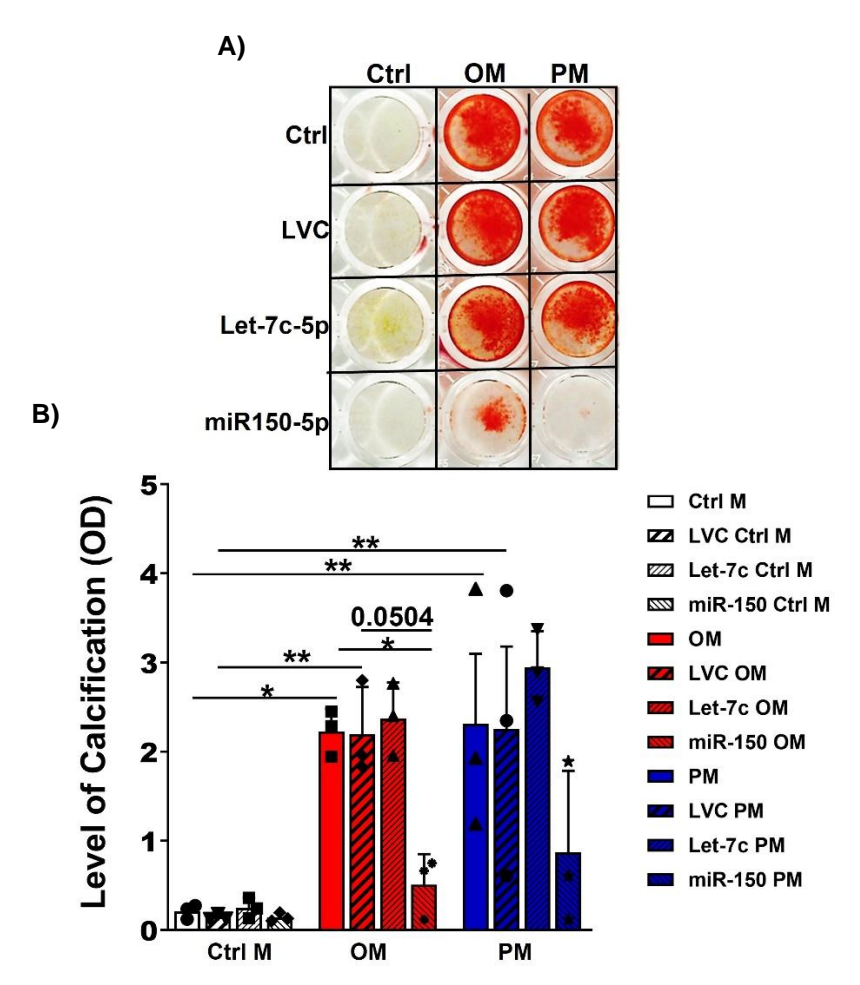


Figure 43.Representative picture of alizarin red in VICs overexpressing miRNA-150-5p and Let-7c-5p.

**A)** The alizarin red staining of VICs transduced with the lentivirus overexpressing miRNA-150-5p and Let-7c-5p which were further calcified in the OM and PM. miRNA-150-5p reduced the calcification in both OM and PM. Let-7c-5p had no impacts on the calcification (n=3). **B)** Alizarin red quantification using cetylpyridinium chloride showed that miRNA-150-5p reduced the mineralization intensity in VICs cultured in OM and PM. Let-7c-5p showed no impact on the calcification in OM and PM (n=3). The absorbance was measured at 405nm. \*p < 0.05, \*\*p < 0.01, two-way ANOVA.

### 3.3.3. miRNA-150-5p and Let-7c-5p reduces calcific markers in calcified VICs

To validate the osteogenic differentiation of VICs, I assessed the expression levels of the calcification-related genes such as *ALPL*, *RUNX2*, *SPP1* and *OPG* in VICs treated with OM and PM for 3 days by using qPCR analysis (Figure 44).

In OM, the expression level of *RUNX2* and *ALPL* was significantly increased, while increased tendency in *OPG* and no changes in *SPP1* were observed (Figure 44). Furthermore, the qPCR analysis showed that the expression levels of *RUNX2*, *ALPL*, *SPP1* and *OGP* were not significantly changed in PM (Figure 44). I further investigated the potential role of miRNA-150-5p and Let-7c-5p on calcific markers. The qPCR results unrevealed that miRNA-150-5p led to the reduction in *RUNX2* and *ALPL* expression in

VICs cultured in OM (Figure 44). These findings are consistent with the role of miRNA-150-5p as observed in the alizarin red staining analysis of VICs (chapter 3.3.2) Moreover, I observed that Let7c-5p significantly decreased the expression level of *RUNX2* and *ALPL* in OM medium (Figure 44).

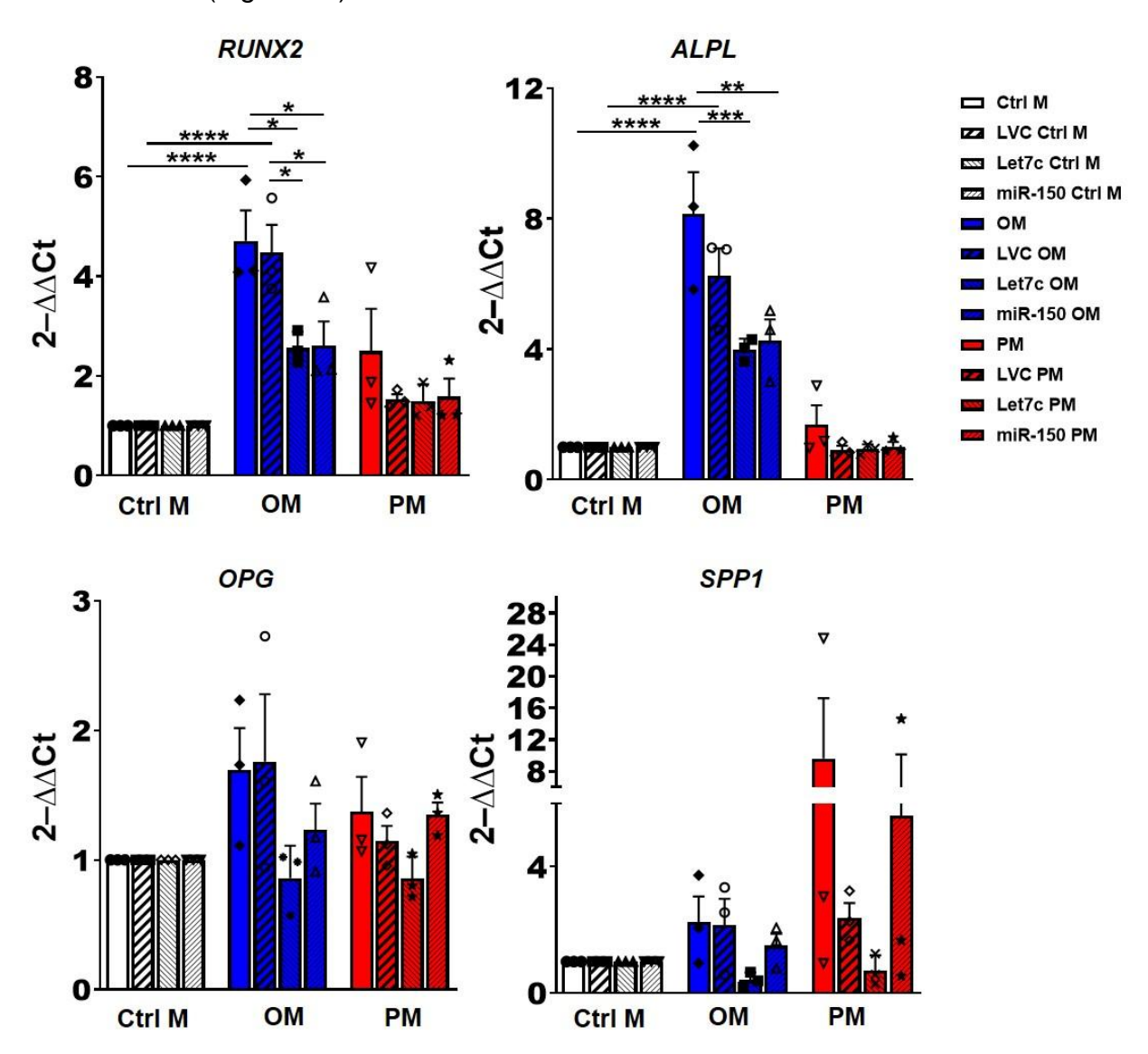


Figure 44. Relative gene expression analysis of calcification markers in VICs overexpressing miRNA-150-5p and Let-7c-5p, cultured in OM and PM.

The qPCR results showed the significantly overexpression of RUNX2 and ALPL and increased tendency in OPG in VICs cultured in OM for 3 days. SPP1 remained unchanged in OM. The calcific markers showed no significant changes in PM. MiRNA-150 and Let-7c reduced the expression level of RUNX2 and ALPL in VICs cultured in OM, but did not change their expressions in PM (n=3). \*p < 0.05, \*\*p < 0.01, \*\*\*p < 0.001, \*\*\*p < 0.001, \*\*\*p < 0.001, \*\*\*p < 0.0001, \*\*p < 0.0001,

### 3.3.4. miRNA-150-5p and Let-7c-5p reduces TNAP activity in VICs cultured in OM

In OM, TNAP targets  $\beta$ -glycerol phosphate, contributing to the formation of nascent hydroxyapatite crystals and cardiovascular calcification (Goto et al. 2019). Therefore, TNAP activity is a necessary factor for calcification in OM, whereas its role appears less significant in PM (Goto et al. 2019). Therefore, I analyzed the activity of TNAP only in OM, and these findings confirmed the increased activity of TNAP in VICs cultured in OM. The data showed that miRNA-150-5p and Let-7c-5p reduced the TNAP activity in OM. It would be important to increase the number of samples to reduce the inherent heterogeneity in future experiments (Figure 45).

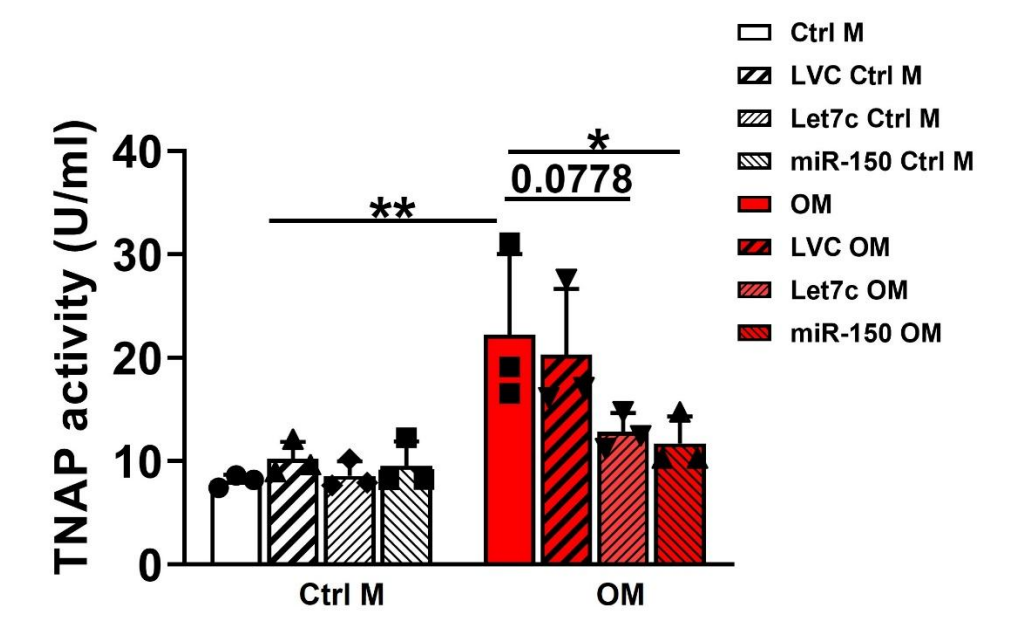


Figure 45. Effect of miRNA-150-5p and Let-7c-5p on TNAP activity in VICs treated with OM. TNAP activity was significantly increased in VICs cultured in OM. miRNA-150-5p significantly reduced the TNAP activity in VICs cultured in OM. \*p < 0.05, two-way ANOVA.

Taken together, these data showed that miRNA-150-5p ameliorated calcification in VICs cultured in OM, supported by the reduction of alizarin red staining, calcific markers and TNAP activity. Moreover, I observed the acute effects of Let-7c-5p in the reduction of calcification, as evidenced by a decreased expression level of calcific markers and TNAP activity. However, these effects were not sustained during the long-term OM treatment of VICs, evidenced by alizarin red staining.

## 4. Discussion

AVS is the most common valvular disease in the elderly population and mainly characterized by the thickening of the valve leaflets and calcification leading to aortic stiffening and stenosis (Kostyunin et al. 2019). Studies investigating the calcification in AVS have found that AVS is a slow and progressive disease rather than passive (Kostyunin et al. 2019). In recent years, switching from cardiac catheterization to doppler electrocardiography has enhanced diagnostic capabilities. Despite these advancements, morbidity and mortality associated with AVS remain a major concern. (Kostyunin et al. 2019). Recently, several studies have been conducted to understand the molecular mechanisms leading to AVS. However, the underlying mechanisms remain poorly understood. EVs and their roles in intercellular communications in diseased heart valves and atherosclerotic plaques have attracted much attention. Importantly, several studies have addressed the potential of EV-miRNAs as key regulators in cardiovascular disease. (Krohn et al. 2016).

This study aimed to investigate the role of EV derived miRNAs in AVS. I specifically focused on two critical mediators of calcification: EndMT and osteogenic differentiation of VICs.

### 4.1. Identification of Dysregulated Tissue-derived EV-miRNAs in AVS

In the diseased heart valve, EVs are continuously released upon the exposure to the pathological stimuli such as lipoproteins, cytokines, oxidative stress, and the shear stress (Diehl et al. 2008). In the coronary artery disease, elevated levels of circulating EVs are associated with cardiovascular mortality and angiogenesis (Sinning et al. 2011). Besides, circulating EVs are increased in atherosclerosis and are associated with unstable plaques and increased risk of atherothrombosis (Bernal-Mizrachi et al. 2004).

In the past decades, studies have mainly focused on the miRNA profiling in AVS tissue using qPCR based screening or microarray, and quite a few studies addressed miRNA profiling in EVs in AVS (Wang et al. 2017). Given the fundamental role of miRNAs as potential regulators of AVS, NGS was performed to investigate the expression pattern of EV-associated miRNAs in patients with AVS. I identified miRNAs in IEVs and sEVs isolated from calcific aortic valve tissue. Among them, miRNA-150-5p was significantly upregulated and miRNA-486-5p and miRNA-486-3p were significantly downregulated in IEVs, while miRNA-671-5p, miRNA-642a-5p, miRNA-486-5p, miRNA-486-3p, miRNA-342-5p, and Let-7g-3p were significantly upregulated and Let-7c-5p, miRNA-30b-5p and miRNA-181c-5p were significantly downregulated in sEVs.

Using miRTarBase, I identified the predicted target genes of these significantly dysregulated miRNAs. GO analysis showed that these target genes were mainly enriched in gene expression regulation, mRNA and miRNA transcription regulation, apoptotic process, EMT, and TGF- $\beta$  receptor binding. Signaling pathway analysis indicated that these miRNAs are linked to the cell cycle regulation and proliferation, Inflammatory

signaling, hypoxia and P53 signaling pathway, DNA modification, MAPK signaling pathway and TGF signaling pathway. These data indicate the potential roles of EV-miRNAs in modulating various signaling pathways that might contribute to the pathophysiology of AVS. Inflammation plays an important role in the pathogenesis of AVS, and increased plasma levels of pro-inflammatory cytokines such as IL-2, IL-6 and TNF-α are correlated with the severity of disease (Kapelouzou et al. 2015; Toli et al. 2008). The MAPK pathway plays a role in VIC calcification via ERK1/2, and its inhibition reduces myofibroblastic and osteoblastic markers. (Gu and Masters 2009). I also demonstrated the potential role of EV-miRNAs in the Hypoxia-Inducible Factor-2 (HIF-2) pathway. HIF-2, activated by NF-κB, regulates VEGF and collagen X in the calcification process (Akahori et al. 2018). In addition, P53 regulates calcification by promoting the transcription of Notch1, which inhibits calcification process (Raddatz et al. 2020). The suppression of p53 in AVS leads to increased cadherin-11 expression, which contributes to the osteogenic differentiation of VICs (Raddatz et al. 2020).

For further miRNA validation, I performed a literature review to focus the analysis on miRNAs directly implicated in cardiovascular diseases. Among the significantly dysregulated miRNAs, miRNA-150-5p, miRNA-486-5p, miRNA-486-3p, miRNA-342-5p, Let-7g-3p, Let-7c-5p and miRNA-30b-5p were found to be relevant to cardiovascular diseases.

So far, research on miRNA-150-5p has primarily focused on its role in cardiovascular diseases including MI and atherosclerosis, where it has been implicated in regulating key cellular processes such as apoptosis and inflammation. For instance, EV-derived miRNA-150-5p is decreased in MI mice; this miRNA is transferred via sEVs from macrophages into the cardiomyocytes and reduces apoptosis via the suppression of Tp53, and elevation of insulin-like growth factor 1 (IGF-1), a known regulator of cell survival. (Zheng et al. 2021). Let-7c-5p is upregulated in hypertensive patients with carotid plagues and contributes to apoptosis through the suppression of BCL-XL (Qin et al. 2012; Minin et al. 2021). Telocytes (TCs) are a newly described type of interstitial cells, and have a protective role in pathological condition by promoting cardiomyocyte regeneration and angiogenesis (Yang et al. 2021). It has been shown that the EV-miRNA-30b-5p transfer from TCs into the VICs reduces the formation of calcium deposition via the effects on RUNX2 and the Wnt/β-catenin pathway (Yang et al. 2021). Profiling miRNAs in sEVs obtained from the mouse bone marrow-derived macrophages exposed to high glucose (BMDM-HG-exo) shows an increased expression level of miRNA-486-5p. The treatment of Apoe-/- mice with BMDM-HG-exo leads to a significant increase in the size and severity of atherosclerotic lesions, which is associated with the higher accumulation of apoptotic bodies and macrophages (Bouchareychas and Duong 2021). Studies have reported the downregulated miRNA-671-5p in MI. Interestingly, the transfer of sEVs isolated from adipose-derived mesenchymal stem cells can recover miRNA-671-5p expression in MI. Furthermore, the transfer of sEVs-miRNA-671-5p alleviates MI symptoms via directly targeting TGF-β receptor 2 (TGFBR2). TGFBR2 promotes the phosphorylation of SMAD2, a key signaling molecule. Therefore, by targeting TGFBR2,

sEVs-miRNA-671-5p reduces SMAD2 phosphorylation.(Wang et al. 2021). Patients with CAD shows increased expression of miR-342-5p (Ahmadi et al. 2018). Notably, this increase was positively associated with high levels of inflammatory cytokines including IL-6 and TNF-α in these patients (Ahmadi et al. 2018). Zhang et al reported the important role of let-7g in oxLDL-induced atherosclerosis by targeting ox-LDL receptor LOX-1 and inducing apoptosis via targeting caspase-3 in vascular endothelial cells (Zhang et al. 2013).

Using Taqman qPCR, I further validated the significantly upregulation of miRNA-150-5p in IEVs and downregulation of Let-7c-5p and miRNA-30b-5p in sEVs. The expression level of miRNA-486-5p, miRNA-486-3p, miRNA-342-5p, Let-7g-3p remained unchanged in IEV and/or sEV in patients with AVS compared to the control samples; therefore, I mainly focused on miRNA-150-5p, Let-7c-5p and miRNA-30b-5p to identify their roles in AVS.

### 4.2. Effects of Candidate miRNAs in VECs

The stability of ECs is crucial for maintaining homeostasis, and alterations in the integrity of ECs are a key and early pathogenic mechanism in AVS. EndMT is an early stage of endothelial dysfunction and contributes to the progression of AVS. Further insights into the role of this process are therefore of great importance. For this reason, i investigated the role of candidate miRNAs in an EndMT model using VECs. Given the lack of a standardized protocol for inducing EndMT in VECs, I firstly established an EndMT model. For this, VECs were treated with TGF- $\beta$ 1, BMP2, IL-1 $\beta$  and TNF $\alpha$  for 7 days. Among these, TNF $\alpha$  treatment led to the most pronounced EndMT, with downregulated endothelial marker *VWF* and upregulated mesenchymal markers *ACTA2*, *VIM*, and *SLUG*. These findings were consistent with microscopic images of VECs treated with TNF $\alpha$  demonstrating a mesenchymal morphology of cells. IL-1 $\beta$  also induced some EndMT-related changes, though less significantly, while TGF- $\beta$ 1 and BMP2 had minimal effects. These finding were in line with the study showing that TNF $\alpha$  is a potent inducer of EndMT in human VECs, while other stimulators such as TGF- $\beta$ 1 show no significant impacts on EndMT markers (Nehl et al. 2022).

Next, I investigated the role of miRNA-150-5p, Let-7c-5p and miR-30b-5p on EndMT. Given the sensitivity of primary ECs to the toxicity of commonly used transfection reagents and the rapid degradation of exogenous nucleic acids, I utilized lentiviruses to overexpress miRNA-150-5p, Let-7c-5p, and miR-30b-5p in VECs. Following transduction, cells were treated with 25ng/ml TNFα for 7 days. The qPCR data revealed that miRNA-150-5p prevented the downregulation of *VWF* and the increase of *ACTA2*, *SLUG* and *VIM* by TNFα. Let-7c-5p significantly increased the expression levels of *ACTA2*, and had no impacts on other EndMT markers. Furthermore, miR-30b-5p significantly reduced the expression level of VIM but had no impacts on the other EndMT markers. Moreover, microscopy images of VECs overexpressing miRNA-150-5p treated with 25ng/ml TNFα showed more EC phenotype while VECs transduced with let-7c-5p and miR-30b-5p

maintained a spindle-like mesenchymal morphology, similar to control cells treated with 25ng/ml TNFα.

Given the promising role of miRNA-150-5p in preventing EndMT in TNFα-treated VECs, I investigated the role of this miRNA in cellular processes relevant to endothelial function. Interestingly, the data revealed that miRNA-150-5p enhanced the tube formation in VECs while reducing cell migration. These effects suggested that miRNA-150-5p may contribute to maintaining the endothelial characteristics of VECs and potentially reduce their capacity to invade the valve during EndMT.

The aortic valve endothelium has significant heterogeneity, mainly resulting from distinct blood flow patterns on its two sides. Under physiological conditions, the ventricular side of the aortic valve is exposed to high laminar flow, whereas the aortic side experiences low oscillatory flow (Simmons et al. 2004). However, pathological conditions disrupt these flow patterns resulting in increased turbulent flow on outflow surfaces, which can contribute to endothelial dysfunction and injury (Atkins and Sucosky 2014). Given these findings suggesting a protective role for miRNA-150-5p, I investigated whether its expression differs between the aortic and ventricular sides of the valve in AVS patients. Therefore, I isolated RNAs using a cold aluminum rod from both sides of aortic valve and analyzed the expression level of miRNA-150-5p. These data showed that miRNA-150-5p is expressed from both sides with no significant differences between two sides.

# 4.3. hsa-miRNA-150-5p in VECs Cultured under the Laminar Flow

Given the role of distinct blood flow patterns in regulating endothelial function, I aimed to investigate how laminar shear stress influences the expression of miRNA-150-5p in cultured VECs. I successfully established VEC cultures under laminar flow that closely resembled physiological conditions (20dyn/cm<sup>2</sup>). VECs cultured for 24h under laminar flow were aligned parallel to the direction of flow. Moreover, the qPCR data revealed the upregulation of KLF2 and KLF4 and downregulation of their targets VCAM-1. It has been shown that laminar flow can activate the protective signaling pathway MEK5/Erk5, and its downstream regulated genes KLF2 and KLF4 (Ohnesorge et al. 2010a). KLF4 suppresses endothelial migration and angiogenesis, and together with KLF2, mediates many vasoprotective responses, including increased eNOS expression and reduced VCAM, thereby decreasing inflammation (Pan 2009). Using MEK5D as a mutant for MRK5 leads to the constant activation of MEK5, resulting in vasoprotective responses mediated by KLF2 and KLF4. Therefore, activation of MEK5/Erk5/KLF4 pathway has been suggested as a potential treatment for vascular diseases (Ohnesorge et al. 2010b). I further identified the miRNA profile in VECs exposed to laminar flow, and the data revealed that laminar flow increased the expression level of miRNA-150-5p in VECs compared to the static condition. The upregulation of miRNA-150-5p in VECs under the laminar flow was further validated by Taqman qPCR. To my knowledge, this is the first report identifying laminar shear-sensitive miRNAs in VECs and demonstrating miRNA-

150-5p overexpression under laminar flow condition. However, I did not explore the functional role of this miRNA in turbulent flow. Nonetheless, I speculate that this could open up new avenues for studying miRNA-150-5p and its gene regulatory networks in flow research.

# 4.4. Role of IEV-Mediated Transfer of miRNA-150-5p in Intracellular Communication in VECs

EV-mediated cell-cell communication is crucial in intracellular crosstalk and has molecular and phenotypic effects on ECs, CMs, and SMCs (Hosen et al. 2022; Zietzer et al. 2020). A recent study has demonstrated that the increased expression of circulating IEV-derived miRNA-122-5p is negatively associated with left ventricular ejection fraction (LVEF) improvement in patients with AVS after TAVR. This study elucidated that miR-122-5p specifically interacts with heterogeneous nuclear ribonucleoprotein (hnRNPU) for sorting into the IEVs. This IEV-miRAN-122-5p can be further transferred from endothelial cells into the cardiomyocytes, leading to a decrease in the expression of the anti-apoptotic gene *BCL2* in cardiomyocytes, increased apoptosis, and consequently, impaired cardiac function (Hosen et al. 2022). Furthermore, the study by Zietzer et al has shown the selective incorporation of miRNA-30c-5p into IEVs through binding to hnRNPU and controls the function of human coronary artery endothelial cells (HCAECs) (Zietzer et al. 2020).

Given the role of EVs in intracellular communications, I further investigated the transfer of miRNA-150-5p between VECs via IEVs. For this, I-VECs were generated using Large T antigen lentiviruses and transduced with a lentivirus overexpressing miRNA-150-5p. IEVs were isolated from the culture media and characterized using SEM and NTA. Afterward, VECs were treated with IEVs. Fluorescence microscopy and qPCR confirmed the uptake of PKH67-labelled IEVs (a lipophilic membrane dye) and the increased expression of miRNA in recipient VECs, respectively. Subsequently, I investigated the role of IEV-miRNA-150-5p in the EndMT model to determine if miRNA-150-5p carried by IEVs could also efficiently impact on EndMT. For this, I treated VECs with EndMT medium after the treatment of VECs with IEV-miRNA-150-5p. Interestingly, these data showed that IEV-miRNA-150-5p significantly increased the expression level of *SLUG* remained unchanged compared to control samples treated only with EndMT medium. Therefore, I suggested that IEV-miRNA-150-5p may reduce EndMT in VECs, potentially impacting AVS.

# 4.5. Identification of miRNA-150-5p Target Genes in VECs

Given the promising role of miRNA-150-5p in VECs, sequencing was performed on VECs transduced with the lentivirus to overexpress miRNA-150-5p to identify its target genes in VECs and gain insights into its potential molecular functions. Using NGS, I identified a total of 104 significantly upregulated and 247 significantly downregulated genes in VECs overexpressing miRNA-150-5p compared to VECs transduced with the LVC.

Subsequently, I performed GO analysis for both upregulated and downregulated genes to gain insights into the potential biological functions.

Upregulated exhibited GO genes enrichment in terms associated with metalloendopeptidase activity, insulin-like growth factor binding, and protein tyrosine kinase binding. Interestingly, GO analysis of the cellular component category revealed that these genes were mainly found in the collagen containing extracellular matrix, autolysosome and extracellular vesicles. This suggests a potential role for miRNA-150-5p in regulating ECM remodeling processes and extracellular vesicles. Moreover, enrichment analysis of molecular function revealed that these upregulated genes are mainly involved in extracellular structure organization, regulation of the ERK1 and ERK2 cascade, and importantly, negative regulation of EMT. The impacts of miRNA-150-5p in EMT, a process closely related to the EndMT suggests a potential protective role for this miRNA in VECs. KEGG signaling pathway analysis showed that these genes are involved in the RAS signaling, fluid shear sensitive and atherosclerosis and VEGF signaling pathways. Based on these findings, key pathways relevant to AVS were further explored. For instance, The ACE2/angiotensin-(1-7)/Mas receptor axis and AT2 receptors mitigate inflammation and proliferation, while ACE/AngII/AT1 induces these processes (Peltonen et al. 2011). VEGFR1 and VEGFR2 regulate monocyte migration and endothelial function (Álvarez-Aznar et al. 2017). Elevated levels of VEGFR1, VEGFR2 and VEGF-A as proangiogenic factors and VEGFR3, VEGF-C and VEGF-D as pro-lymphogenic factors have been reported in male AVS patients (Matilla et al. 2022). Enhanced activity of ERK1/2 drives vascular and valvular calcification, while its inhibition enhances AMPKa, P53, and LRP6/DKK1, suppressing β-catenin-mediated calcification (Zeng et al. 2021; Adhikari et al. 2023).

I further conducted PPI and GRN analysis to gain insights about the hub genes/proteins and their interactions with other genes. These analyses revealed key genes in EndMT regulation including SHC2, which is relevant to the VEGF signalling pathway, and INSR, PLA2G4C and EFNA1, which are relevant to the MAPK signalling pathway.

The GO molecular function analysis showed that the downregulated genes were associated with tubulin binding, metal ion binding, oxidoreductase activity and calcium binding. The analysis of cell component and biological process indicated the contribution of downregulated genes in cell cycle process as well as spindle and microtubule organization. Moreover, KEGG analysis indicated the involvement of these downregulated genes in the cell cycle, ECM receptor interaction, P53 signaling and AMPK signaling pathways which are all implicated in AVS. Abnormal composition, and disorganization of the ECM are among the earliest detectable changes in AVS. It has been shown that dysregulated gene expression of ECM proteins increases cell migration, as well as the mesenchymal phenotype and activated ERK signaling in porcine VECs. Different GAG composition in 3 hydrogel model affects its stiffness and increases EndMT via affecting cell adhesion molecules and EC invasion (Sudip Dahal et al. 2017). Moreover, AMPK signaling plays a role in mediating the metabolic effects of hydrogen

sulfide (H2S) and contributes to endothelial cell stress attenuation and EndMT inhibition in atherosclerosis (Souilhol et al. 2018). In addition, I performed PPI and GRN analysis for downregulated genes and identified hub genes/proteins associated with EndMT signalling pathways, including COL1A1, COL1A2, ITGA4, ITGA9, CD44, and HMMR linked to ECM receptor pathways, and CCNA1, CCNA2, ADIPOR2, and SCD linked to the AMPK signaling pathway.

The miRNA-mRNA interaction leads to mRNA degradation by miRNA binding to the 3' UTR of the mRNA or translation inhibition (Economou et al. 2015). Therefore, I performed a further investigation to identify the direct target genes of miRNA-150-5p within downregulated genes associated with EndMT signalling pathways. Using Target scan, RNA 22, Pictar and miRDB, I evaluated the binding sites of miRNA-150-5p among downregulated genes associated with EndMT. I assessed the miRNA-mRNA duplex binding pattern and minimum free energy (MFE) of hybridization. MFE <-15 kcal/mol as was used as a threshold. I identified *COL1A1* with MFE= -28.80 and *ADIPOR2* with MFE= -22.30 as potential target genes for miRNA-150-5p. These two genes had binding sites that were conserved across different species. Xu et al has reported the upregulation of *COL1A1* together with other mesenchymal markers such as *COL3A1* and *ACTA2*, and the downregulation of endothelial markers such as *CD34* and *VWF* in patients with AVS compared to healthy controls. The upregulation of *COL1A1* was further validated in an *in vitro* model using TGF-β to induce EndMT (Xu et al. 2020).

ADIPOR2 regulates energy homeostasis and lipid oxidation with an anti-inflammatory and anti-apoptosis effects through the AMPK/p38 MAPK (Kreth et al. 2014) While its role in metabolic disorders is debated, studies suggest its involvement in vascular health. AdipoR2-/- mice exhibit resistance to high-fat diet-induced obesity, improved glucose clearance, and reduced atherosclerotic plaque formation (Lindgren et al. 2013).

Atherosclerosis is characterized by the accumulation of cholesterol-laden macrophages, known as foam cells. Interestingly, studies have shown that miRNA-150-5p is upregulated in oxLDL-treated THP-1 macrophages. Overexpression of miRNA-150-5p inhibits lipid accumulation and foam cell formation while enhancing cholesterol efflux either by increasing ATP-binding cassette transporters ABCA1 and ABCG1 or by upregulating Apo-A1 and HDL. This process is regulated by ADIPOR2, which is a direct target gene of miRNA-150-5p (Li and Zhang 2016). In vascular ECs, AdipoR2, also a target gene of miR-449a, plays a crucial role in anti-inflammatory effects and plaque lesion development. TNFa inhibited the recruitment of ADIPOR2 into lipid rafts, disrupting its interaction with E-cadherin and enhancing EC proliferation, migration and EndMT (Jiang et al. 2019). An increased expression level of miRNA-150-5p has been reported in patients with chronic heart failure (CHF). In vitro data have shown that miRNA-150-5p adiponectin resistance via targeting ADIPOR2. Adiponectin exerts cardioprotective actions, and impaired adiponectin signalling may contribute to the progression of CHF (Kreth et al. 2014).

In conclusion, I identified *COL1A1* and *ADIPOR2* as potential direct target genes of miRNA-150-5p. Further studies are needed to explore the role of miRNA-150-5p via targeting *COL1A1* and *ADIPOR2* in the EndMT model to provide further insights into the cardioprotective role of this miRNA in AVS.

### 4.6. Effects of Candidate miRNAs in VICs

In this study, I identified that miRNA-150-5p might protect VECs from EndMT and improve their function. Besides, through literature review, I found that Let-7c-5p, similar to my data, was significantly downregulated in patients with AVS (Zhang et al. 2021; Wang et al. 2017). This alignment with the published data further validates the robustness of the applied methodology. Therefore, I investigated the role of miRNA-150-5p and Let-7c-5p on calcification in VICs.

For this, VICs were isolated from AVS patients, and calcification was induced with including OM and PM. Alizarin red staining revealed donor-dependent variability in calcification. A study by Goto et al. has demonstrated that the calcification of VICs specifically in OM medium depends on patient samples, passage number of VICs and TNAP activity, whereas the calcification of VICs in PM is donor-,TNAP-, and passage-independent (Goto et al. 2019). This variability might be partly due to a higher number of calcification-resistant VICs compared to calcification-prone VICs (Goto et al. 2019).

I further investigated the role of miRNA-150-5p and Let-7c-5p in calcification. For this, VICs were transduced with the lentivirus to overexpress miRNA-150-5p and Let-7c-5p and treated with OM and PM. The qPCR data analysis showed that calcific markers including *RUNX2* and *ALPL* were significantly upregulated in non-transduced VICs cultured in OM; however, *OPG* and *SPP1* remained unchanged. Besides, VICs treated with PM showed no significant changes in the expression level of calcific markers. This could be due to the short-term treatment of VICs with OM and PM medium (3 days) for RNA isolation, in contrast to the long-term treatment (14 days) of VICs used for alizarin red staining. Further analysis of different time points of calcification might help to find the optimal duration for observing the significant changes in calcific markers in VICs treated with PM. In the current study, I identified that miRNA-150-5p reduced the expression levels of osteogenic markers including *RUNX2* and *ALPL*. Similarly, Let-7c-5p decreased significantly the expression levels of *RUNX2* and *ALPL* in VICs treated with OM.

Furthermore, I measured TNAP activity in calcified VICs in OM, as previous studies have shown that TNAP activity is only increased in OM but not in PM(Goto et al. 2019). This is because OM contains  $\beta$ -glycerophosphate, which TNAP hydrolyzes into inorganic phosphate. Inorganic phosphate provides phosphate ions for hydroxyapatite crystal formation and the development of calcification foci. In contrast, PM contains high levels of inorganic phosphates as a driver of VIC calcification; this medium induces calcification in a TNAP-independent manner. Additionally, TNAP hydrolyzes pyrophosphate (PPi) as a calcification inhibitor and thereby contributing to calcification (Goto et al. 2019). The data showed that TNAP activity was significantly increased in VICs cultured in OM. The

data revealed that miRNA-150-5p significantly decreased TNAP activity in VICs treated with OM compared to the non-transduced cells. Furthermore, I observed a tendency of decreased TNAP activity in VICs overexpressing Let-7c-5p. A larger sample size might provide further insight into the robustness of this observation. These findings suggest that Let-7c-5p may only acutely decrease the calcification in VICs, as evidenced by no changes in Alizarin red staining which were observed after 14 days treatment of VICs with either OM or PM. Further studies are needed to elucidate its role in calcification in AVS.

To my knowledge, the involvement of IEV-miR-150 in osteogenic differentiation of VICs has not been previously documented. Thus, my study presents novel insights into the role of miRNA-150-5p in calcification of VICs. MiRNA-150-5p has been implicated in both beneficial and detrimental effects in cardiovascular disease. For example, miR-150 has an ischemic stress-responsive protector role against CM apoptosis both in vivo and in vitro. Mice deficient for miR-150-5p are sensitized to MI and showed increased cardiac apoptosis and fibrosis as well as loss of pump function. It was claimed that the cardioprotective roles of miR-150 during ischemic injury were in part attributed to the direct repression of the pro-apoptotic genes including EGR2(zinc-binding transcription factor induced by ischemia) and P2RX7 (pro-inflammatory ATP receptor) in cardiomyocytes. It has been shown that the expression of miRNA-150-5p is regulated by β-arrestin1 which mediates the maturation of pre-miRNA-150-5p from pri-miRNA-150-5p (Tang et al. 2015). In contrast, global-knockout mice experiments have revealed that miR-150 deficiency has a protective effect on atherosclerosis development by reducing inflammatory cytokines and decreased infiltrated machrophages. In vitro experiments have further suggested that the anti-inflammatory response associated with miRNA-150-5p deficiency in atherosclerosis is directly linked to the increased expression of the cytoskeletal protein PDZ and LIM domain 1 (PDLIM1) in macrophages which inhibits p65 and Nf-κB activation (Gong et al. 2018). However, Zhang et al. has reported an elevated level of miRNA-150-5p in the plasma of atherosclerosis patients. Their study has indicated that miRNA-150 is secreted from monocytes and selectively packaged into large EVs. They have shown that treatment of human microvascular endothelial (HMEC-1) with IEV isolated from atherosclerosis patients with the increased level of miRNA-150-5p enhances cell migration and tube formation through inhibition of c-Myb (Li et al. 2013). These studies have highlighted the complex roles of miRNA-150-5p in cardiovascular diseases.

While the current study has identified the protective role of IEV-miRNA-150-5p in EndMT and calcification, a key limitation is the lack of investigation into the shuttling of miRNA-150-5p via IEVs for direct cell-to-cell communication between VECs and VICs. Utilizing co-culture models could shed light on how IEV-miRNA-150 released from VECs, possibly triggered by increased flow, inflammatory response or other stimulators, influences VIC calcification. Besides, validation of these findings in an *in vivo* model would provide valuable insights into the potential therapeutic targeting of IEV-miRNA150-5p in AVS.

# 5. Summary

Aortic valve stenosis (AVS) is the most prevalent valvular disease in elderly. Extracellular vesicles (EVs), including large EVs (IEVs) and small EVs (sEVs), have recently gained attention in cardiovascular diseases. In this study, I elucidated the potential role of EV-miRNAs in AVS by investigating endothelial to mesenchymal transition (EndMT) and osteogenic differentiation of VICs.

Herein, I identified and validated miRNA-150-5p as an upregulated miRNA in IEVs isolated from patients with AVS who underwent surgical aortic valve replacement. Conversely, Let-7c-5p and miRNA30b-5p were downregulated in sEVs. To elucidate their roles in AVS, EndMT model was established. The overexpression of miRNA-150-5p mitigated EndMT in VECs as evidenced by increased expression of endothelial marker VWF and decreased expression of mesenchymal markers such as ACTA2, and VIM, and EndMT transcription factor SLUG. The microscopic analysis of VECs further supported these findings. Cells overexpressing miRNA-150-5p retained their endothelial morphology. However, Let-7c-5p and miRNA-30b-5p had no significant impacts on EndMT in VECs. I further assessed the role of miRNA-150-5p in VEC function, and the data showed that miRNA-150-5p improved VEC function by reducing cell migration and increasing tube formation. Given the valve heterogeneity, mainly caused by different blood flow pattern, I analyzed the expression level of miRNA-150-5p from the aortic and ventricular sides of the aortic valve. The analysis indicated that this miRNA was expressed from both sides. To further investigate the relationship between miR-150-5p and blood flow, VECs were exposed to laminar flow, and the data showed that miRNA-150-5p was increased under the laminar flow, suggesting a protective role of miRNA-150-5p in VECs. Given the role of EVs in intracellular communications, IEVs containing miRNA-150-5p were co-incubated with VECs to determine their role in EndMT. I identified that IEV-miRNA-150-5p reduced EndMT by increasing the expression level of VWF and decreasing ACTA2 and VIM. To gain more insights into the potential target genes of miRNA-150-5p, NGS was performed in VECs overexpressing miRNA-150-5p. Upregulated target genes were enriched in pathways such as RAS signaling, VEGF signaling, flow shear stress and atherosclerosis, while downregulated genes were enriched in pathways such as ECM receptor interaction, P53 signaling and AMPK signaling pathways which are linked to the AVS pathology. In silico analysis highlighted COL1A1 and ADIPOR2 as direct target genes of miRNA-150-5p. KEGG signaling pathway analysis showed that these two genes were linked to ECM receptor interaction and AMPK signaling pathway, respectively, both implicated in EndMT.

Besides, I investigated the role of miRNA-150-5p in osteogenic differentiation of VICs. For this, I used osteogenic medium (OM) and pro-calcifying medium (PM) for the osteogenic differentiation of VICs. Alizarin red staining showed that miRNA-150-5p decreased the calcification in VICs cultured in OM and PM. Consistent with these findings, I observed that miRNA-150-5p reduced the expression of the calcification-related genes *RUNX2* and *ALPL* as well as the TNAP activity in VICs cultured in OM.

In conclusion, my study shows that IEV derived miRNA-150-5p may play a protective role in AVS by mediating two main mechanisms leading to AVS such as EndMT and calcification.

## **Publication bibliography**

Adhikari, Radhika; Jung, Jaehun; Shiwakoti, Saugat; Park, Eun-Young; Kim, Hyun-Jung; Ko, Ju-Young et al. (2023): Capsaicin inhibits aortic valvular interstitial cell calcification via the redox-sensitive NFκB/AKT/ERK1/2 pathway. In *Biochemical Pharmacology* 212, p. 115530. DOI: 10.1016/j.bcp.2023.115530.

Ahmadi, Reza; Heidarian, Esfandiar; Fadaei, Reza; Moradi, Nariman; Malek, Mojtaba; Fallah, Soudabeh (2018): miR-342-5p Expression Levels in Coronary Artery Disease Patients and its Association with Inflammatory Cytokines. In *Clinical Laboratory* 64 (4), pp. 603–609. DOI: 10.7754/Clin.Lab.2017.171208.

Akahori, Hirokuni; Tsujino, Takeshi; Masuyama, Tohru; Ishihara, Masaharu (2018): Mechanisms of aortic stenosis. In *Journal of cardiology* 71 (3), pp. 215–220. DOI: 10.1016/j.jjcc.2017.11.007.

Álvarez-Aznar, Alberto; Muhl, Lars; Gaengel, Konstantin (2017): VEGF Receptor Tyrosine Kinases: Key Regulators of Vascular Function. In *Current Topics in Developmental Biology* 123, pp. 433–482. DOI: 10.1016/bs.ctdb.2016.10.001.

Atkins; Sucosky (2014): Etiology of bicuspid aortic valve disease: focus on hemodynamics. Available online at https://www.ncbi.nlm.nih.gov/pmc/articles/pmc4278157/.

Atkin-Smith, Georgia K.; Tixeira, Rochelle; Paone, Stephanie; Mathivanan, Suresh; Collins, Christine; Liem, Michael et al. (2015): A novel mechanism of generating extracellular vesicles during apoptosis via a beads-on-a-string membrane structure. In *Nat Commun* 6 (1), p. 7439. DOI: 10.1038/ncomms8439.

Bäck, Magnus; Michel, Jean-Baptiste (2021): From organic and inorganic phosphates to valvular and vascular calcifications. In *Cardiovasc Res* 117 (9), pp. 2016–2029. DOI: 10.1093/cvr/cvab038.

Bartel, David P. (2004): MicroRNAs: genomics, biogenesis, mechanism, and function. In *Cell* 116 (2), pp. 281–297. DOI: 10.1016/S0092-8674(04)00045-5.

Baumgartner, Helmut (2006): Hemodynamic assessment of aortic stenosis: are there still lessons to learn? In *Journal of the American College of Cardiology* 47 (1), pp. 138–140. DOI: 10.1016/j.jacc.2005.10.001.

Bermejo, J.; Yotti, R. (2007): Low-gradient aortic valve stenosis: value and limitations of dobutamine stress testing. In *Heart* 93 (3), pp. 298–302. DOI: 10.1136/hrt.2005.066860.

Bernal-Mizrachi, Leon; Jy, Wenche; Fierro, Christian; Macdonough, Rick; Velazques, Hermes A.; Purow, Joshua et al. (2004): Endothelial microparticles correlate with high-risk angiographic lesions in acute coronary syndromes. In *International Journal of Cardiology* 97 (3), pp. 439–446. DOI: 10.1016/j.ijcard.2003.10.029.

Blaser, Mark C.; Buffolo, Fabrizio; Halu, Arda; Turner, Mandy E.; Schlotter, Florian; Higashi, Hideyuki et al. (2023): Multiomics of Tissue Extracellular Vesicles Identifies Unique Modulators of Atherosclerosis and Calcific Aortic Valve Stenosis. In *Circulation* 148 (8), pp. 661–678. DOI: 10.1161/CIRCULATIONAHA.122.063402.

Bouchareychas, Laura; Duong, Phat (2021): High glucose macrophage exosomes enhance atherosclerosis by driving cellular proliferation & hematopoiesis. Available online at https://www.cell.com/iscience/pdf/s2589-0042(21)00815-4.pdf.

Boulanger, Chantal M.; Amabile, Nicolas; Tedgui, Alain (2006): Circulating microparticles: a potential prognostic marker for atherosclerotic vascular disease. In *Hypertension* 48 (2), pp. 180–186. DOI: 10.1161/01.HYP.0000231507.00962.b5.

Charitos, Efstratios I.; Sievers, Hans-Hinrich (2013): Anatomy of the aortic root: implications for valve-sparing surgery. In *Annals of cardiothoracic surgery* 2 (1), pp. 53–56. DOI: 10.3978/j.issn.2225-319X.2012.11.18.

Chen, Jian-Fu; Murchison, Elizabeth P.; Tang, Ruhang; Callis, Thomas E.; Tatsuguchi, Mariko; Deng, Zhongliang et al. (2008): Targeted deletion of Dicer in the heart leads to dilated cardiomyopathy and heart failure. In *Proceedings of the National Academy of Sciences of the United States of America* 105 (6), pp. 2111–2116. DOI: 10.1073/pnas.0710228105.

Chironi, Gilles; Simon, Alain; Hugel, Bénédicte; Del Pino, Muriel; Gariepy, Jérôme; Freyssinet, Jean-Marie; Tedgui, Alain (2006): Circulating leukocyte-derived microparticles predict subclinical atherosclerosis burden in asymptomatic subjects. In *Arteriosclerosis, Thrombosis, and Vascular Biology* 26 (12), pp. 2775–2780. DOI: 10.1161/01.ATV.0000249639.36915.04.

Choi, Dong-Sic; Kim, Dae-Kyum; Kim, Yoon-Keun; Gho, Yong Song (2013): Proteomics, transcriptomics and lipidomics of exosomes and ectosomes. In *PROTEOMICS* 13 (10-11), pp. 1554–1571. DOI: 10.1002/pmic.201200329.

Coffey, Sean; Cox, Brian; Williams, Michael J. A. (2014): The prevalence, incidence, progression, and risks of aortic valve sclerosis: a systematic review and meta-analysis. In *Journal of the American College of Cardiology* 63 (25 Pt A), pp. 2852–2861. DOI: 10.1016/j.jacc.2014.04.018.

Coffey, Sean; Williams, Michael J. A.; Phillips, L. Vicky; Galvin, Ivor F.; Bunton, Richard W.; Jones, Gregory T. (2016): Integrated microRNA and messenger RNA analysis in aortic stenosis. In *Sci Rep* 6 (1), p. 36904. DOI: 10.1038/srep36904.

Coté, Nancy; Mahmut, Ablajan; Bosse, Yohan; Couture, Christian; Pagé, Sylvain; Trahan, Sylvain et al. (2013): Inflammation is associated with the remodeling of calcific aortic valve disease. In *Inflammation* 36 (3), pp. 573–581. DOI: 10.1007/s10753-012-9579-6.

Cowell, S. Joanna; Newby, David E.; Boon, Nicholas A.; Elder, Andrew T. (2004): Calcific aortic stenosis: same old story? In *Age Ageing* 33 (6), pp. 538–544. DOI: 10.1093/ageing/afh175.

Da Silva, Rose Mary Ferreira Lisboa; Brugada, Josep (2022): Cardiac and Vascular Causes of Syncope and Atherosclerosis. In *Curr Cardiol Rep* 24 (10), pp. 1241–1249. DOI: 10.1007/s11886-022-01757-7.

Deb, Nandini; Ali, Mir S.; Mathews, Ashley; Chang, Ya-Wen; Lacerda, Carla (2021): Shear type and magnitude affect aortic valve endothelial cell morphology, orientation, and differentiation. In *Experimental biology and medicine (Maywood, N.J.)* 246 (21), pp. 2278–2289. DOI: 10.1177/15353702211023359.

Di Minno, Alessandro; Zanobini, Marco; Myasoedova, Veronika A.; Valerio, Vincenza; Songia, Paola; Saccocci, Matteo et al. (2017): Could circulating fetuin A be a biomarker of aortic valve stenosis? In *International Journal of Cardiology* 249, pp. 426–430. DOI: 10.1016/j.ijcard.2017.05.040.

Diehl, Philipp; Nagy, Ferenc; Sossong, Verena; Helbing, Thomas; Beyersdorf, Friedhelm; Olschewski, Manfred et al. (2008): Increased levels of circulating microparticles in patients with

severe aortic valve stenosis. In *Thromb Haemost* 99 (4), pp. 711–719. DOI: 10.1160/th07-05-0334.

Economou, Evangelos K.; Oikonomou, Evangelos; Siasos, Gerasimos; Papageorgiou, Nikolaos; Tsalamandris, Sotiris; Mourouzis, Konsantinos et al. (2015): The role of microRNAs in coronary artery disease: From pathophysiology to diagnosis and treatment. In *Atherosclerosis* 241 (2), pp. 624–633. DOI: 10.1016/j.atherosclerosis.2015.06.037.

Ewels, Philip A.; Peltzer, Alexander; Fillinger, Sven; Patel, Harshil; Alneberg, Johannes; Wilm, Andreas et al. (2020): The nf-core framework for community-curated bioinformatics pipelines. In *Nat Biotechnol* 38 (3), pp. 276–278. DOI: 10.1038/s41587-020-0439-x.

Fabian, Marc Robert; Sonenberg, Nahum; Filipowicz, Witold (2010): Regulation of mRNA translation and stability by microRNAs. In *Annual review of biochemistry* 79, pp. 351–379. DOI: 10.1146/annurev-biochem-060308-103103.

Faccini, Julien; Ruidavets, Jean-Bernard; Cordelier, Pierre; Martins, Frédéric; Maoret, Jean-José; Bongard, Vanina et al. (2017): Circulating miR-155, miR-145 and let-7c as diagnostic biomarkers of the coronary artery disease. In *Sci Rep* 7 (1), p. 42916. DOI: 10.1038/srep42916.

Fan, Jiajie; Shi Shanshan; Yunxiang Qiu, Zhijie Zheng, Luyan Yu (2019): MicroRNA-486-5p down-regulation protects cardiomyocytes against hypoxia-induced cell injury by targeting IGF-1. Available online at https://www.ncbi.nlm.nih.gov/pmc/articles/pmc6949569/.

Ferrari, Enrico; Segesser, Ludwig Karl von (2010): Transcatheter aortic valve implantation (TAVI): state of the art techniques and future perspectives. In *Swiss Med Wkly* 140, w13127. DOI: 10.4414/smw.2010.13127.

Fichtlscherer, Stephan; Rosa, Salvatore de; Fox, Henrik; Schwietz, Thomas; Fischer, Ariane; Liebetrau, Christoph et al. (2010): Circulating microRNAs in patients with coronary artery disease. In *Circulation Research* 107 (5), pp. 677–684. DOI: 10.1161/CIRCRESAHA.109.215566.

Filipowicz, Witold; Bhattacharyya, Suvendra N.; Sonenberg, Nahum (2008): Mechanisms of post-transcriptional regulation by microRNAs: are the answers in sight? In *Nat Rev Genet* 9 (2), pp. 102–114. DOI: 10.1038/nrg2290.

Freeman, Rosario V.; Otto, Catherine M. (2005): Spectrum of calcific aortic valve disease: pathogenesis, disease progression, and treatment strategies. In *Circulation* 111 (24), pp. 3316–3326. DOI: 10.1161/CIRCULATIONAHA.104.486738.

Gan, Lu; Xie, Dina; Liu, Jing; Bond Lau, Wayne; Christopher, Theodore A.; Lopez, Bernard et al. (2020): Small Extracellular Microvesicles Mediated Pathological Communications Between Dysfunctional Adipocytes and Cardiomyocytes as a Novel Mechanism Exacerbating Ischemia/Reperfusion Injury in Diabetic Mice. In *Circulation* 141 (12), pp. 968–983. DOI: 10.1161/CIRCULATIONAHA.119.042640.

Gautam, Vibhav; Singh, Archita; Singh, Sharmila; Sarkar, Ananda K. (2016): An Efficient LCM-Based Method for Tissue Specific Expression Analysis of Genes and miRNAs. In *Sci Rep* 6 (1), p. 21577. DOI: 10.1038/srep21577.

Gleason, Thomas G.; Reardon, Michael J.; Popma, Jeffrey J.; Deeb, G. Michael; Yakubov, Steven J.; Lee, Joon S. et al. (2018): 5-Year Outcomes of Self-Expanding Transcatheter Versus Surgical Aortic Valve Replacement in High-Risk Patients. In *Journal of the American College of Cardiology* 72 (22), pp. 2687–2696. DOI: 10.1016/j.jacc.2018.08.2146.

Gong, Fu-Han; Cheng, Wen-Lin; Wang, Haiping; Gao, Maomao; Qin, Juan-Juan; Zhang, Yan et al. (2018): Reduced atherosclerosis lesion size, inflammatory response in miR-150 knockout mice via macrophage effects. In *Journal of Lipid Research* 59 (4), pp. 658–669. DOI: 10.1194/jlr.M082651.

Goody, Philip Roger; Hosen, Mohammed Rabiul; Christmann, Dominik; Niepmann, Sven Thomas; Zietzer, Andreas; Adam, Matti et al. (2020): Aortic Valve Stenosis: From Basic Mechanisms to Novel Therapeutic Targets. In *Arteriosclerosis, Thrombosis, and Vascular Biology* 40 (4), pp. 885–900. DOI: 10.1161/ATVBAHA.119.313067.

Goto, Shinji; Rogers, Maximillian A.; Blaser, Mark C.; Higashi, Hideyuki; Lee, Lang H.; Schlotter, Florian et al. (2019): Standardization of Human Calcific Aortic Valve Disease in vitro Modeling Reveals Passage-Dependent Calcification. In *Front. Cardiovasc. Med.* 6, p. 49. DOI: 10.3389/fcvm.2019.00049.

Gregory, Carl A.; Gunn, W. Grady; Peister, Alexandra; Prockop, Darwin J. (2004): An Alizarin redbased assay of mineralization by adherent cells in culture: comparison with cetylpyridinium chloride extraction. In *Analytical Biochemistry* 329 (1), pp. 77–84. DOI: 10.1016/j.ab.2004.02.002.

Ground, Marcus; Callon, Karen; Walker, Rob; Milsom, Paget; Cornish, Jillian (2023): Valvular Interstitial Cells: Physiology, Isolation, and Culture. In: Technologies in Cell Culture - A Journey From Basics to Advanced Applications [Working Title]: IntechOpen.

Gu, Xiaoxiao; Masters, Kristyn S. (2009): Role of the MAPK/ERK pathway in valvular interstitial cell calcification. In *American journal of physiology*. *Heart and circulatory physiology* 296 (6), H1748-57. DOI: 10.1152/ajpheart.00099.2009.

Gu, Zuguang; Eils, Roland; Schlesner, Matthias (2016): Complex heatmaps reveal patterns and correlations in multidimensional genomic data. In *Bioinformatics (Oxford, England)* 32 (18), pp. 2847–2849. DOI: 10.1093/bioinformatics/btw313.

Helske, Satu; Syväranta, Suvi; Lindstedt, Ken A.; Lappalainen, Jani; Oörni, Katariina; Mäyränpää, Mikko I. et al. (2006): Increased expression of elastolytic cathepsins S, K, and V and their inhibitor cystatin C in stenotic aortic valves. In *Arteriosclerosis, Thrombosis, and Vascular Biology* 26 (8), pp. 1791–1798. DOI: 10.1161/01.ATV.0000228824.01604.63.

Hjortnaes, Jesper; Shapero, Kayle; Goettsch, Claudia; Hutcheson, Joshua D.; Keegan, Joshua; Kluin, Jolanda et al. (2015): Valvular interstitial cells suppress calcification of valvular endothelial cells. In *Atherosclerosis* 242 (1), pp. 251–260. DOI: 10.1016/j.atherosclerosis.2015.07.008.

Ho, Siew Yen (2019): Morphology and Surgical Anatomy of the Aorta and Pulmonary Trunk. In Olaf Stanger, John Pepper, Lars G. Svensson (Eds.): Surgical management of aortic pathology. Current fundamentals for the clinical management of aortic disease. Vienna: Springer, pp. 63–75. Available online at https://link.springer.com/chapter/10.1007/978-3-7091-4874-7\_3.

Hosen, Mohammed Rabiul; Goody, Philip Roger; Zietzer, Andreas; Xiang, Xu; Niepmann, Sven Thomas; Sedaghat, Alexander et al. (2022): Circulating MicroRNA-122-5p Is Associated With a Lack of Improvement in Left Ventricular Function After Transcatheter Aortic Valve Replacement and Regulates Viability of Cardiomyocytes Through Extracellular Vesicles. In *Circulation* 146 (24), pp. 1836–1854. DOI: 10.1161/CIRCULATIONAHA.122.060258.

Hutcheson, Joshua D.; Chen, Joseph; Sewell-Loftin, M. K.; Ryzhova, Larisa M.; Fisher, Charles I.; Su, Yan Ru; Merryman, W. David (2013): Cadherin-11 regulates cell-cell tension necessary for

calcific nodule formation by valvular myofibroblasts. In *Arteriosclerosis, Thrombosis, and Vascular Biology* 33 (1), pp. 114–120. DOI: 10.1161/ATVBAHA.112.300278.

Jander, Nikolaus; Gohlke-Bärwolf, Christa; Bahlmann, Edda; Gerdts, Eva; Boman, Kurt; Chambers, John B. et al. (2014): Indexing aortic valve area by body surface area increases the prevalence of severe aortic stenosis. In *Heart* 100 (1), pp. 28–33. DOI: 10.1136/heartjnl-2013-304443.

Jansen, Felix; Schäfer, Lisa; Wang, Han; Schmitz, Theresa; Flender, Anna; Schueler, Robert et al. (2017a): Kinetics of Circulating MicroRNAs in Response to Cardiac Stress in Patients With Coronary Artery Disease. In *Journal of the American Heart Association* 6 (8). DOI: 10.1161/JAHA.116.005270.

Jansen, Felix; Xiang, Xu; Werner, Nikos (2017b): Role and function of extracellular vesicles in calcific aortic valve disease. In *Eur Heart J* 38 (36), pp. 2714–2716. DOI: 10.1093/eurheartj/ehx477.

Jayachandran, Muthuvel; Litwiller, Robert D.; Owen, Whyte G.; Heit, John A.; Behrenbeck, Thomas; Mulvagh, Sharon L. et al. (2008): Characterization of blood borne microparticles as markers of premature coronary calcification in newly menopausal women. In *American journal of physiology*. *Heart and circulatory physiology* 295 (3), H931-H938. DOI: 10.1152/ajpheart.00193.2008.

Jiang, Lei; Hao, Chuanji; Li, Zhenfu; Zhang, Ping; Wang, Shizhong; Yang, Sumin et al. (2019): miR-449a induces EndMT, promotes the development of atherosclerosis by targeting the interaction between AdipoR2 and E-cadherin in Lipid Rafts. In *Biomedicine & pharmacotherapy* = *Biomedecine & pharmacotherapie* 109, pp. 2293–2304. DOI: 10.1016/j.biopha.2018.11.114.

Kaden, Jens J.; Dempfle, Carl-Erik; Grobholz, Rainer; Fischer, Carolin S.; Vocke, Daniela C.; Kiliç, Refika et al. (2005): Inflammatory regulation of extracellular matrix remodeling in calcific aortic valve stenosis. In *Cardiovascular Pathology* 14 (2), pp. 80–87. DOI: 10.1016/j.carpath.2005.01.002.

Kalra, Hina; Adda, Christopher G.; Liem, Michael; Ang, Ching-Seng; Mechler, Adam; Simpson, Richard J. et al. (2013): Comparative proteomics evaluation of plasma exosome isolation techniques and assessment of the stability of exosomes in normal human blood plasma. In *PROTEOMICS* 13 (22), pp. 3354–3364. DOI: 10.1002/pmic.201300282.

Kant, Shashi; Tran, Khanh-Van; Kvandova, Miroslava; Caliz, Amada D.; Yoo, Hyung-Jin; Learnard, Heather et al. (2022): PGC1α Regulates the Endothelial Response to Fluid Shear Stress via Telomerase Reverse Transcriptase Control of Heme Oxygenase-1. In *Arteriosclerosis, Thrombosis, and Vascular Biology* 42 (1), pp. 19–34. DOI: 10.1161/ATVBAHA.121.317066.

Kapelouzou, Alkistis; Tsourelis, Loukas; Kaklamanis, Loukas; Degiannis, Dimitrios; Kogerakis, Nektarios; Cokkinos, Dennis V. (2015): Serum and tissue biomarkers in aortic stenosis. In *Global Cardiology Science and Practice* 2015 (4), p. 49. DOI: 10.5339/gcsp.2015.49.

Klinkner, Denise B.; Densmore, John C.; Kaul, Sushma; Noll, LeAnne; Lim, Hyun J.; Weihrauch, Dorothee et al. (2006): Endothelium-derived microparticles inhibit human cardiac valve endothelial cell function. In *Shock* 25 (6), pp. 575–580. DOI: 10.1097/01.shk.0000209558.69575.80.

Kostyunin, Alexander E.; Yuzhalin, Arseniy E.; Ovcharenko, Evgeniy A.; Kutikhin, Anton G. (2019): Development of calcific aortic valve disease: Do we know enough for new clinical trials? In *Journal of Molecular and Cellular Cardiology* 132, pp. 189–209. DOI: 10.1016/j.yjmcc.2019.05.016.

Kovacic, Jason C.; Dimmeler, Stefanie; Harvey, Richard P.; Finkel, Toren; Aikawa, Elena; Krenning, Guido; Baker, Andrew H. (2019): Endothelial to Mesenchymal Transition in Cardiovascular Disease: JACC State-of-the-Art Review. In *Journal of the American College of Cardiology* 73 (2), pp. 190–209. DOI: 10.1016/j.jacc.2018.09.089.

Kreth, Simone; Ledderose, Carola; Schütz, Stefanie; Beiras, Andres; Heyn, Jens; Weis, Florian; Beiras-Fernandez, Andres (2014): MicroRNA-150 inhibits expression of adiponectin receptor 2 and is a potential therapeutic target in patients with chronic heart failure. In *The Journal of heart and lung transplantation : the official publication of the International Society for Heart Transplantation* 33 (3), pp. 252–260. DOI: 10.1016/j.healun.2013.10.014.

Krohn, Jona B.; Hutcheson, Joshua D.; Martínez-Martínez, Eduardo; Aikawa, Elena (2016): Extracellular vesicles in cardiovascular calcification: expanding current paradigms. In *The Journal of Physiology* 594 (11), pp. 2895–2903. DOI: 10.1113/JP271338.

Laird, Dougal F.; Mucalo, Michael R.; Yokogawa, Yoshiyuki (2006): Growth of calcium hydroxyapatite (Ca-HAp) on cholesterol and cholestanol crystals from a simulated body fluid: A possible insight into the pathological calcifications associated with atherosclerosis. In *Journal of Colloid and Interface Science* 295 (2), pp. 348–363. DOI: 10.1016/j.jcis.2005.09.013.

Lê, Sébastien; Josse, Julie; Husson, François (2008): FactoMineR: An R Package for Multivariate Analysis. In *J. Stat. Soft.* 25 (1), pp. 1–18. DOI: 10.18637/jss.v025.i01.

Leopold, Jane A. (2012): Cellular mechanisms of aortic valve calcification. In *Circulation. Cardiovascular interventions* 5 (4), pp. 605–614. DOI: 10.1161/CIRCINTERVENTIONS.112.971028.

Li, Jing; Zhang, Suhua (2016): microRNA-150 inhibits the formation of macrophage foam cells through targeting adiponectin receptor 2. In *Biochemical and biophysical research communications* 476 (4), pp. 218–224. DOI: 10.1016/j.bbrc.2016.05.096.

Li, Jing; Zhang, Yujing; Liu, Yuchen; Dai, Xin; Li, Wenyang; Cai, Xing et al. (2013): Microvesicle-mediated transfer of microRNA-150 from monocytes to endothelial cells promotes angiogenesis. In *Journal of Biological Chemistry* 288 (32), pp. 23586–23596. DOI: 10.1074/jbc.M113.489302.

Lindgren, Anna; Levin, Malin; Rodrigo Blomqvist, Sandra; Wikström, Johannes; Ahnmark, Andrea; Mogensen, Christina et al. (2013): Adiponectin receptor 2 deficiency results in reduced atherosclerosis in the brachiocephalic artery in apolipoprotein E deficient mice. In *PLOS ONE* 8 (11), e80330. DOI: 10.1371/journal.pone.0080330.

Liu, Yangyang; Li, Qian; Hosen, Mohammed Rabiul; Zietzer, Andreas; Flender, Anna; Levermann, Paula et al. (2019): Atherosclerotic Conditions Promote the Packaging of Functional MicroRNA-92a-3p Into Endothelial Microvesicles. In *Circulation Research* 124 (4), pp. 575–587. DOI: 10.1161/CIRCRESAHA.118.314010.

Ljungberg, Johan (2018): Cardiovascular risk factors in aortic stenosis. Umeå universitet. Available online at https://www.diva-portal.org/smash/record.jsf?pid=diva2:1179001.

Love, Michael I.; Huber, Wolfgang; Anders, Simon (2014): Moderated estimation of fold change and dispersion for RNA-seq data with DESeq2. In *Genome biology* 15 (12), p. 550. DOI: 10.1186/s13059-014-0550-8.

Ma, Xiaochun; Zhao, Diming; Yuan, Peidong; Li, Jinzhang; Yun, Yan; Cui, Yuqi et al. (2020): Endothelial-to-Mesenchymal Transition in Calcific Aortic Valve Disease. In *Acta Cardiologica Sinica* 36 (3), pp. 183–194. DOI: 10.6515/ACS.202005\_36(3).20200213A.

Mallat, Z.; Benamer, H.; Hugel, B.; Benessiano, J.; Steg, P. G.; Freyssinet, J. M.; Tedgui, A. (2000): Elevated levels of shed membrane microparticles with procoagulant potential in the peripheral circulating blood of patients with acute coronary syndromes. In *Circulation* 101 (8), pp. 841–843. DOI: 10.1161/01.CIR.101.8.841.

Mathonnet, Géraldine; Fabian, Marc R.; Svitkin, Yuri V.; Parsyan, Armen; Huck, Laurent; Murata, Takayuki et al. (2007): MicroRNA inhibition of translation initiation in vitro by targeting the capbinding complex eIF4F. In *Science* 317 (5845), pp. 1764–1767. DOI: 10.1126/science.1146067.

Matilla, Lara; Martín-Núñez, Ernesto; Garaikoetxea, Mattie; Navarro, Adela; Vico, Julieta Anabela; Arrieta, Vanessa et al. (2022): Characterization of the sex-specific pattern of angiogenesis and lymphangiogenesis in aortic stenosis. In *Front. Cardiovasc. Med.* 9, p. 971802. DOI: 10.3389/fcvm.2022.971802.

Minin, Eduarda O. Z.; Paim, Layde R.; Lopes, Elisangela C. P.; Bueno, Larissa C. M.; Carvalho-Romano, Luís F. R. S.; Marques, Edmilson R. et al. (2021): Association of Circulating miR-145-5p and miR-let7c and Atherosclerotic Plaques in Hypertensive Patients. In *Biomolecules* 11 (12), p. 1840. DOI: 10.3390/biom11121840.

Mittelbrunn, Maria; Sánchez-Madrid, Francisco (2012): Intercellular communication: diverse structures for exchange of genetic information. In *Nat Rev Mol Cell Biol* 13 (5), pp. 328–335. DOI: 10.1038/nrm3335.

Mo, Liang; Ma, Chao; Wang, Zhangzheng; Li, Jianxiong; He, Wei; Niu, Wei et al. (2022): Integrated Bioinformatic Analysis of the Shared Molecular Mechanisms Between Osteoporosis and Atherosclerosis. In *Front. Endocrinol.* 13, p. 950030. DOI: 10.3389/fendo.2022.950030.

Mohler, Emile R. (2004): Mechanisms of aortic valve calcification. In *The American journal of cardiology* 94 (11), 1396-402, A6. DOI: 10.1016/j.amjcard.2004.08.013.

Mongkoldhumrongkul, Napachanok; Yacoub, Magdi H.; Chester, Adrian H. (2016): Valve Endothelial Cells - Not Just Any Old Endothelial Cells. In *Current vascular pharmacology* 14 (2), pp. 146–154. DOI: 10.2174/1570161114666151202205504.

Nader, Joseph; Metzinger, Laurent; Maitrias, Pierre; Caus, Thierry; Metzinger-Le Meuth, Valérie (2020): Aortic valve calcification in the era of non-coding RNAs: The revolution to come in aortic stenosis management? In *Non-coding RNA Research* 5 (2), pp. 41–47. DOI: 10.1016/j.ncrna.2020.02.005.

Nehl, D.; Goody, PR.; Maus, K.; Pfeifer, A.; Aikawa, E.; Bakthiary, F. et al. (2022): Porcine and human aortic valve endothelial and interstitial cell isolation and characterization: Cold Spring Harbor Laboratory.

Nigam (2010): Altered microRNAs in bicuspid aortic valve: a comparison between stenotic and insufficient valves. Available online at https://www.ncbi.nlm.nih.gov/pmc/articles/pmc4242684/.

Nishimura, Riko; Hata, Kenji; Matsubara, Takuma; Wakabayashi, Makoto; Yoneda, Toshiyuki (2012): Regulation of bone and cartilage development by network between BMP signalling and transcription factors. In *J Biochem* 151 (3), pp. 247–254. DOI: 10.1093/jb/mvs004.

Ohnesorge, Nils; Viemann, Dorothee; Schmidt, Nicole; Czymai, Tobias; Spiering, Désirée; Schmolke, Mirco et al. (2010b): Erk5 activation elicits a vasoprotective endothelial phenotype via induction of Kruppel-like factor 4 (KLF4). In *Journal of Biological Chemistry* 285 (34), pp. 26199–26210. DOI: 10.1074/jbc.M110.103127.

Osman, Narin; Grande-Allen, K. Jane; Ballinger, Mandy L.; Getachew, Robel; Marasco, Silvana; O'Brien, Kevin D.; Little, Peter J. (2013): Smad2-dependent glycosaminoglycan elongation in aortic valve interstitial cells enhances binding of LDL to proteoglycans. In *Cardiovascular pathology: the official journal of the Society for Cardiovascular Pathology* 22 (2), pp. 146–155. DOI: 10.1016/j.carpath.2012.07.002.

Otto, C. M.; Kuusisto, J.; Reichenbach, D. D.; Gown, A. M.; O'Brien, K. D. (1994): Characterization of the early lesion of 'degenerative' valvular aortic stenosis. Histological and immunohistochemical studies. In *Circulation* 90 (2), pp. 844–853. DOI: 10.1161/01.cir.90.2.844.

Otto, C. M.; Pearlman, A. S.; Gardner, C. L. (1989): Hemodynamic progression of aortic stenosis in adults assessed by Doppler echocardiography. In *Journal of the American College of Cardiology* 13 (3), pp. 545–550. DOI: 10.1016/0735-1097(89)90590-1.

Otto, Catherine M. (2006): Valvular aortic stenosis: disease severity and timing of intervention. In *Journal of the American College of Cardiology* 47 (11), pp. 2141–2151. DOI: 10.1016/j.jacc.2006.03.002.

Pan, Shi (2009): Molecular mechanisms responsible for the atheroprotective effects of laminar shear stress. In *Antioxidants & Redox Signaling* 11 (7), pp. 1669–1682. DOI: 10.1089/ars.2009.2487.

Patel, Vishal; Carrion, Katrina; Hollands, Andrew; Hinton, Andrew; Thomas Gallegos,§ Jeffrey Dyo,\* Roman Sasik,¶ Emma Leire,† Gary Hardiman,l# Salah A. Mohamed,\*\* Sanjay Nigam,§ Charles C. King,‡ Victor Nizet,† and Vishal Nigam\*††,2 (2015): The stretch responsive microRNA miR-148a-3p is a novel repressor of IKBKB, NF-κB signaling, and inflammatory gene expression in human aortic valve cells. Available online at https://www.ncbi.nlm.nih.gov/pmc/articles/pmc4771066/.

Peltonen, Tuomas; Näpänkangas, Juha; Ohtonen, Pasi; Aro, Jani; Peltonen, Jenni; Soini, Ylermi et al. (2011): (Pro)renin receptors and angiotensin converting enzyme 2/angiotensin-(1-7)/Mas receptor axis in human aortic valve stenosis. In *Atherosclerosis* 216 (1), pp. 35–43. DOI: 10.1016/j.atherosclerosis.2011.01.018.

Piazza, Nicoló; Jaegere, Peter de; Schultz, Carl; Becker, Anton E.; Serruys, Patrick W.; Anderson, Robert H. (2008): Anatomy of the aortic valvar complex and its implications for transcatheter implantation of the aortic valve. In *Circulation. Cardiovascular interventions* 1 (1), pp. 74–81. DOI: 10.1161/CIRCINTERVENTIONS.108.780858.

Poggio, Paolo; Songia, Paola; Moschetta, Donato; Valerio, Vincenza; Myasoedova, Veronika; Perrucci, Gianluca L.; Pompilio, Giulio (2019): MiRNA profiling revealed enhanced susceptibility to oxidative stress of endothelial cells from bicuspid aortic valve. In *Journal of Molecular and Cellular Cardiology* 131, pp. 146–154. DOI: 10.1016/j.yjmcc.2019.04.024.

Poon, Ivan K. H.; Chiu, Yu-Hsin; Armstrong, Allison J.; Kinchen, Jason M.; Juncadella, Ignacio J.; Bayliss, Douglas A.; Ravichandran, Kodi S. (2014): Unexpected link between an antibiotic, pannexin channels and apoptosis. In *Nature* 507 (7492), pp. 329–334. DOI: 10.1038/nature13147.

Qin, Bing; Xiao, Bo; Liang, Desheng; Li, Ye; Jiang, Ting; Yang, Huan (2012): MicroRNA let-7c inhibits Bcl-xl expression and regulates ox-LDL-induced endothelial apoptosis. In *BMB Reports* 45 (8), pp. 464–469. DOI: 10.5483/bmbrep.2012.45.8.033.

Raddatz, Michael A.; Vander Roest, Mark J.; Merryman, W. David (2020): Notch1 suppression by microRNA-34a: a new mechanism of calcific aortic valve disease. In *Cardiovasc Res* 116 (5), pp. 871–873. DOI: 10.1093/cvr/cvz280.

Rajamannan (2011): Calcific aortic valve disease: not simply a degenerative process a review and agenda for research from the National Heart and Lung and Blood Institute Aortic ... Available online at https://www.ncbi.nlm.nih.gov/pmc/articles/pmc3306614/.

Rana, Mukaram (2022): Aortic Valve Stenosis: Diagnostic Approaches and Recommendations of the 2021 ESC/EACTS Guidelines for the Management of Valvular Heart Disease -A Review of the Literature. In *Cardiology and cardiovascular medicine* 6 (3), pp. 315–324. DOI: 10.26502/fccm.92920267.

Rao, Ravi M.; Yang, Lin; Garcia-Cardena, Guillermo; Luscinskas, Francis W. (2007): Endothelial-dependent mechanisms of leukocyte recruitment to the vascular wall. In *Circulation Research* 101 (3), pp. 234–247. DOI: 10.1161/CIRCRESAHA.107.151860b.

Rautou, Pierre-Emmanuel; Vion, Anne-Clémence; Amabile, Nicolas; Chironi, Gilles; Simon, Alain; Tedgui, Alain; Boulanger, Chantal M. (2011): Microparticles, vascular function, and atherothrombosis. In *Circulation Research* 109 (5), pp. 593–606. DOI: 10.1161/CIRCRESAHA.110.233163.

Robinson, Mark D.; McCarthy, Davis J.; Smyth, Gordon K. (2010): edgeR: a Bioconductor package for differential expression analysis of digital gene expression data. In *Bioinformatics* 26 (1), pp. 139–140. DOI: 10.1093/bioinformatics/btp616.

Ross, J.; Braunwald, E. (1968): Aortic stenosis. In *Circulation* 38 (1 Suppl), pp. 61–67. DOI: 10.1161/01.CIR.38.1S5.V-61.

Rozeik; Wheatley; Gourlay (2014): The aortic valve: structure, complications and implications for transcatheter aortic valve replacement. In *Perfusion* 29 (4), pp. 285–300. DOI: 10.1177/0267659114521650.

Rutkovskiy, Arkady; Malashicheva, Anna; Sullivan, Gareth; Bogdanova, Maria; Kostareva, Anna; Stensløkken, Kåre-Olav et al. (2017): Valve Interstitial Cells: The Key to Understanding the Pathophysiology of Heart Valve Calcification. In *Journal of the American Heart Association* 6 (9). DOI: 10.1161/JAHA.117.006339.

Schmidt, Ulf; Frewer, Andreas (2007): History and theory of human experimentation. The declaration of Helsinki and modern medical ethics. Edited by Ulf Schmidt, Andreas Frewer. Stuttgart: Franz Steiner Verlag (Geschichte und Philosophie der Medizin, Bd. 2). Available online at https://kar.kent.ac.uk/13343.

Schoen, Frederick J. (2008): Evolving concepts of cardiac valve dynamics: the continuum of development, functional structure, pathobiology, and tissue engineering. In *Circulation* 118 (18), pp. 1864–1880. DOI: 10.1161/CIRCULATIONAHA.108.805911.

Shen, Yaqi; Shen, Zhuqing; Miao, Lei; Xin, Xiaoming; Lin, Shizhou; Zhu, Yichun et al. (2015): miRNA-30 family inhibition protects against cardiac ischemic injury by regulating cystathionine-γ-lyase expression. In *Antioxidants & Redox Signaling* 22 (3), pp. 224–240. DOI: 10.1089/ars.2014.5909.

Simak, J.; Gelderman, M. P.; Yu, H.; Wright, V.; Baird, A. E. (2006): Circulating endothelial microparticles in acute ischemic stroke: a link to severity, lesion volume and outcome. In *Journal of thrombosis and haemostasis : JTH* 4 (6), pp. 1296–1302. DOI: 10.1111/j.1538-7836.2006.01911.x.

Simionescu, Dan T.; Lovekamp, Joshua J.; Vyavahare, Narendra R. (2003): Glycosaminoglycan-degrading enzymes in porcine aortic heart valves: implications for bioprosthetic heart valve degeneration. In *The Journal of heart valve disease* 12 (2), pp. 217–225. Available online at https://www.researchgate.net/profile/dan-simionescu/publication/10798679\_glycosaminoglycan-degrading\_enzymes\_in\_porcine\_aortic\_heart\_valves\_implications\_for\_bioprosthetic\_heart\_valve e degeneration.

Simmons, Craig A.; Zilberberg, Jenny; Davies, Peter F. (2004): A rapid, reliable method to isolate high quality endothelial RNA from small spatially-defined locations. In *Annals of Biomedical Engineering* 32 (10), pp. 1453–1459. DOI: 10.1114/B:ABME.0000042360.57960.2b.

Simons, Mikael; Raposo, Graça (2009): Exosomes--vesicular carriers for intercellular communication. In *Current Opinion in Cell Biology* 21 (4), pp. 575–581. DOI: 10.1016/j.ceb.2009.03.007.

Sinning, Jan-Malte; Losch, Jan; Walenta, Katrin; Böhm, Michael; Nickenig, Georg; Werner, Nikos (2011): Circulating CD31+/Annexin V+ microparticles correlate with cardiovascular outcomes. In *Eur Heart J* 32 (16), pp. 2034–2041. DOI: 10.1093/eurheartj/ehq478.

Sohel, Mahmodul Hasan (2016): Extracellular/Circulating MicroRNAs: Release Mechanisms, Functions and Challenges. In *Achievements in the Life Sciences* 10 (2), pp. 175–186. DOI: 10.1016/j.als.2016.11.007.

Souilhol, Celine; Harmsen, Martin C.; Evans, Paul C.; Krenning, Guido (2018): Endothelial-mesenchymal transition in atherosclerosis. In *Cardiovasc Res* 114 (4), pp. 565–577. DOI: 10.1093/cvr/cvx253.

Spiess (2013): R: A language and environment for statistical computing. Available online at https://apps.dtic.mil/sti/citations/ad1039033.

Stewart, B. F.; Siscovick, D.; Lind, B. K.; Gardin, J. M.; Gottdiener, J. S.; Smith, V. E. et al. (1997): Clinical factors associated with calcific aortic valve disease. Cardiovascular Health Study. In *Journal of the American College of Cardiology* 29 (3), pp. 630–634. DOI: 10.1016/S0735-1097(96)00563-3.

Sudip Dahal; Peter Huang; Bruce T. Murray; Gretchen J. Mahler (2017): Endothelial to mesenchymal transformation is induced by altered extracellular matrix in aortic valve endothelial cells. In *Journal of Biomedical Materials Research Part A* 105 (10), pp. 2729–2741. DOI: 10.1002/jbm.a.36133.

Tang, Yaoping; Wang, Yongchao; Park, Kyoung-mi; Hu, Qiuping; Teoh, Jian-peng; Broskova, Zuzana et al. (2015): MicroRNA-150 protects the mouse heart from ischaemic injury by regulating cell death. In *Cardiovasc Res* 106 (3), pp. 387–397. DOI: 10.1093/cvr/cvv121.

Toli, Konstantina; Paraskevas, Kosmas I.; Poulakou, Maria V.; Agrogiannis, Georgios; Kavantzas, Nikolaos; Xanthopoulos, Vassilios et al. (2008): Association between plasma levels and immunolocalization of cytokines in heart valve lesions: a possible target for treatment? In *Expert Opinion on Therapeutic Targets* 12 (10), pp. 1209–1215. DOI: 10.1517/14728222.12.10.1209.

van Niel, Guillaume; D'Angelo, Gisela; Raposo, Graça (2018): Shedding light on the cell biology of extracellular vesicles. In *Nat Rev Mol Cell Biol* 19 (4), pp. 213–228. DOI: 10.1038/nrm.2017.125.

Vesely, I. (1998): The role of elastin in aortic valve mechanics. In *Journal of Biomechanics* 31 (2), pp. 115–123. DOI: 10.1016/S0021-9290(97)00122-X.

Wang, Hui; Shi, Jing; Li, Beibei; Zhou, Qiulian; Kong, Xiangqing; Bei, Yihua (2017): MicroRNA Expression Signature in Human Calcific Aortic Valve Disease. In *BioMed Research International* 2017, p. 4820275. DOI: 10.1155/2017/4820275.

Wang, Xue; Zhu, Yuhai; Wu, Chengcheng; Liu, Wennan; He, Yujie; Yang, Qing (2021): Adipose-Derived Mesenchymal Stem Cells-Derived Exosomes Carry MicroRNA-671 to Alleviate Myocardial Infarction Through Inactivating the TGFBR2/Smad2 Axis. In *Inflammation* 44 (5), pp. 1815–1830. DOI: 10.1007/s10753-021-01460-9.

Wei, Tianling; Folkersen, Lasse; Ehrenborg, Ewa; Gabrielsen, Anders (2016): MicroRNA 486-3P as a stability marker in acute coronary syndrome. In *Biosci Rep* 36 (3). DOI: 10.1042/BSR20160023.

Wei, Yuanyuan; Nazari-Jahantigh, Maliheh; Chan, Lily; Zhu, Mengyu; Heyll, Kathrin; Corbalán-Campos, Judit et al. (2013): The microRNA-342-5p fosters inflammatory macrophage activation through an Akt1- and microRNA-155-dependent pathway during atherosclerosis. In *Circulation* 127 (15), pp. 1609–1619. DOI: 10.1161/CIRCULATIONAHA.112.000736.

Wickham, Hadley (2016): Data Analysis. In : ggplot2: Springer, Cham, pp. 189–201. Available online at https://link.springer.com/chapter/10.1007/978-3-319-24277-4\_9.

Winter, Julia; Jung, Stephanie; Keller, Sarina; Gregory, Richard I.; Diederichs, Sven (2009): Many roads to maturity: microRNA biogenesis pathways and their regulation. In *Nat Cell Biol* 11 (3), pp. 228–234. DOI: 10.1038/ncb0309-228.

Xu, Kang; Xie, Shangbo; Huang, Yuming; Zhou, Tingwen; Liu, Ming; Zhu, Peng et al. (2020): Cell-Type Transcriptome Atlas of Human Aortic Valves Reveal Cell Heterogeneity and Endothelial to Mesenchymal Transition Involved in Calcific Aortic Valve Disease. In *Arteriosclerosis, Thrombosis, and Vascular Biology* 40 (12), pp. 2910–2921. DOI: 10.1161/ATVBAHA.120.314789.

Xue, Tingmao; Yam, Judy Wai Ping (2022): Role of Small Extracellular Vesicles in Liver Diseases: Pathogenesis, Diagnosis, and Treatment. In *Journal of Clinical and Translational Hepatology* 10 (6), pp. 1176–1185. DOI: 10.14218/JCTH.2022.00008.

Yanagawa, Bobby; Lovren, Fina; Pan, Yi; Garg, Vinay; Quan, Adrian; Tang, Gilbert et al. (2012): miRNA-141 is a novel regulator of BMP-2-mediated calcification in aortic stenosis. In *The Journal of Thoracic and Cardiovascular Surgery* 144 (1), pp. 256–262. DOI: 10.1016/j.jtcvs.2011.10.097.

Yáñez-Mó, María; Siljander, Pia R-M; Andreu, Zoraida; Zavec, Apolonija Bedina; Borràs, Francesc E.; Buzas, Edit I. et al. (2015): Biological properties of extracellular vesicles and their physiological functions. In *Journal of Extracellular Vesicles* 4, p. 27066. DOI: 10.3402/jev.v4.27066.

Yang, Rong; Tang, Yihu; Chen, Xiaowen; Yang, Yang (2021): Telocytes-derived extracellular vesicles alleviate aortic valve calcification by carrying miR-30b. In *ESC Heart Failure* 8 (5), pp. 3935–3946. DOI: 10.1002/ehf2.13460.

Yeang; Wilkinson (2016): Lipoprotein (a) and oxidized phospholipids in calcific aortic valve stenosis. Available online at https://www.ncbi.nlm.nih.gov/pmc/articles/pmc4956483/.

Yin, Qiulin; He, Mingyan; Huang, Li; Zhang, Xuehong; Zhan, Junfeng; Hu, Jing (2021): IncRNA ZFAS1 promotes ox-LDL induced EndMT through miR-150-5p/Notch3 signaling axis. In *Microvascular Research* 134, p. 104118. DOI: 10.1016/j.mvr.2020.104118.

Zeng, Peng; Yang, Jie; Liu, Lipei; Yang, Xiaoxiao; Yao, Zhi; Ma, Chuanrui et al. (2021): ERK1/2 inhibition reduces vascular calcification by activating miR-126-3p-DKK1/LRP6 pathway. In *Theranostics* 11 (3), pp. 1129–1146. DOI: 10.7150/thno.49771.

Zhang, Fan; Cheng, Naixuan; Han, Yingchun; Zhang, Congcong; Zhang, Haibo (2021): miRNA Expression Profiling Uncovers a Role of miR-139-5p in Regulating the Calcification of Human Aortic Valve Interstitial Cells. In *Frontiers in genetics* 12, p. 722564. DOI: 10.3389/fgene.2021.722564.

Zhang, Mi; Liu, Xiaohong; Zhang, Xiwu; Song, Zhigang; Han, Lin; He, Yuanyuan; Xu, Zhiyun (2014): MicroRNA-30b is a multifunctional regulator of aortic valve interstitial cells. In *The Journal of Thoracic and Cardiovascular Surgery* 147 (3), 1073-1080.e2. DOI: 10.1016/j.jtcvs.2013.05.011.

Zhang, Yefei; Chen, Naiyun; Zhang, Jihao; Tong, Yaling (2013): Hsa-let-7g miRNA targets caspase-3 and inhibits the apoptosis induced by ox-LDL in endothelial cells. In *International Journal of Molecular Sciences* 14 (11), pp. 22708–22720. DOI: 10.3390/ijms141122708.

Zhao, Yong; Ransom, Joshua F.; Li, Ankang; Vedantham, Vasanth; Drehle, Morgan von; Muth, Alecia N. et al. (2007): Dysregulation of cardiogenesis, cardiac conduction, and cell cycle in mice lacking miRNA-1-2. In *Cell* 129 (2), pp. 303–317. DOI: 10.1016/j.cell.2007.03.030.

Zheng, Suxia; Gong, Maolei; Chen, Jing (2021): Extracellular vesicles enriched with miR-150 released by macrophages regulates the TP53-IGF-1 axis to alleviate myocardial infarction. In *American journal of physiology. Heart and circulatory physiology* 320 (3), H969-H979. DOI: 10.1152/ajpheart.00304.2020.

Zhu, Bin; Liu, Wei; Xu, Qiang; Liu, Hong-Liang (2022): MicroRNA-486-5p functions as a diagnostic marker for carotid artery stenosis and prevents endothelial dysfunction through inhibiting inflammation and oxidative stress. In *Bioengineered* 13 (4), pp. 8667–8675. DOI: 10.1080/21655979.2022.2054500.

Zietzer, Andreas; Hosen, Mohammed Rabiul; Wang, Han; Goody, Philip Roger; Sylvester, Marc; Latz, Eicke et al. (2020): The RNA-binding protein hnRNPU regulates the sorting of microRNA-30c-5p into large extracellular vesicles. In *Journal of Extracellular Vesicles* 9 (1), p. 1786967. DOI: 10.1080/20013078.2020.1786967.

## **List of Figures**

Figure 1. Schematic figure of the aortic root.	1
Figure 2. Aortic valve structure.	
Figure 3. Pathophysiology and progression of aortic valve stenosis (AVS)	
Figure 4. Mechanisms of EndMT and Calcification in AVS.	
Figure 5. Biogenesis of extracellular vesicles (EVs)	
Figure 6. miRNA biogenesis.	
Figure 7. Schematic illustration of VIC isolation from calcific aortic valve.	
Figure 8. Representative figure of ibidi pump system	
Figure 9. Representative figure of ibidi 2 well culture-insert.	
Figure 10. A representative picture of primary miRNA structure.	
Figure 11. Side specific cell and RNA isolation from VECs (Figure adapted from Simmons et al.	
(Simmons et al. 2004).	39
Figure 12. Stem-Loop RT PCR.	
Figure 13. Representative figure of sequencing data in IEV- and sEV-derived miRNAs in AVS com	
to Al.	
Figure 14. Gene ontology (GO) and signaling pathway analysis of EV-miRNA target genes	
Figure 15. IEV-miRNA validation.	
Figure 16.sEV-miRNA validation.	
Figure 17. VEC Characterization.	
Figure 18. Morphology of VECs in EndMT model.	
Figure 19. Gene expression levels of EndMT Markers treated with 10ng/ml TGF-β1, 50ng/ml BMP2	
10ng/ml IL-1β and 25ng/ml TNFα for 7 days.	
Figure 20. Validation of miRNAs overexpression in VECs after transduction.	
Figure 21. EndMT markers in VECs Overexpressing miRNA-150-5p and treated with TNFα	
Figure 22. EndMT markers in VECs overexpressing hinting 130-5p and treated with 110 d	
rigure 22. Endivir markers in vEGs overexpressing Let-76-5p and militing-50b-5p and treated with	
Figure 23. Microscopic images of VECs overexpressing miRNA-150-5p, Let-7c-5p, and miR-30b-5	
the TNFα treatment to induce EndMT (n=3).	
Figure 24. Effects of miRNA-150-5p on tube formation of VECs	
Figure 25. Effect of miRNA-150-5p on migration ability of VECs.	
Figure 26. qPCR analysis of miRNA-150-5p expression on aortic and ventricular sides of the aortic	
showing the similar expression level of miRNA-150-5p in both regions (n=3). Statistical analysis was	
performed using Student's t-test.	
Figure 27. representative microscopic picture of VECs cultured under laminar flow and static condi	
Figure 28. Gene expression pattern of shear sensitive genes in VECs exposed to laminar flow 20 c	
for 24h.	
Figure 29. miRNA profiling in VECs exposed to laminar flow compared to control cells	
Figure 30. Immortalized VECs (I-VECs).	
Figure 31. Characterization of IEVs isolated from immortalized VECs.	
Figure 31. Characterization of 1EVs isolated from infinitionalized VECs.	
Figure 33. EndMT markers in VECs treated with IEVs containing increased level of miRNA-150 (n=	
· ·	
Figure 34. Representative figure of mRNA sequencing data in VECs overexpressing miRNA-150-5	•
Figure 35. Functional enrichment analysis of upregulated target genes of miRNA-150-5p.	
Figure 36. Functional enrichment analysis of downregulated target genes of miRNA-150-5p	
Figure 37. Venn diagram illustrating the signaling pathways associated with EndMT in both upregulated target genes of miRNA 150.5p.	
and downregulated target genes of miRNA-150-5p	
Figure 39. GRNs and PPIs analysis of downregulated target genes of miRNA-150-5p	
Figure 40. Characterization of isolated VICs from the calcific aortic valve.	
Figure 41. VIC calcification in 6 different patients with AVS.	
i iguio 71. Vio valviilvalivii iii v uiiigigiil paligiilo Willi AVO	

Figure 42. Validation of miRNA-150-5p and Let-7c-5p overexpression in VICs after transduction	84
Figure 43.Representative picture of alizarin red in VICs overexpressing miRNA-150-5p and Let-7c	-5p85
Figure 44. Relative gene expression analysis of calcification markers in VICs overexpressing miRI	NA-150-
5p and Let-7c-5p, cultured in OM and PM	
Figure 45. Effect of miRNA-150-5p and Let-7c-5p on TNAP activity in VICs treated with OM	87
List of Tables	
Table 1. Grading of AVS (Rana 2022)	6
Table 2: Cell culture medium used for VIC experiments	
Table 3: Cell culture medium used for VEC experiments	20
Table 4. PBS	28
Table 5. PFA 4%	
Table 6. BSA-glycine-PBS-T	
Table 7. List of primary and secondary antibodies.	
Table 8. List of primers used to amplify miRNAs and the length of corresponding PCR product	
Table 9. PCR reaction mix.	
Table 10. PCR program used for DNA Insert Amplification.	
Table 11. 50X TAE buffer	
Table 12. Restriction digestion reaction	
Table 13. Ligation reaction	
Table 14. LB Medium	
Table 15. Miniprep buffers	
Table 16. Restriction digestion for miRNA-150-5p	
Table 17. Restriction digestion for Let-7c-5p	
Table 18. Restriction digestion for miRNA-30b-5p	
Table 19. RIPA buffer	
Table 20. cDNA synthesis program	
Table 21. List of primers	
Table 22. qPCR thermal program	
Table 23. cDNA components	
Table 24. cDNA synthesis program	
Table 25. List of RT and PCR primers	
Table 26. qPCR thermal program.	
Table 27. cDNA synthesis program.	
Table 28. qPCR thermal program	
Table 29. Baseline patient characteristics.	
Table 30. List of significantly dysregulated miRNAs in EVs isolated from the aortic valve	
Table 31. List of validated EV-miRNAs in cardiovascular diseases	
Table 32. Baseline patient characteristics.	
Table 33. miRNA-mRNA Hybridization and the pattern of binding site	81